Author:

Morten Ziebell

Institute:

Neurobiology Research Unit 9201, Rigshospitalet

University:

University of Copenhagen, Faculty of Health Sciences, Denmark

Title:

Evaluation of the superselective radioligand [^{123}I]PE2I for imaging of the dopamine transporter in SPECT.

Supervisor:

Professor, MD, DMSc, Gitte Moos Knudsen

Assessment committee:

Associate Professor, Chief Physician, Senior MD, Lars Friberg, Department of Clinical Physiology and Nuclear Medicine, Bispebjerg University Hospital, Copenhagen, Denmark. (University representative)

Professor, MD, PhD, Jan Booij, Department of Nuclear Medicine, University of Amsterdam, Academic Medical Center, Amsterdam, the Netherlands.

Chief Physician, PhD, Anna M. Catafau, Barcelona Imaging Group (BenIG), Barcelona, Spain.

Preface

Sometimes when doing research, you find yourself in the middle of a single detail within one of your methods and you tend to forget where you came from. So before I begin this thesis and focus on details of a single method for measuring one single protein in the brain, I want to draw the attention of the reader towards one main point that helped me keeping my focus, interest and attention in my research: The methods and research that are evaluated in this thesis overall relate to the fact that we as a population are getting older. The global average lifespan has doubled within the last 200 years from 31 to 65.6 years, and the average lifespan in many developed countries today is over 80 years (World Health Organisation (WHO)). As a consequence the prevalence of age related neurodegenerative diseases such as Parkinson's and Alzheimer's Disease[1] has evolved dramatically. In 2006 approximately 24 million people suffered from dementia and it is estimated that the number of people suffering from dementia will double every 20 years (Ferri *et al* 2005). Likewise, in 2005 1 % of people over the age of 60 suffered from Parkinson's disease (de Lau and Breteler 2006) a number expected to increase 25 % by the year of 2030 (WHO 2010). Hence the need for research in this area is crucial.

So please remember to turn to this page if you tend to forget "where I came from".

Morten Ziebell, October 2010

---

[1] Alzheimer Alois (1907). "*Über eine eigenartige Erkrankung der Hirnrinde"*. Allgemeine Zeitschrift fur Psychiatrie und Psychisch-Gerichtlich Medizin **64** (1–2): 146–148.

"An Essay on the Shaking Palsy", by James Parkinson, Published by Sherwood, Neely, and Jones London, 1817.

Table of contents

Acknowledgements

Denne Ph.d.-afhandling markerer afslutningen på et langt og godt forløb ved Neurobiologisk Forskningsenhed (NRU). Her har jeg været siden jeg var "en lille dreng" (citat, Gitte). Jeg startede som stud. med. i 2002 som "altmuligmand" for læge, dr. med. Lars H. Pinborg, og under hans kyndige hænder og med hans store engagement i kvantificering af hjernens receptorer blev min egen begejstring for forskning vakt. NRU har gamle traditioner ud i forskning i hjernens blodgennemstrømning ved grundlægger Professor Niels A Lassen og senere Professor Olaf B Paulsen, og har under ledelse af Professor Gitte Moos Knudsen bibeholdt dets høje internationale anerkendte forskning, nu med fokus på hjernens receptorer. NRU er en spændende "multiuddannelses-kulturel" og dynamisk forskningsenhed med mange udfordringer i samarbejde og formidling. Tiden som Ph.d.-studerende er en uddannelse i forskning, og i det finder man ikke bedre uddannelsessted end NRU.

Jeg vil gerne takke ledelsen og især Gitte for hendes personlige, økonomiske og ikke mindst faglige opbakning samt Lars for hans store faglige kunnen, hjælp og inspiration. Dernæst vil jeg gerne takke mine medforfattere for deres bidrag til de artikler som ligger til grund for min afhandling. Særligt vil jeg gerne fremhæve mine fantastisk gode arbejdskollegaer fra SPECT laboratoriet, som om nogen har muliggjort denne Ph.d. herunder bioanalytiker Karin Stahr, Svitlana Olsen og Glenna Skoubo, samt ikke mindst laboratoriets Chef bioanalytiker Gerda Thomsen, som med hendes store engagement og smittende humør har hjulpet mig i gode som i mindre gode tider, praktisk som personligt. Jeg vil gerne takke arbejdskollegaer fra NRU, venner og familie for støtte, gode tider og overbærenhed med distræte perioder. Sidst men ikke mindst vil jeg takke min bedste ven og livsledsager, min kloge kone Mette Louise for at have fulgt og støttet mig under hele perioden på NRU, samt for at være der som den bedste mor man kan tænke sig for vores børn Marius og Laura Amalie, tak smukke.

List of articles

Pinborg LH, Ziebell M, Frokjaer VG, de Nijs R, Svarer C, Haugbol S, Yndgaard S, Knudsen GM (2005) Quantification of 123I-PE2I binding to dopamine transporter with SPECT after bolus and bolus/infusion. *J Nucl Med* 46:1119-27.

Ziebell M, Thomsen G, Knudsen GM, de Nijs R, Svarer C, Wagner A, Pinborg LH (2007) Reproducibility of [123I]PE2I binding to dopamine transporters with SPECT. *Eur J Nucl Med Mol Imaging* 34:101-9.

Ziebell M, Pinborg LH, Thomsen G, de Nijs R, Svarer C, Wagner A, Knudsen GM (2010) MRI-guided region-of-interest delineation is comparable to manual delineation in dopamine transporter SPECT quantification in patients: a reproducibility study. *J Nucl Med Technol* 38:61-8.

Ziebell M, Holm-Hansen S, Thomsen G, Wagner A, Jensen P, Pinborg LH, Knudsen GM (2010) Serotonin transporters in dopamine transporter imaging: A head-to-head comparison of dopamine transporter SPECT radioligands [123I]FP-CIT and [123I]PE2I. *J Nucl Med* 51:1885-91.

Abbreviations

AAAD	Aromatic-L-amino-acid decarboxylase
AUC	Area Under the Curve
$B_{available}$	Receptors available for binding
B_{max}	Receptor density
β-CIT	2-beta-carbomethoxy-3 beta-(4-iodophenyl)tropane
BBB	Blood brain barrier
B/I	Bolus infusion ratio
BP	Binding Potential
BP_{ND}	Binding Potential of the non-displaceable tracer
BP_P	Binding Potential of the total plasma concentration
BP_1	Former notation of the BP_P
BP_2	Former notation of the BP_{ND}
BR	Binding Ratio
CT	Computer Tomography
D1-5	Dopamine receptor 1-5
DA	Dopamine, 3,4-dihydroxyphenethylamine
DAT	Dopamine transporter
DaTSCAN	FP-CIT
5-HT	Serotonin
FP-CIT	2-beta-carbomethoxy-3 beta-(4-iodophenyl)-N-(3-fluoropropyl)nortropane
f_{ND}	Free fraction in non-displaceable compartment
GABA	γ-Aminobutyric acid
K_D	Equilibrium dissociation constant
L-DOPA	3,4-dihydroxyphenylalanine
MAO	Monoamine oxidase enzymes
MD	Manual delineation
MRD	MRI-defined probability map based ROI delineation
MRI	Magnetic Resonance Imaging
NET	Norepinephrine transporter
PET	Positron Emission Tomography
PD	Parkinson's disease
PE2I	N-(3-iodoprop-2E-enyl)-2-beta-carbomethoxy-3beta-(4-methylphenyl),
ROI	Region of interest
SBR	Striatal binding ratio
SERT	Serotonin transporter
SNpc	Substantia Nigra Pars Compacta
SPECT	Single Photon Emission Computer Tomography
SRTM	Simplified Reference tissue model
SSRI	Selective Serotonin Reuptake inhibitor
SVI	Striatal volume of interest
TAC	Time activity curves
^{99m}Tc-TRODAT-1	(99m)Tc-[2[[2-[[[3-(4-chlorophenyl)-8-methyl-8-azabicyclo[3,2,1]-oct-2-yl]-methyl](2-mercaptoethyl) amino]ethyl]amino]ethane-thiolato(3-)-N2,N2',S2,S2]oxo-[1R-(exo-exo)
VOI	Volume of interest
VMAT	Vesicular monoamine transporter

Background

Dopamine

In 2000 a Swedish scientist, Arvid Carlsson, received the Nobel Prize for his work with 3,4-dihydroxyphenethylamine, dopamine (DA) (Carlsson et al 1957). DA was synthesised in 1910 by George Barger and colleagues (Barger and Dale 1910). They found it to be a weak sympathomimetic compound and so it was left unexplored for more than three decades. What Arvid Carlsson found out years later, was that dopamine was a neurotransmitter by itself and not only a precursor for norepinephrine and epinephrine. In the same period the enzyme aromatic-L-amino-acid decarboxylase (also called dopa decarboxylase or AAAD) was discovery by a German scientist (Holtz 1959). The discovery of this enzyme, which in mammalian tissues converts 3,4-dihydroxyphenylalanine (L-DOPA) to dopamine, provided a mechanism for the formation of dopamine in the brain because unlike dopamine itself, L-DOPA can cross the blood brain barrier (BBB). Since then the neurotransmitter dopamine has been the subject of enormous scientific interest; mentioned in almost 65.000 papers when combined with search term "brain" in a Pubmed search in September 2010.

DA neurons play a key role in many basic functions of the brain, such as motivation, motor behaviour and working memory. It constitutes one of its main functions in the reward system of the brain and thereby indirectly controls the learning of many of our specific behaviours (for review (Wise 2004)). Altogether DA acts as a central neurotransmitter for our good health – mentally as physically. The DA neurons are located in groups deep within the brain and the projections of the DA neurons were originally identified and localized using the Falck – Hillarp histoflourocense method (Falck *et al* 1982). The most prominent cell group of DA neurons that accounts for 90 % of the total amount is located in the mesencephalon. There are 3 overall pathways in this DA system, fig. 1: In two of the pathways DA neuron cell bodies located in the ventral tegmental area project to the frontal cortex and the nucleus accumbens. In

the third pathway, "the nigrostriatal pathway" DA neurons in the substantia nigra pars compacta (SNpc) project axons to the dorsal striatum (putamen and caudate nucleus), as part of the basal ganglia. This nigrostriatal pathway was first described in 1964 (Anden *et al* 1964) and will be the focus of this thesis.

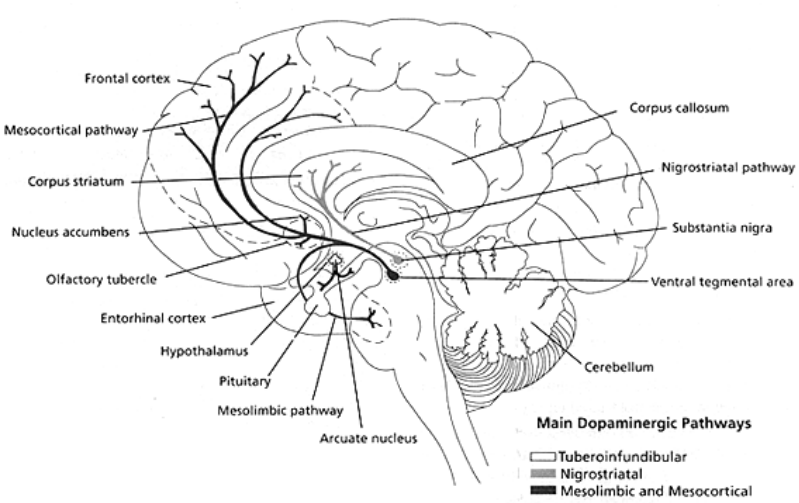

Figure 1. A sketch of the dopaminergic projections from the SNpc and the ventral tegmental area. (Source: *Aust Prescr* 1994; 17: 17-21).

The basal ganglia

The basal ganglia or basal nuclei are a group of nuclei situated in the forebrain (prosencephalon), fig. 2. The main components are the striatum, pallidum, substantia nigra and the subthalamic nucleus.

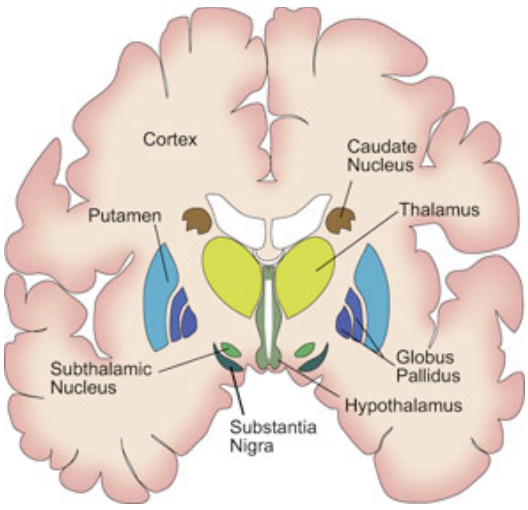

Figure 2. An overview of the different nuclei that make up the basal ganglia (thalamus, however not conventionally regarded as such). (Source: The Dana Foundation, unknown illustrator).

The striatum is mostly known for its part in planning and modulation of movement pathways, but it is also involved in different cognitive functions and in the reward system of the brain (Wise 2004). The striatum receives input not only from the SNpc but also from other brain areas such as the brain stem (raphe nucleus) that sends projections from serotonergic (5-HT) neurons (Varnas *et al* 2004). However, the most dominant input comes from the neocortex, except the primary visual and auditory cortex, thus making striatum the major input center of the whole brain.

The striatum consists mostly of medium spiny neurons, which are inhibitory neurons that use γ-Aminobutyric acid (GABA) as neurotransmitter. The medium spiny neurons contain different types of neuropeptide receptors (Substance P, dynorphin and dopamine). Within the basal ganglia there is a very complex system of neuronal circuits. Two are major, fig. 3: "The direct pathway" where medium spiny neurons send their axons to the internal part of the globus pallidus and the substantia nigra, and "the indirect pathway" where they send their axons to the external part of the globus pallidus. In a complex pattern the net result of excitatory inputs towards medium spiny neurons in these two circuits either stimulates (the direct pathway) or inhibits (the indirect pathway) upper motor neurons and thereby movement.

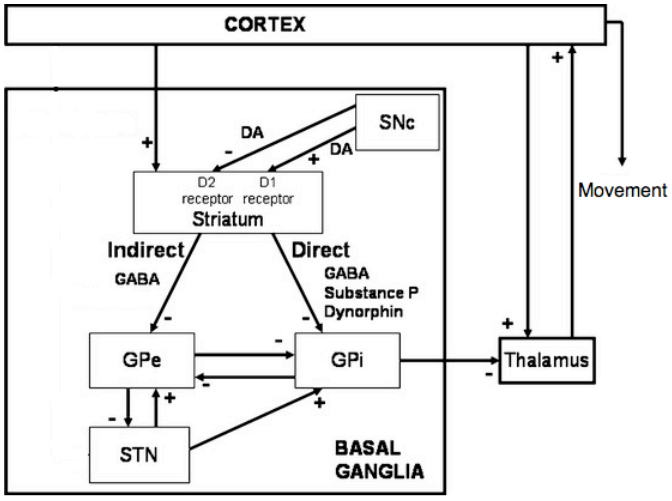

Figure 3. Scheme of the basal ganglia circuit. SNc Substantia nigra pars compacta; STN subthalamic nucleus; GPe & GPi external and internal part of the globus pallidus. (Source: Moroney, R, *Jour of Comput Neurosc* Vol. 25 Issue 3)

Not surprisingly dysfunction of the basal ganglia primarily leads to diseases associated with symptoms of movement dysfunction known as movement disorders such as Parkinson's disease (PD), Huntington's disease (HD), Lewy body dementia (DLB) and various other atypical Parkinson syndromes associated with basal ganglia pathology. These diseases involve different localisation in the basal ganglia. In HD there is a massive loss of medium spiny neurons in the striatum (Paulsen 2009), whereas loss of neurons (i.e. dopaminergic neurons) is located in the SNpc in PD (Damier *et al* 1999).

Dopamine transmission

The neurotransmission in the nigro-striatal pathway takes place in the dorsal striatum. DA is synthesized in the core of the DA neurons in SNpc and transported to the synapse where it is stored in presynaptic vesicles. When the DA neuron is triggered by electrical stimuli the DA is released into the synapse where it acts through DA receptors on the postsynaptic membrane. There are at least 5 receptors (D1-D5) belonging to the family of G-protein coupled transmembrane receptors (Girault and Greengard 2004). D1 and D2 receptors are located in the striatum where they are involved in the direct and indirect motor loop (Missale *et al* 1998).

Immediately after DA has carried out its action on the postsynaptic membrane it is removed from the synaptic cleft ensuring the effect of a new DA release at the next neurotransmission. Most of the extracellular DA is re-cycled by reuptake in the presynaptic cell by the dopamine transporter (DAT). Inside the cell, DA is either degraded by the monoamine oxidase (MAO) enzymes or vesicle-stored through the vesicular monoamine transporters (mainly type 2, VMAT2) (Rice and Cragg 2008). This thesis has its main focus on *in vivo* imaging of the DAT as a surrogate marker for the DA neurotransmission to assign the state of function of the nigro-striatal pathway.

The dopamine transporter

The DAT, along with the serotonin and norepinephrine transporter (SERT and NET), are plasma membrane spanning proteins belonging to the SLC6 gene family transporters fig. 4, (Gether *et al* 2006).

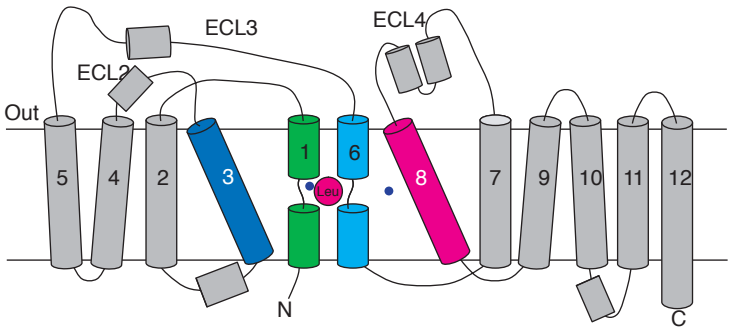

Figure 4. High-resolution structure of Na^+ - Cl^- -coupled neurotransmitter transporter homolog (SLC6 family). (Source Gether *et al* 2006).

The DAT constitutes of 620 amino acids residues (Uhl 2003) that actively clears extracellular dopamine, using the energy of cellular ionic electrochemical gradients (Gether *et al* 2006). DA uptake is dependent on the co-transport of Na^+ and Cl^-, and is driven by the ion concentration gradient facilitated by the Na^+/K^+ ATPase (Uhl 2003). The DAT is a target of several clinically used drugs such as methylphenidate, d-amphetamine, and modafinil. In addition, the reinforcing and euphoric effects of the powerfully addictive stimulants cocaine and d-

methamphetamine are primarily mediated by blocking the DAT leading to elevated extracellular DA concentration (Mortensen and Amara 2003; Piccini 2003).

DAT is expressed exclusively in DA neurons (Ciliax *et al* 1995) and thus constitutes a specific marker of these neurons. Sub-localization is predominantly in axons and therefore high concentrations are observed in regions receiving DA afferents (striatum). However, DAT is not located in the synaptic zone but extrasynaptic, along the axons (Hersch *et al* 1997). Recently the idea of the DA synapse has been challenged and it has been proposed that DAT has its main role in the lifetime of extrasynaptic DA concentration more than a transporter for synaptic DA spillover, suggesting that DAT functions to regulate DA concentrations within a wide area rather than within the synaptic cleft fig. 5 (Piccini 2003; Rice and Cragg 2008).

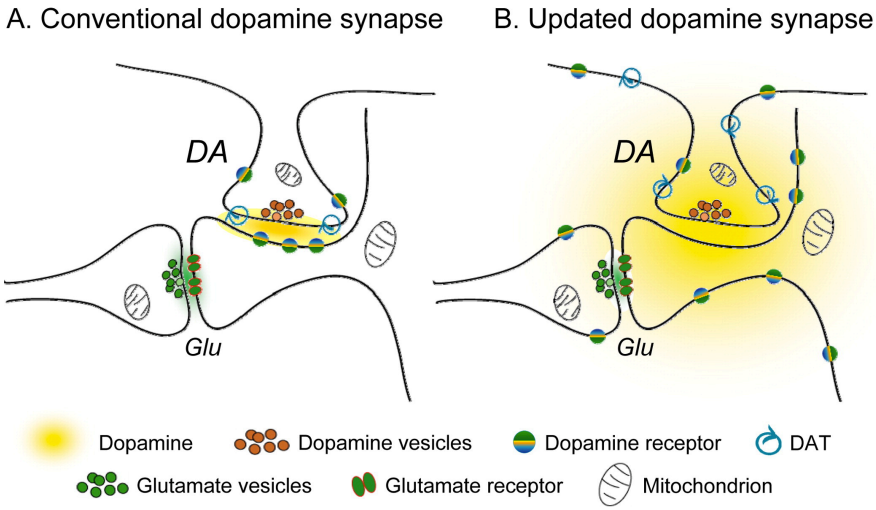

Fig. 5. Illustration of the conventional (A) and the updated (B) DA synapse (Source (Rice and Cragg 2008)).

The cell surface concentration of the DAT is dynamic and regulated primarily by membrane endocytosis (Eriksen *et al* 2009) rather than *de novo* synthesis, which is relatively slow (Kimmel *et al* 2000). The rate of DAT cell surface up-/downregulation can be very rapid (seconds to minutes) and slow (days to weeks) which can be observed by the paradox effect on DAT expression after acute and long-term exposure to cocaine (Daws *et al* 2002; Letchworth *et al* 2001). In addition to drug induced regulation of the DAT, there are several proteins

associated with regulation of the DAT, amongst those also some that play key roles in e.g. Parkinson's disease (for review (Eriksen *et al* 2010)).

Parkinson's disease

PD was first described by James Parkinson (Parkinson 1817) and is characterised by 4 core symptoms: rigidity, bradykinesia, tremor and postural instability. PD is the second most common neurodegenerative disorder after Alzheimer's disease with a 2005 prevalence of 1 % of people above 60 years (de Lau and Breteler 2006). Median age of onset of PD is 60 and average duration from diagnosis until death is 15 years (Katzenschlager *et al* 2008). However, late stages of PD involves severe disabilities with low quality of life and huge economic consequences for the society (Chen 2010).

PD is considered a sporadic disease by which aging is the major risk factor, similar to other neurodegenerative disorders. Surprisingly, considering the substantial focus on the topic, very few environmental factors causing PD have been identified (Dick *et al* 2007). In recent years there has been focus on smoking and caffeine both known to cause release of dopamine in different nuclei in the basal ganglia (Lichtensteiger *et al* 1982; Solinas *et al* 2002). However, currently the proposed protective effect of these stimulants is somewhat controversial (Evans *et al* 2006). Genetic studies have shown involvement of genes in which mutations can lead to L-dopa responsive parkinsonism and in 10-15 % of patients with PD there is a positive family history compatible with a Mendelian inheritance (Gasser 2007).

The pathological hallmark of PD is the regional loss of DA cells in the SNpc that correlates to duration of disease (Damier *et al* 1999). The loss of DA neurons in PD is more precisely an increased acceleration in striatal neurodegeneration estimated to ~ 46 % per decade compared to the normal age-related loss of 6 % (Fearnley and Lees 1991; Pirker *et al* 2002; van Dyck *et al* 2002).

Involvement of the 5-HT system in PD is more unresolved. A post mortem brain study showed a marked decrease in many different markers of the 5-HT system, only the SERT binding showed a wide overlap with the normal controls (Kish *et al* 2008) and this preservation in the early PD patients has recently been confirmed in a PET study (Strecker *et al* 2010). Data have shown that there could be a "reactive" hyper-innervation of 5-HT neurons accompanying the DA neurodegeneration (Maeda *et al* 2003) and that this innervation plays an important role in L-DOPA induced dyskinesias experienced by some of the patients when treated (Eskow *et al* 2009). Other midbrain areas may also be involved in PD although these mostly do not correlate to disease duration and hence their relation to the neurodegeneration in PD are disputed (Damier *et al* 1999).

Diagnosis of PD

There are many clinical differential diagnoses to PD and especially in the beginning when symptoms are weak and history is short it can be difficult to diagnose the disease. In one study the concordance between an initial clinical diagnosis and a final diagnose settled by autopsy (>10 years later) showed a sensitivity of 75%, and a specificity of 42% (Walker *et al* 2007). However, as a consequence of the natural clinical progression of PD and other related diseases with striatal neurodegeneration, one can increase the clinical predictive values by following the patients since their symptoms will definitely persist and often worsen over time (Litvan *et al* 1998). Clinicopathological studies suggest that when established PD is diagnosed according to current U.K. Brain Bank criteria, which is only possible when the PD patients have had symptoms for many years, there is a more than 80% concordance between expert clinical impression and the presence of nigral Lewy bodies (Hughes *et al* 1992).

Treatment of PD

Even though rasagiline vs. placebo in a large double-blind delayed-start trial seemed to slow the clinical progression of PD (Olanow *et al* 2009), the cure for PD remains unfound and symptomatic treatment is the only opportunity.

Biomarkers in PD

For PD and other related striatal neurodegenerative diseases the need for biomarkers in support of a clinical diagnosis or to assess progression of the disease in, e.g., intervention studies has long been a subject of intense investigation. Explored biomarkers in the cerebrospinal fluid include α-synuclein, tau protein and amyloid beta measurements but as of today most published reports have identify cerebrospinal fluid biochemistry as a useless diagnostic tool (Eller and Williams 2009).

Despite the cell loss in SNpc, conventional MRI shows normal SNpc structure in patients with PD and is therefore not diagnostically helpful (Stern *et al* 1989). Newer methods such as Inversion recovery sequences (Minati *et al* 2007) and T2-weighted sequences (Michaeli *et al* 2007) are promising techniques, but even these MR images show a considerable overlap between PD and healthy controls. Newer 3 Tesla volumetric T1-weighted MRI studies have shown slight atrophy of the putamen compared to normal age matched controls, but failed to detect a reduction in SNpc volume in patients with PD, possibly because of difficulties in accurately defining the border of the SNpc (Geng *et al* 2006). So far the most promising results have been achieved by diffusion tensor imaging, where a recent study was able to differentiate 14 healthy subjects from 14 PD patients, because all the patients with PD showed a reduced Nigral fractional anisotropy (Vaillancourt *et al* 2009). These results should be replicated and evaluated in larger populations of PD patients.

Methods

SPECT imaging

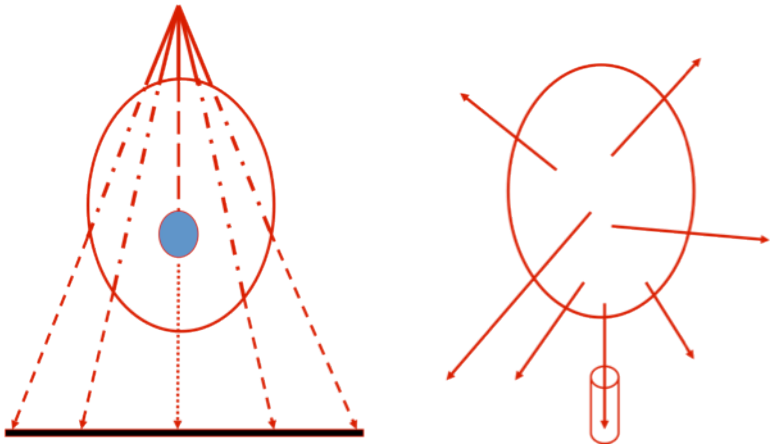

Transmission Emission

Figure 6. Illustration of the difference between a normal x-ray (to the left) that uses an external source that emits gamma ray's (transmission) and SPECT/PET where injection of radiotracer converts the subject into the radioactive source emitting gamma ray's (emission).

Single Photon Emission Computer Tomography (SPECT) began early after the introduction of computer science in the 1960s (Kuhl and Edwards 1963). Some of the pioneer work in SPECT brain imaging actually took place in Copenhagen (Lassen *et al* 1981). The method is a non-invasive technique that allows scientists to study various physiological and pathophysiological human brain functions *in vivo*. The basic technique requires injection of a molecule labelled with a radioactive gamma-emitting radioisotope (radionuclide) into the bloodstream of the patient. SPECT imaging is based on the injection of tracer amounts of the labelled molecule (nano- to picomoles, ie, much lower than the mili- to micromolar levels that elicit a pharmacologic response). The radioactive decay results in emission of photons (fig. 6) and these gamma ray's carry information of the location of the decay e.g. in the brain and thus the biodistribution of the radiotracer. Usually the half-life of the isotopes is much higher in SPECT than in Photon Emission Tomografy (PET) and thereby allows for transportation of the

radioligand outside production facilities, lowering the costs and making the clinical application easier. As a downside the emission of only one gamma ray in SPECT, opposite the consequently two gamma ray's in PET, compromises the precision of position where the radioactive decay took place and results in much lower spatial resolution in SPECT compared to PET (≈10mm vs. ≈5mm).

The main isotopes used in SPECT are ^{123}Xe, ^{131}I, ^{123}I and Tc99m. Since many molecules contain iodine one can substitute the naturally occurring ^{127}I with its radioactive counterpart isotope without changing the chemical properties of the labelled molecule.

The ideal target protein for radioligands should be a protein that exactly reflects a biological process that changes with the progression of disease, e.g., be proportional to the cell loss of DA neurons in PD. Further, the binding of the radioligand to the target protein should have multiple qualities: a high reproducibility of quantification outcomes, posses a high target to background ratio with a suitable reference region devoid of that protein, be selective to the target, be reversible allowing for displacement by unlabelled tracer, have no radiolabelled metabolites capable of crossing the BBB and finally, of course be safe and tolerable for patients and healthy volunteers.

Imaging the nigro-striatal pathway

With the introduction of PET and SPECT new insight into the neurobiology of the nigro-striatal pathway followed. The potential of PET and SPECT brain imaging provided the clinicians with new diagnostic tools (Catafau and Tolosa 2004; Vlaar *et al* 2008) and the pharmaceutical companies and the researchers with a biomarker for disease progression and evaluation of treatment efficacy (Fahn *et al* 2004; Group 2002).

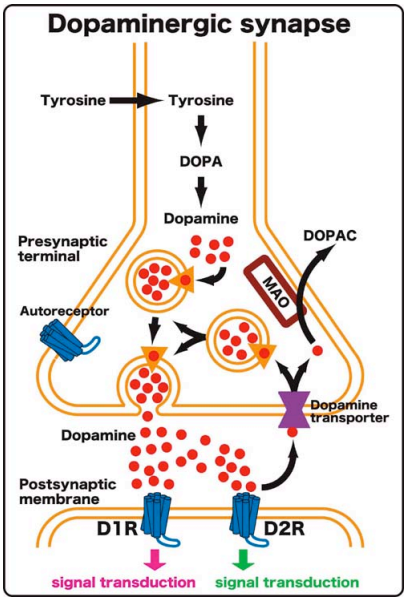

Figure 7. The conventional DA synapse. The figure illustrates various proteins that could be encountered as targets for radiotracer binding. Presynaptic: DAT, VMAT (yellow triangles) or DOPA. Postsynaptic: D1 or D2. (Source: the internet, unknown illustrator.)

The first target to be imaged in humans (by PET) was the postsynaptic receptors (Wagner *et al* 1983). Of course this was especially interesting when looking at diseases with a postsynaptic pathology, e.g., as in Huntington's Disease (Pinborg *et al* 2001). It was also with postsynaptic radioligands that scientists were able to show endogenous release of dopamine into the synaptic cleft after stimulation (Laruelle *et al* 1996), thereby for the first time *in vivo* supporting the hypothesis of hyperactivity of the DA neurotransmission in schizophrenia. Since then these receptors have been the focus of intense investigation and for example used in evaluation of antipsychotic drugs (Catafau *et al* 2006; Corripio *et al* 2005).

Imaging disease progression in PD is different, since the pathology is primarily presynaptic. The function of the presynaptic DA neurons can be assessed with PET/SPECT in 3 ways (fig. 7) (Brooks *et al* 2003): 1) L-DOPA uptake and catalyzation to dopamine ([^{18}F]-fluorodopa), 2) VMAT ([^{11}C]- or [^{18}F]-dihydrotetrabenazine or 3) the DAT.

[^{18}F]-fluorodopa is a PET ligand that has been widely used in PD. It was first synthesized more than 30 years ago (Garnett *et al* 1978). The accumulation of [^{18}F] activity in striatum during [^{18}F]-fluorodopa PET can be attributed to uptake of [^{18}F]-fluorodopa in the presynaptic membrane, followed by its conversion to [^{18}F]-fluorodopamine by AAAD, and uptake and trapping of [^{18}F]-fluorodopamine into synaptic vesicles. Although reproducibility of [^{18}F]-

fluorodopa is high and within the range of DAT ligands (Vingerhoets *et al* 1996) the problem with [^{18}F]-flourodopa is its failure to accurately reflect DA synthesis: It is also taken up, metabolized and stored in other monoamine neurons in the striatum (Brown *et al* 1999)) and in humans it gives rise to a radiolabeled metabolite (Luxen *et al* 1992). Using [^{18}F]-fluorodopa as a biomarker is not optimal since studies have shown that there is a compensatory upregulation of the synthesis and release of DA in PD animal models in early phases of PD (Zigmond *et al* 1990), this initial upregulation is to be seen in contrast to the downregulation of the DAT (Fernandez *et al* 2001; Lee *et al* 2000; Tedroff *et al* 1999). This upregulation makes the timing of the PET scan in early stages of PD crucial to the interpretation of the scan results and makes interpretation of scientific data difficult.

The lack of selectivity seems also to be the problem for radioligands that bind to the VMAT. The VMATs are ATP-dependent transporters, which are nonselective and effective for both dopamine, norepinephrine and serotonin. As a consequence, imaging of VMAT in the brain provides a measurement reflecting the total number of all three neurons (Frey *et al* 2001). Studies have shown that there seems to be no initial downregulation of VMAT compared to that of the DAT (Kilbourn *et al* 2000; Lee *et al* 2000), making it less sensitive in diagnosing de novo PD patients. On the other hand VMAT is influenced to a lesser extend by L-DOPA, deprenyl, cocaine, and amphetamine (Wilson and Kish 1996) which could make it more useful as a biomarker for treatment efficacy.

Notably, [^{18}F]-fluorodopa and [^{18}F]-dihydrotetrabenazine have the same general pros and cons being PET ligands as compared to the SPECT ligands (previously addressed).

Radioligands for DAT

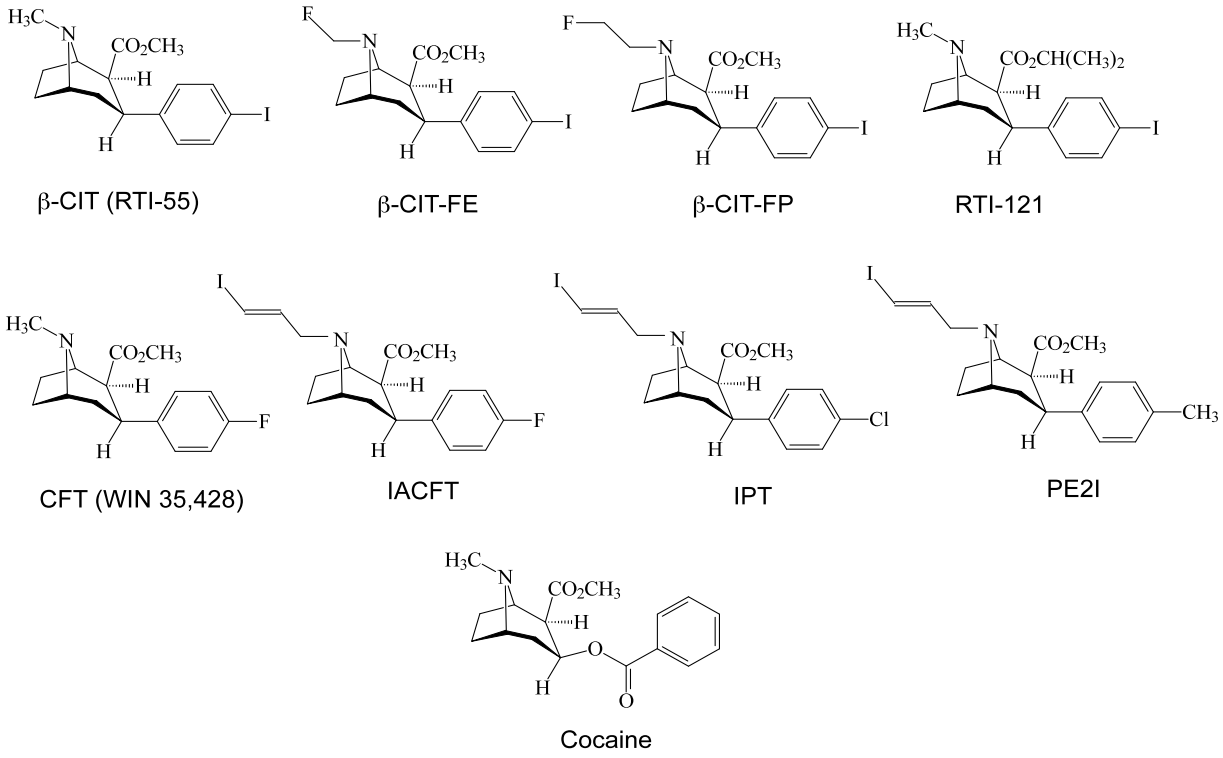

Figure 8. Radiotracers for PET/SPECT imaging.

[^{11}C]cocaine was the first radioligand to be used for imaging the cerebral dopamine transporter *in vivo* (Fowler *et al* 1989). A number of other radioligands have subsequently been developed and tested as PET- or SPECT ligands, however most of these ligands have been cocaine derivates (figure 8). With the introduction of 2-beta-carbomethoxy-3 beta-(4-iodophenyl)tropane ([^{123}I]β-CIT) (Neumeyer *et al* 1991), brain imaging of DAT became a clinically useful method for supplementary diagnosis of movement disorders. As a ligand [^{123}I]β-CIT has several serious downsides as it has equal affinity for DAT as for SERT and because of its slow kinetics it requires imaging to be conducted 24 hours after bolus injection. A few years later 2-beta-carbomethoxy-3 beta-(4-iodophenyl)-N-(3-fluoropropyl)nortropane (FP-CIT) was synthesized (Neumeyer *et al* 1994) and its cerebral distribution and dosimetry in healthy volunteers was subsequently reported in 1998 (Booij *et al* 1998a). [^{123}I]FP-CIT has an improved selectivity for DAT vs. SERT as compared to [^{123}I]β-CIT, se table 1.

Table 1. From (Ziebell *et al* 2010a)

SERT and DAT Binding Affinity of Inhibitor (K_i), as Measured in Rat Brain Homogenates

Ligand	K_i DAT (nM), ^{3}H-GBR-12935	K_i SERT (nM), ^{3}H-paroxetine	SERT-to-DAT ratio
^{123}I-β-CIT*	27	3	0.1
^{123}I-FP-CIT†	3.5	9.7	2.8
^{123}I-PE2I*	17	500	29.4

*According to study of Abi-Dargham et al. (5).
†According to study of Emond et al. (8).

Furthermore, due to its lower DAT affinity [^{123}I]FP-CIT has much faster kinetic properties with a striatal peak time of 148 minutes after IV injection. As a result it has a reduced timespan of 3 hours from tracer injection to SPECT scan, making it more feasible for scanning of out hospital patients (Abi-Dargham *et al* 1996). With a bolus injection and without measurements of the arterial input function, the outcome parameter (the binding ratio between a target and a reference region) does, however, become sensitive to intersubject variation in the plasma clearance rate of the radioligand (Carson *et al* 1993), this will be discussed later. [^{123}I]FP-CIT was licensed as DaTSCAN in Europe in 2000 and since then, it has become a frequently used SPECT radioligand, particularly as an ancillary tool to diagnose patients with movement disorders. In 2006 more than 500 European SPECT-centres were using [^{123}I]FP-CIT for clinical purposes (Booij and Kemp 2008). The radioligand has also been widely employed in both preclinical and clinical studies; a Pubmed search October 2010 shows that it is currently mentioned in over 300 scientific papers.

In 1997 the ligand 123-I-labelled N-(3-iodoprop-2E-enyl)-2-beta-carbomethoxy-3beta-(4-methylphenyl), named PE2I, was synthesized (Emond *et al* 1997) and a dosimetry study in humans was published in 1998 (Kuikka *et al* 1998).

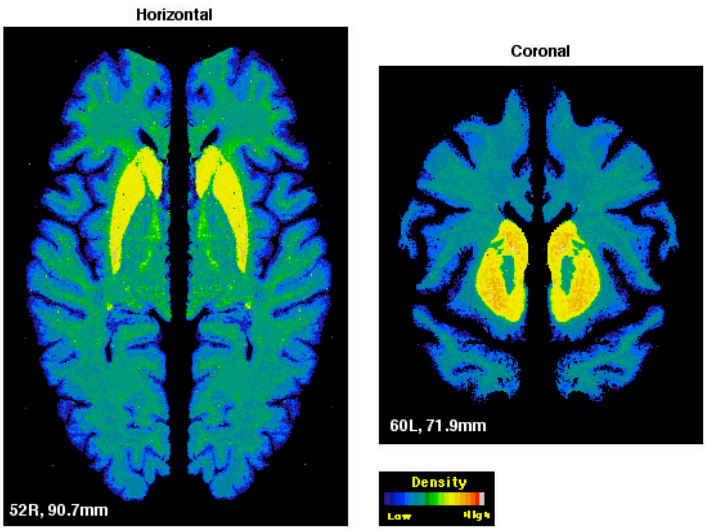

Figure 9. Distribution of DAT in the human brain using whole hemisphere autoradiography and [^{125}I]PE2I. The light green seen in the brain slice reveals a slight white matter binding (Source (Hall *et al* 1999)).

[^{123}I]PE2I has an approximately 30-fold higher *in vitro* affinity for DAT than for SERT and thus *in vitro* results have shown that binding of [^{125}I]PE2I is not affected by citalopram nor maprotiline (Hall *et al* 1999). The lipophilicity is high compared to that of the β-CIT (log p = 4.68, vs. log p = 4.36), and as a consequence it accumulates slightly in the white matter, fig 9. (Hall *et al* 1999). Because of its lower affinity to DAT, [^{123}I]PE2I has faster kinetics than [^{123}I]FP-CIT with a striatal peak time between 30-60 min (Pinborg *et al* 2002).
PE2I has also proven suitable as a [^{11}C] labelled PET probe (Delorenzo *et al* 2009) even also as [^{18}F]-labelled (Schou *et al* 2009), however in both circumstances the administration in humans have resulted in radiolabelled metabolites, warranting further detailed evaluations. In [^{123}I]-labelled form neither PE2I, nor FP-CIT gave rise to radiolabelled BBB permeable metabolites (Seibyl *et al* 1998; Videbaek *et al* 1999). In spite of its favourable properties, [^{123}I]PE2I is currently not licensed as a SPECT radioligand for clinical use.

Along with [^{123}I]PE2I a novel ^{99m}Tc tracer was synthesised (99m)Tc-[2[[2-[[[3-(4-chlorophenyl)-8-methyl-8-azabicyclo[3,2,1]-oct-2-yl]-methyl](2-mercaptoethyl) amino]ethyl]amino]ethane-thiolato(3-)-N2,N2',S2,S2]oxo-[1R-(exo-exo) namely ^{99m}Tc-TRODAT-1 (Kung et al 1997). This ^{99m}Tc-based tracer has several advantages; it is less

expensive than the cyclotron-produced ^{123}I tracers and can be readily produced by a commercially available ^{99}Mo/ ^{99m}Tc generator. But even though ^{99m}Tc-TRODAT-1 has a high DAT:SERT selectivity (26:1) it has the disadvantage of having a very low target to background that compromises the sensitivity of the scan (Hwang *et al* 2004).

Quantification of target proteins by SPECT/PET

As previously mentioned it is important when measuring a biological system *in vivo*, not to interfere with the function of the system. Therefore, the labeled + unlabelled compound should not occupy more than 5-10% of the receptors, preferentially less. In most SPECT studies occupancy is less than 1 %. *In vitro* quantification of radiotracers bound to target proteins is based on the equilibrium binding reaction:

$$R + F \leftrightarrow B$$

where R is the receptor (or transporter), F is free ligand and B a complex of both.
In 1984 the binding potential was introduced for PET imaging (Mintun *et al* 1984) and defined as:

$$BP = \frac{B_{MAX}}{K_D}$$

where B_{max} equals the receptor density and K_D the radioligand equilibrium dissociation constant or the affinity of the radioligand. In the simplest form BP is a ratio of specifically bound tracer in the brain to the free concentration in the brain. This can be derived from the Michaelis–Menten equation (which is used to describe *in vitro* receptor binding):

$$B = \frac{B_{MAX} * F}{K_D + F}$$

$$\Rightarrow \frac{B}{F} = \frac{B_{MAX}}{K_D} = BP$$, because in radiotracer studies $F<<<K_D$.

Since measurement of the free concentrations in the brain would require invasive procedures and thus rejecting PET and SPECT as non-invasive methods, several simplified models for measuring the BP were established. The first assumption in these models is that the free radiotracer in blood diffuses unstirred across the BBB. By this assumption one can measure the BP in a specific region of interest (ROI) in the brain as the ratio of specifically bound radioligand in the ROI to the concentration in either plasma (BP_P) defined as:

$$BP_P = \frac{specifically\ bound\ radioligand}{total\ parent\ radioligand\ in\ plasma}$$

or to that of a reference region representing the concentration of non-displaceable radioligand in the brain (BP_{ND}):

$$BP_{ND} = \frac{specifically\ bound\ radioligand}{non-displaceable\ radioligand\ in\ brain\ tissue}$$

Non-displaceable radioligand equals the sum of the free and non-specific bound radioligand concentration. The specific bound radioligand is the total radioligand bound in the ROI minus the non-displaceable radioligand. Non-displaceable binding is usually represented by a region, which is assumed to be devoid of the specific receptor i.e. a reference region. By delineation of a ROI in a SPECT/PET image the mean counts of gamma-ray's can be measured as a linear function of radioligand concentration. Thus calculating the BP_{ND} without even measuring radioligand concentration in the blood:

$$BP_{ND} = \frac{C_{ROI} - C_{REFERECE}}{C_{REFERENCE}} = \frac{C_{ROI}}{C_{REFERENCE}} - 1$$

C_{ROI} = concentration in the ROI, $C_{REFERENCE}$ = concentration in reference region.

Yet, very importantly, the BP_{ND} is not a representation of the true *BP*, since several precautions are to be taken when calculating the BP_{ND}:

First of all, only a subset of receptors/transporters is available *in vivo*, hence the BP_{ND} does not represent the total receptor concentration but a reflection of the maximum amount available for binding (B_{avail}). Secondly, as the target proteins are not saturated with tracer, the BP_{ND} is directly correlated to the free fraction of the non-displaceable compartment (f_{ND}) i.e. the fraction of radioligand that is freely dissolved in tissue water in the brain, hence:

$$BP_{ND} = f_{ND} * B_{AVAILABLE} / K_D$$

Last, but not least, calculating the BP_{ND} by a concentration ratio presupposes that the concentration in plasma and brain tissue is at steady state conditions (*in vivo* terms of *in vitro* equilibrium (Innis *et al* 2007)). In clinical centers this is sometimes ignored to an extent that may compromise quantification accuracy. In these cases BP is often measured when tracers appear in a steady state because of a very slow washout from the brain. However, this is a pseudo steady state condition, also termed transient equilibrium or pseudo-equlibrium. In theory, an individual binding ratio calculated at transient equilibrium could overestimate true steady state BP_{ND} if the individual terminal plasma clearance rate is high; a problem originally addressed by *Carson* (Carson *et al* 1993).

There are several ways of calculating a true BP_{ND} and one of them is by obtaining true steady state conditions. One way this can be achieved is by a constant infusion of the radioligand, however this would be a very time consuming affair because of the continuously biologic half-life (metabolism and decay) of the radioligand. The steady state condition can therefore be hasten by the use of a bolus plus constant infusion design (Carson *et al* 1993).). The idea is to hasten a true steady state of the tracer in plasma and in the brain by an initial injection of a

tracer bolus prior to the tracer infusion. The ratio between the bolus and the constant infusion can be calculated from bolus injection data. The result of the calculated size of bolus relative to that of the infusion is often described as a ratio of the bolus size to the infusion velocity defined as the bolus-to-infusion ratio B/I ratio (h) (Carson *et al* 1993; Pinborg *et al* 2000; Pinborg *et al* 2003). The bolus infusion idea is illustrated in figure 10.

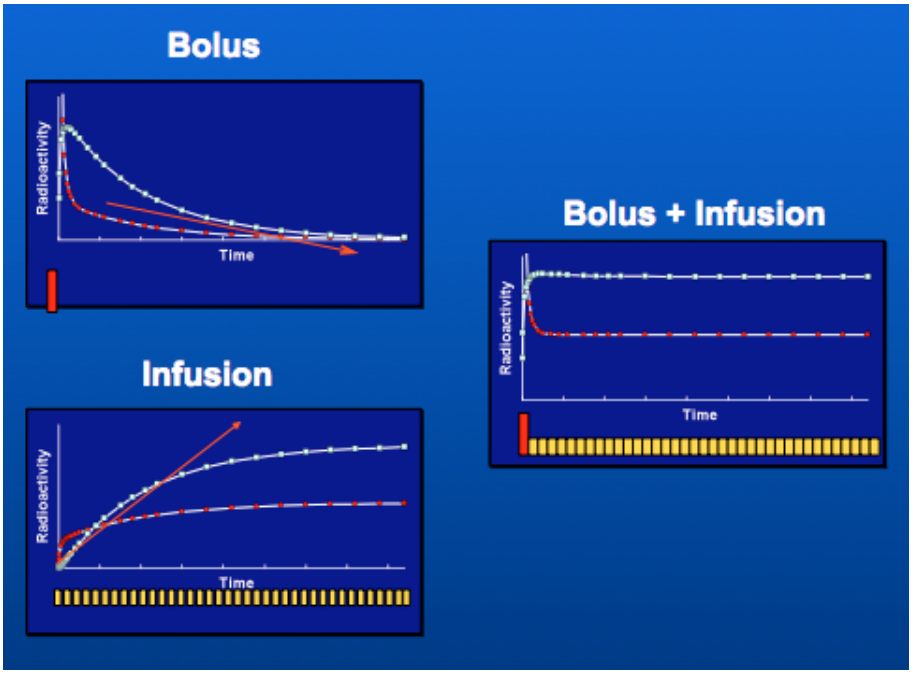

Figure 10. Light blue dots indicate time activity curves (TAC) for a brain region and red dots the plasma curve. Ideally, the infusion velocity should equal the terminal plasma clearance rate from a bolus injection, both indicated by the red arrows (Illustration kindly provided by Pinborg LH).

In addition to precise calculations of the BP_{ND} the steady state condition ease interpretation of pharmacological challenge to the target protein in the ROI, by e.g. "cold" ligand. That is, the TAC for the ROI will approach that of the reference region if the drug has affinity and thus compete with the radioligand for the target protein.

Calculating the true BP_{ND} can also be achieved using either kinetic analysis such as the Logan analysis (Logan *et al* 1990) or graphical analysis such as the Simplified Tissue Reference

Model (SRTM) (Lammertsma and Hume 1996). These analyses are attractive methods since they rely on data from bolus injection alone. The drawbacks are that the methods are more vulnerable to noise in the data and often require longer scanning time, which hinders their clinical use (Pinborg *et al* 2005).

Finally, visual semi-quantification can also be achieved. Especially in the clinical setting this is a very popular time saving method and it is used in many centers of nuclear medicine. A visual quantification, by an experienced reader, can very often be sufficient to tell if the image is normal or abnormal. However, visual quantification cannot give any exact estimates of the receptor concentration in a ROI and is therefore useless in research perspectives. Despite of this fact a visual quantification is from time to time observed in a scientific paper (McKeith *et al* 2007).

Aims

This PhD-thesis covers the investigation of the SPECT DAT radioligand [^{123}I]PE2I which includes the following steps:

1) Establishment of a bolus/infusion (B/I) protocol for [^{123}I]PE2I that enable steady state conditions in plasma and brain.

2) Test of reproducibility of the B/I method in healthy subjects and in patients with decreased striatal binding of [^{123}I]PE2I.

3) Evaluation of different ROI delineation methods for [^{123}I]PE2I quantification.

4) Comparison of binding potential and contribution of serotonin transporter binding in [^{123}I]PE2I images as compared to the commonly used [^{123}I]FP-CIT.

Results and discussion

The bolus infusion method for [^{123}I]PE2I

The first aim of this study was to establish a bolus infusion method for [^{123}I]PE2I thereby enabling easy and reliable quantification of [^{123}I]PE2I binding to DAT in the human brain. The group had been working with [^{123}I]PE2I for a few years before I started my research. The use of [^{123}I]PE2I began in 1998 as part of an EU-project. With MD, DMSc Lars H. Pinborg as head of the trials the conclusion was that the non-invasive Logan analysis, a graphical analysis method provided the most accurate method for quantification (Pinborg *et al* 2002). This method is very accurate and does not require arterial blood samples, but the recommended study time of 120 min could be a problem in an every day clinical practice since it would compromise scanning capacity to 3 per scanner per day. In addition 2 hours spend in a scanner is not feasible for many elderly persons and Logan analysis is compromised significantly if the patient is to abort the SPECT scan. Therefore we chose to see if we could set up a bolus infusion method initially described by Carson (Carson *et al* 1993), a method that the group previously had experience with (Pinborg *et al* 2000; Pinborg *et al* 2003). Five healthy volunteers were included (paper 1), and all of them were studied twice at 2 separate days. In addition, we tested the calculated B/I ratio in another independent group of 7 healthy volunteers, (paper 2).

Based on the first bolus studies we calculated the average bolus infusion ratio to be 2.5 h in the first 5 healthy volunteers (fig. 11). In order to reduce the time from bolus injection to steady state conditions we increased the ratio slightly, to 2.7 h.

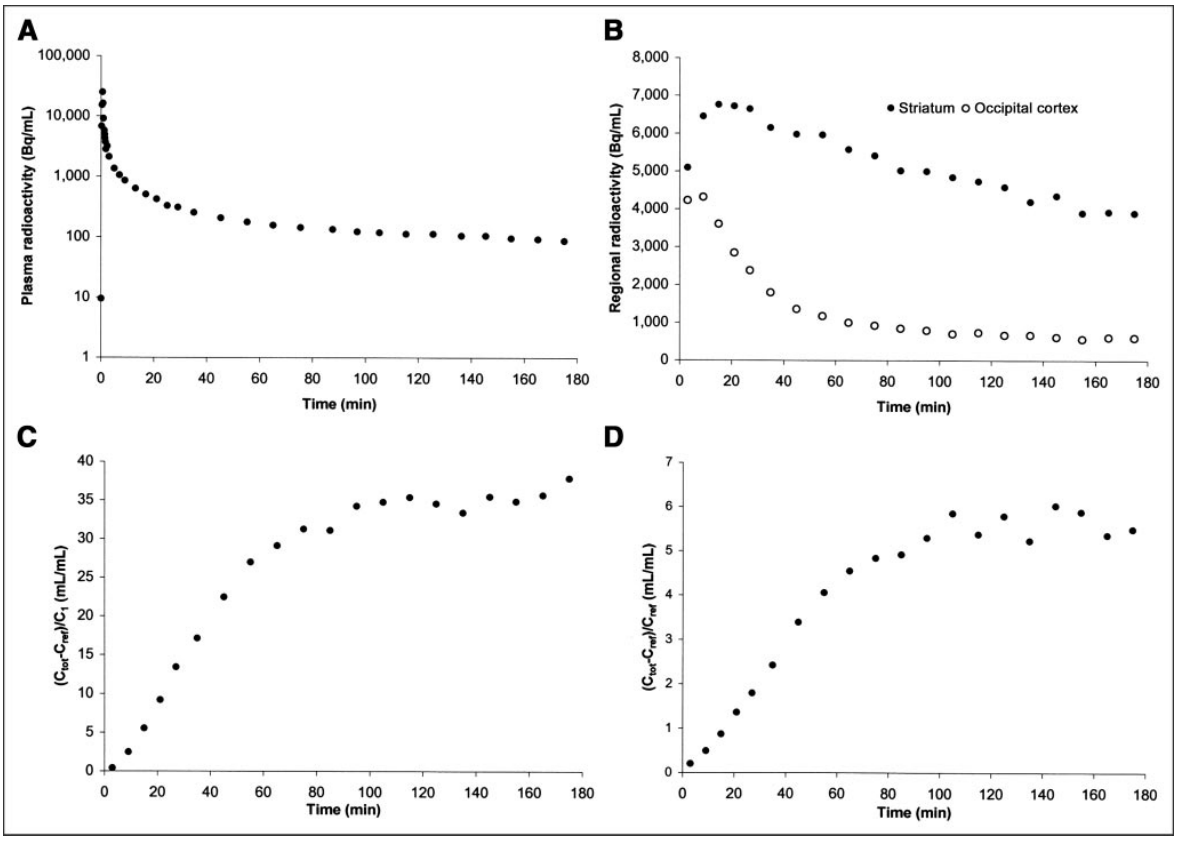

FIGURE 2. Average ^{123}I-PE2I bolus data: time course for metabolite-corrected plasma radioactivity (A), time course for striatum and occipital cortex radioactivity (B), time course for $(C_{tot} - C_{ref})/C_1$ (C), and time course for $(C_{tot} - C_{ref})/C_{ref}$ (D).

Figure 11. The results of the bolus injection studies from (Pinborg *et al* 2005). Figures 2C and 2D show the average ratio of striatum-specific binding to metabolite corrected plasma and the average ratio of striatum-specific binding to occipital cortex, respectively, as a function of time. Starting approximately 90 min after bolus injection, the curves became horizontal.

In the second scan of the 5 healthy volunteers, they received a bolus plus constant infusion and the calculated B/I ratio (2.7h) from the bolus alone study was applied. From table 2, one can appreciate the very stable BP_{ND} (at that time denoted BP_2) that we achieved from 120-240 min post injection.

Table 2. From (Pinborg *et al* 2005)

Stability of Outcome Measures, Free Parent Compound, and Individual Optimal Bolus-to-Infusion Ratio

	Bolus/infusion experiments			Bolus experiments	
Subject no.	BP_1 (%/h)	BP_2 (%/h)	Plasma (%/h)	B/I ratio (h)	Confidence interval (h)
1	−0.1	−4.0	4.2	3.7	2.4–8.5
2	6.8*	2.2	−7.2*	2.4	1.3–12.8
3	−3.1	−6.6	−2.8	3.1	2.8–3.6
4	2.8	2.1	−3.4	2.6	1.3–214.0
5	−6.6	−3.1	−4.2	1.8	1.2–4.0
Average ± SD	−0.0 ± 5.2	−1.9 ± 3.9	−1.6 ± 4.9	2.7 ± 0.7	

*Slope of regression line calculated from 120 to 240 min is significantly different from zero ($P < 0.05$). BP_1, BP_2, and plasma stability measures were calculated from bolus/infusion data. Individual bolus-to-infusion ratios and corresponding 95% confidence intervals were calculated from terminal clearance rate from plasma after bolus injection of ^{123}I-PE2I.

To get an estimate of the calculated BP_{ND} from the B/I experiments, we performed various kinetic and graphical analysis on the data from the initial bolus experiments in comparison, please see table 3. This showed that the B/I calculated BP_{ND}'s did not differ significantly from the SRTM (paired students *t* test, P>0.3). However, as can be seen from the table, the B/I and kinetic analysis did significantly underestimate that of the transient equilibrium analysis (P< 0.0002, paired Student t test).

Table 3. From (Pinborg *et al* 2005)

BP_2 Values Calculated Using 5 Different Methods of Quantification

	Bolus/infusion experiments	Bolus experiments			
Subject no.	(120–180 min)	Reference tissue (0–180 min)	Logan analysis (0–180 min)	Peak equilibrium (40–80 min)	Transient equilibrium (90–180 min)
1	4.6	4.6	4.6	4.8	6.0
2	4.6	4.1	3.7	3.8	5.5
3	4.4	4.3	4.2	4.5	5.5
4	4.0	4.2	4.2	4.7	6.0
5	3.9	3.6	3.5	3.5	5.2
Average ± SD	4.3 ± 0.3	4.1 ± 0.4	4.0 ± 0.4	4.3 ± 0.6	5.6 ± 0.4

BP_2 was calculated using Equation 2. Peak equilibrium and transient equilibrium were not calculated at tracer steady state.

There was a very high interindividual B/I ratio and one concern about the B/I method was that it could be very difficult to calculate the individual B/I ratio. We hence did a theoretical simulation in order to calculate the maximum alterations in BP_{ND} that we could expect from wide ranges of individual terminal plasma clearances. In the simulation we changed the B/I

ratio more than 2 fold and as a result only saw a 11% variation in the calculated BP_{ND} values (figure 12).

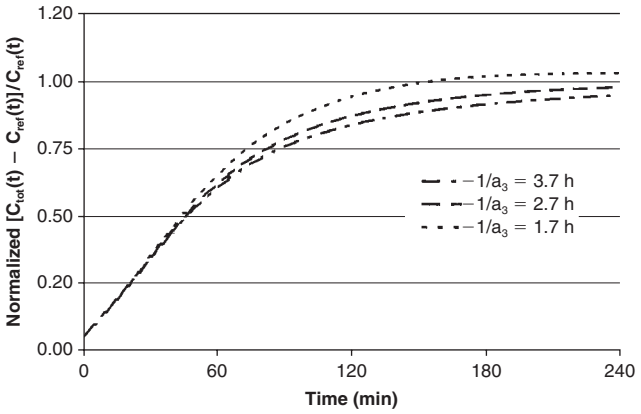

Figure 12. The average normalized BP_{ND} values are 0.99 (B/I = 1.7 h), 0.92 (B/I = 2.7 h), and 0.88 (B/I = 3.7 h). Thus, a 2.2-fold variation in terminal clearance rate from plasma translates into only a 11% variation in the calculated BP_{ND}.

So both in theory and in practice the calculated B/I ratio was quite reliable and stable and calculations of individual B/I ratios were not required. Despite of these convincing data we still wanted to test the stability in an independent sample of patients. In the next study (Ziebell *et al* 2007) we once more tested the stability of BP_{ND} within the time window of 120-180 minutes (figure 13).

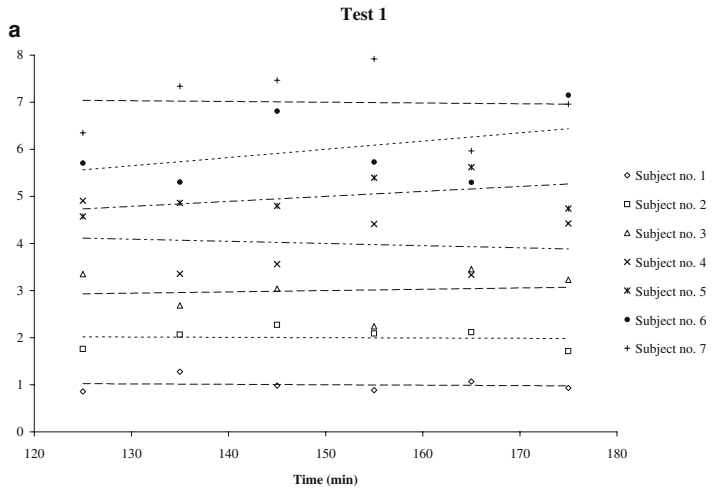

Figure 13. The stability of the BP_{ND} from the first scans of the 7 subjects (Ziebell *et al* 2007).

In table 4 the details outlines the exact values of the stability.

Table 4. From (Ziebell *et al* 2007)

	Study 1			Study 2		
Subject	Striatum	Occipital	BP_2	Striatum	Occipital	BP_2
1	−2.5	−2.0	−5.7	2.8	1.3	2.4
2	−8.4	−7.3	−2.1	1.4	27.1	−26.8
3	−6.2	−8.8	5.3	1.8	−23.4	33.3
4	−5.1	−0.1	−7.0	−6.6	2.5	−7.7
5	−10.0	−13.9	12.6	−9.7	−21.9	14.9
6	0.4	−1.6	−4.0	3.6	5.1	−1.2
7	−7.0	−4.9	−1.5	0.1	−17.7	23.4
Mean	−5.6	−5.5	−0.3	−0.9	−3.9	5.5
SD	3.5	4.9	7.0	5.1	18.3	20.2
ABS mean	5.7	5.5	5.6	3.7	14.2	15.7

SD standard deviation, *ABS* absolute
Stability of striatal and occipital volumes: slope of time-activity curve (120–180 min)×60 min divided by mean values from 120 to 180 min in percent.
Stability of BP_2: slope of time-activity curve (estimated by striatum/occipital −1) from 120 to 180 min×60 min divided by mean values from 120 to 180 min in percent.

Even though there was a significant difference in individual BP_{ND} stability between the first and second scan of the healthy volunteers in the reproducibility study ($p < 0.03$) the overall stability was very low (≈ 5.5%). The fact that the stability measures were lower in the high count striatal ROIs than in the low count occipital cortex ROI imply that the variability was primarily due to random noise. This can be appreciated visually from figure 13 where very little change in the endpoints (120 and 180 min) can cause a large impact on the stability measurements.

Reproducibility of [^{123}I]PE2I

Knowledge of the reproducibility of a method is important; not only to identify the most suitable method for quantification, but also to design studies appropriately in terms of sample size. Especially when performing costly experiments involving SPECT and PET scans an accurate power analysis is crucial to ensure that studies are not underpowered resulting in useless experiments and unnecessary exposure of radiation to healthy volunteers and/or patients. It was therefore natural to conduct reproducibility studies with radioligand [^{122}I]PE2I. Reproducibility studies of brain SPECT imaging outcomes of DAT binding with other radioligands had already been conducted. These were carried out in both healthy volunteers (Booij *et al* 1998b; Seibyl *et al* 1996) and in patients with affected striatal DAT availability (Booij *et al* 1998b; Hwang *et al* 2004; Seibyl *et al* 1997; Tsuchida *et al* 2004) see section table. Traditionally in DAT SPECT imaging the reproducibility is calculated as the absolute value of the difference between to measurements of BP: x_1 and x_2 divided by the mean given as a percentage (Seibyl *et al* 1996).

$$Reproducibility = \frac{|x_1 - x_2|}{(x_1 + x_2)/2} * 100\%$$

This equation can be applied to the reproducibility of the total method or to different steps in the method to explore the contribution to the total reproducibility that is constituted by that particular step in the procedure. As the formula reads, one can see that the reproducibility of a given method is very much dependent of the absolute value of the observations if the difference between observation 1 and 2 remains the same. This is one of the reasons why it is important to conduct calculations of reproducibility in both healthy volunteers and in patients with a low DAT binding, since the latter according to the formula alone, should have a higher reproducibility.

In the second paper we calculated the reproducibility in 7 healthy volunteers (Ziebell *et al* 2007) whereas we chose 8 patients with decreased striatal DAT binding in the third paper. (Ziebell *et al* 2010b).

In both studies the mean reproducibility outcomes were inversely correlated to the volume of the ROI: Ziebell et al 2007: Striatum 5.4 %, putamen 5.9 % and caudate nucleus 8.0 %; Ziebell et al 2010: Striatum11.9 %, putamen 14.8 % and caudate nucleus 19.4 % (table 5 & 6). This was probably related to delineation accuracy because of the low spatial resolution in SPECT.

Table 5. From (Ziebell *et al* 2007)

Subject	1	2	3	4	5	6	7	Mean	SD	Reliability
Striatum BP_2										
Study 1	2.3	3.4	4.2	3.5	3.3	4.3	3.6	3.6	0.7	
Study 2	2.3	3.3	4.5	3.5	3.2	4.5	4.0	3.7	0.8	
Variability (%)	0.5	3.7	−7.0	−1.9	2.6	−3.3	−9.7	−2.2	5.4	0.96
ABS variability (%)	0.5	3.7	7.0	1.9	2.6	3.3	9.7	4.1	3.2	
Caudate nucleus BP_2										
Study 1	2.6	3.8	4.3	3.4	3.7	4.5	3.8	3.8	0.7	
Study 2	2.5	3.6	4.6	3.7	3.3	4.9	4.1	3.9	0.8	
Variability (%)	1.4	5.1	−6.4	−9.2	12.6	−6.5	−6.1	−1.3	8.0	0.95
ABS variability (%)	1.4	5.1	6.4	9.2	12.6	6.5	6.1	6.8	3.5	
Putamen BP_2										
Study 1	2.5	3.5	4.5	3.8	3.6	4.7	3.8	3.8	0.7	
Study 2	2.5	3.4	4.8	3.7	3.7	4.6	4.3	3.8	0.8	
Variability (%)	0.8	3.4	−7.1	4.2	−2.9	0.6	−11.9	−1.9	5.9	0.95
ABS variability (%)	0.8	3.4	7.1	4.2	2.9	0.6	11.9	4.4	4.0	
Striatum BP										

Table 6. From (Ziebell *et al* 2010b)

Summed Intrasubject Variability from 3 Different ROI Application Methods (n = 8)

Method	Caudate nucleus	Putamen	Striatum	ICC
MD (BP_{ND})	19.4% ± 14.3%	14.8% ± 6.0%	11.9% ± 10.0%	0.88
MRD (BP_{ND})	16.4% ± 11.9%	15.8% ± 11.7%	14.6% ± 15.3%*	0.90
SVI (SBR)			10.8% ± 10.2%	0.90

*Calculated striatum = volume-weighted (caudate nucleus + putamen).
ICC = intraclass correlation coefficient.

The final result was comparable to other available SPECT radioligands with an average reproducibility of 4.1 % and 11.9 %, please see table 7. The section table sums up the test-retest results among SPECT DAT radioligands used in clinical practice.

Table 7. (Ziebell *et al* 2010b)

Intrasubject Variability of Various DAT Radioligands for SPECT

Study	Ligand	Total patients (*n*)	Delineation	Intrasubject variability*		Reliability ICC
				Healthy volunteers	Patients	
Ziebell et al. (*17*)	PE2I	7	MD HC	4.1 ± 3.2		0.96
Seibyl et al. (*20*)	β-CIT	7	Template WS	12.8 ± 8.9†		0.82
Booij et al. (*18*)	FP-CIT	6	Template HC	7.3 ± 3.2		0.92†
Tsuchida et al. (*21*)	FP-CIT	10	Template HC	11.1 ± 10.4		0.59
Pirker et al. (*31*)	β-CIT	9	MD HC	8.2 ± 7.2		0.70
Ziebell et al., current study	PE2I	8	MD HC		11.9 ± 10.0	0.88
Seibyl et al. (*20*)	β-CIT	7	Template WS		16.8 ± 13.3†	0.82
Booij et al. (*18*)	FP-CIT	6	Template HC		7.9 ± 6.9	0.72†
Tsuchida et al. (*21*)	FP-CIT	6	Template HC		7.8 ± 8.9	0.95
Hwang et al. (*19*)	Trodat	20	MD HC		10.2 ± 6.2	0.95

*Mean outcome for either BP_{ND} or SBR (±SD).
†Data extracted from publication.
ICC = intraclass correlation coefficient; HC = high-count slides; WS = whole striatum.

The first column shows the individual studies of DAT SPECT reproducibility, some of which originate from the late nineties. However, in spite of the development within the SPECT scanner hardware and the computer power, the procedures of reconstruction and the overall resolution have not changed within the last 14 years. The number of participants has traditionally been low; this is probably because of the large costs of a single SPECT scan compared to e.g. a blood sample. In the fourth column we listed the method used for delineation of ROI. Overall there does not seem to be any significant difference in reproducibility outcome using either manual or template based delineation. I will discuss the subject of delineation later on. The data of main interest is composed of column five, six and seven and show the reproducibility and reliability results. There is not much difference between any of the ligands. However, a difference from 4 to 13 % (seen in e.g. the healthy group) would require more subjects to be included and this difference is not negligible as we have previously shown in another test-retest study (Haugbol *et al* 2007). Overall the results showed what we expected, that reproducibility is higher in patients than in healthy volunteers. Important factors to take into account when designing studies (calculating power of future studies). On average [^{123}I]PE2I had the same reproducibility as the commercially used [^{123}I]FP-CIT. Remarkably [^{123}I]PE2I had a higher reliability.

The reliability or the intraclass correlation coefficient (ICC) has traditionally been used in various reproducibility studies in SPECT and PET and was introduced in SPECT DAT reproducibility studies by Seibyl et al 1996. The ICC is a descriptive statistic outcome, which can be used when quantitative measurements are made on units that are organized into groups. It should be emphasized that no statistical cut off level is present when calculating the ICC. Calculation of ICC in medicine dates back 100 years (Arthur Harris 1913) but the modern way of calculating ICC origins from (Kirk 1982):

$$ICC = \frac{\left(MS_B - MS_W\right)}{(k-1)(MS_B + MS_W)}$$

Where MS_B is the mean sum of squares between subjects, MS_W the mean sum of squares within subjects and k the number of within-subject measurements. The ICC can vary between 0-1.0, but if an ICC is to take the value of ≈ 1.00 it is only possible if the MS_B >>> than MS_W. This is achieved if the data has a high individual variance and at the same time the reproducibility low. As noted, I recalculated the reliability from (Booij *et al* 1998b) which in one example was 1.00. Notably the ICC can be manipulated higher if one simply raises the absolute values e.g. by calculating binding ratios which equals BP_{ND} + 1 instead of BP_{ND} since this would decrease the MS_W without affecting the MS_B. This is illustrated in figure 14.

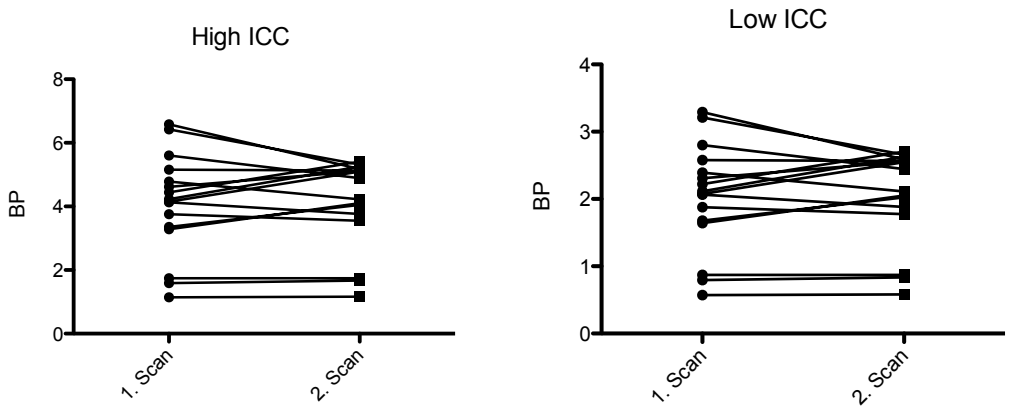

Figure 14. An example of equal reproducibility but different ICC, achieved by simply multiplying the data in 1. and 2. scan in the low ICC study by a factor of two.

The reader should therefore always consider the absolute values of the outcome variable when interpreting results of reproducibility studies.

Delineation of brain region of interest (ROI) in [^{123}I]PE2I DAT imaging

Intrasubject variability in SPECT DAT imaging results from both biological and methodological variation. In the absence of subject-specific anatomical information (e.g. MRI), the ROI delineation is anticipated to be particularly prone to observer bias. To our knowledge this had never been formally assessed in DAT SPECT studies before and was the aim of paper 3. We did also briefly assess this in paper 2 and some of these results are also included in this section.

Overall, there are three principally different ways of delineating ROI's on the SPECT image: a) manual delineation (MD) directly on the SPECT-image; b) template guided delineation and c) delineation based on co-registration with another brain image that provides structural information, such as MRI/CT. In theory there is only limited difference between the MD and the adjustable template based delineation. The largest advantage of template based delineation compared to MD is that it is less time consuming and operator-independent (Koch *et al* 2005). An alternative to an anatomically correct ROI was described by Tossici-Bolt et al., the so-called striatal volume of interest method (SVI) (Tossici-Bolt *et al* 2006). This method requires no structural information on the brain of the individual patients, but involves a template of oversized ROI's, involving all striatal slices. The calculated volume of interest (VOI), the total counts within this volume, the count concentration in a reference region and a population-based estimate of the average striatal volume then forms the basis for the calculation of a striatal binding ratio (SBR) equivalent to the ratio of the specific / non-displaceable uptake. The three different methods can be visualized in figure 15.

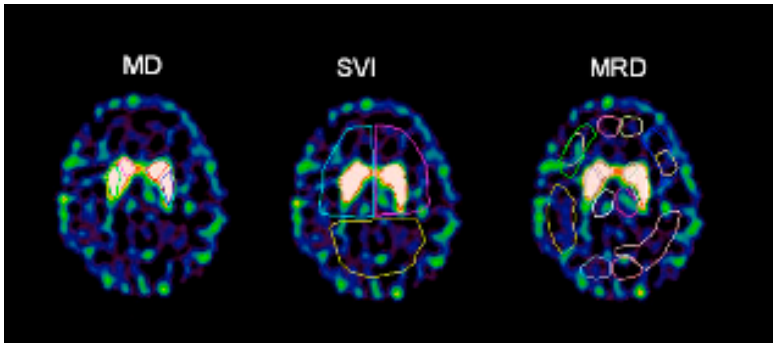

Figure 15. Three different methods of ROI delineation on SPECT images of same brain slice in same individual (Ziebell *et al* 2010b).

In healthy volunteers (paper 2) we showed that MD of ROI directly on SPECT images performed equally well to a MRI-defined probability map based ROI delineation (MRD) in terms of intrasubject variability of BP_{ND} of DAT (Manual 4.1 % vs. MRD 5.2%) (Ziebell *et al* 2007). This was despite the fact that the volume reproducibility of the ROI was 8 times better with the MRD method. The lack of better performance of the MRD method is probably primarily a partial volume effect related to a larger ROI volume using the MRD approach compared with the manual "hot spot" delineation approach, where ROIs are delineated on a few slices only (no attempts were made to manually move the MR-defined volumes to the "hot spots" on the SPECT image).

We expected that the test-retest variability was larger in patients with reduced DAT availability, because the concentration of tracer in the striatal regions of the patients is closer to the non-specific tracer concentrations. In this context, the method for ROI delineation without anatomical information is even more difficult and prone to larger observer bias, and the advantage of including MRI-based anatomical information for assessment of striatal DAT availability in patients with decreased binding would be expected to have greater impact.

The ROI delineation reproducibility for each method is shown in figure 16—that is, the calculated BP_{ND} from the first ROI delineation week 0 is plotted against the BP_{ND} from the

second ROI delineation 4 weeks later. The delineation reproducibility was not significantly different among any of the 3 ROI delineation methods (paired t test, $P > 0.1$).

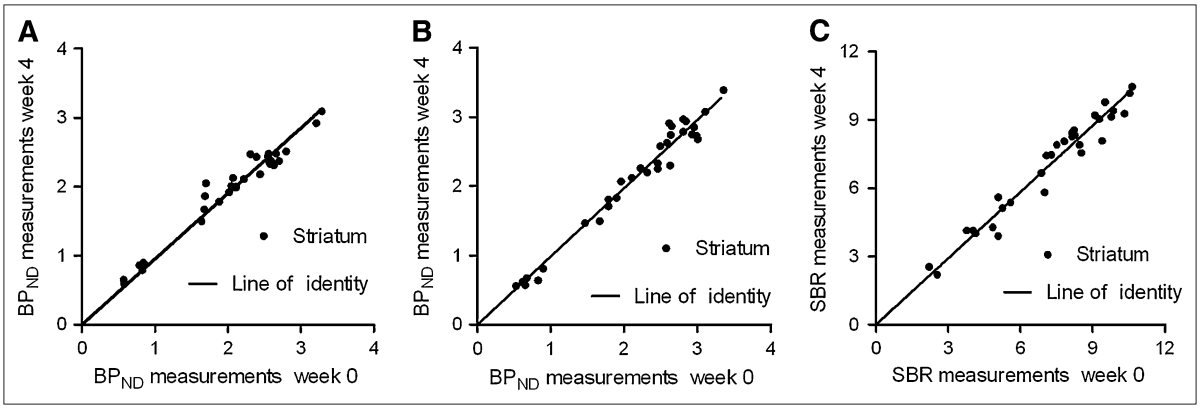

Figure 16. Intraobserver reproducibility of BPND in striatum for different delineation methods. MD (A), probability map–based delineation (B), and SVI (C). For all 3 methods, both test and retest scans were quantified entailing 32 data points (Ziebell *et al* 2010b).

Table 8 summarizes the intraobserver reproducibility of either BP_{ND} or SBR for all 3 ROI delineation methods.

Table 8. From (Ziebell *et al* 2010b).

Summed Intraobserver Reproducibility of 3 Different Methods

Method	Caudate nucleus	Putamen	Striatum	ICC
MD (BP_{ND})	10.2% ± 9.2%	9.7% ± 5.4%	7.0% ± 4.1%	0.97
MRD (BP_{ND})	14.2% ± 12.3%	8.1% ± 7.5%	5.7% ± 5.4%*	0.98
SVI (SBR)			6.7% ± 6.0%	0.98

*Calculated striatum = volume-weighted (caudate nucleus+ putamen).
ICC = intraclass correlation coefficient.
No statistically significant better intraobserver reproducibility was observed for any method (MD vs. MRD, MD vs. SVI, MRD vs. SVI; $P > 0.1$), and all performed equally for intraclass correlation coefficient ($n = 16$).

Even though the results are comparable, the MD method is obviously operator dependent as well as dependent upon prior experience, and is presumably also the most time-consuming. However, the MRD method is not outperforming the other methods and especially in the every day clinical setting it is not worth the effort (since it requires an individual MRI scan in addition to the SPECT scan). The SVI method did not result in a significantly better ROI

delineation reproducibility than the 2 other methods. Further, the absolute value of SBR is linearly related to the actual volume and we found a quite high interindividual variation in the MRI- determined striatal volumes, ranging from 7.2 to 10.4 mL, suggesting that the outcome parameter SBR is determined with some uncertainty if the user applies a population-based average striatal volume.

In addition to the similar ROI delineation reproducibility of the MRD compared to the MD, there was no statistically significant difference (paired t test, $P > 0.4$) in the BP_{ND} values calculated by the methods (Fig. 17). Linear regression analysis showed an excellent correlation with a slope of 0.99 ($R_2 = 0.96$).

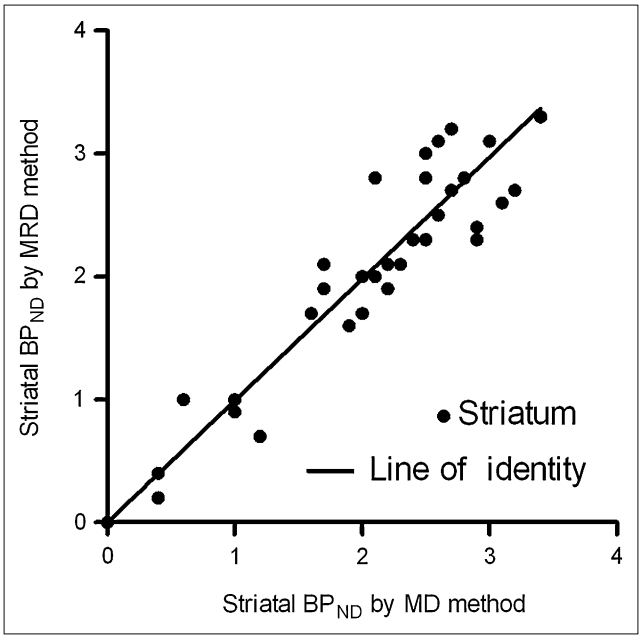

Figure 17. BP_{ND} values for caudate nucleus and putamen by ROI application with MD vs. MRD method. Linear regression analysis showed excellent correlation, $R^2 = 0.96$ (Ziebell *et al* 2010b).

The results of the reproducibility of the delineation methods should be seen in the light of the overall reproducibility of the whole method (table 9) i.e. the intrasubject variability.

Table 9. From (Ziebell *et al* 2010b).

Summed Intrasubject Variability from 3 Different ROI Application Methods (n = 8)

Method	Caudate nucleus	Putamen	Striatum	ICC
MD (BP_{ND})	19.4% ± 14.3%	14.8% ± 6.0%	11.9% ± 10.0%	0.88
MRD (BP_{ND})	16.4% ± 11.9%	15.8% ± 11.7%	14.6% ± 15.3%*	0.90
SVI (SBR)			10.8% ± 10.2%	0.90

*Calculated striatum = volume-weighted (caudate nucleus + putamen).
ICC = intraclass correlation coefficient.

When doing so, it is clear that the performance of the delineation reproducibility is considerable for all three methods, constituting approximately 50% of the intrasubject scan to scan variability in patients with decreased DAT binding.

Head to head comparison of the DAT ligands [^{123}I]PE2I and [^{123}I]FP-CIT

In the fourth and final study (Ziebell *et al* 2010a) we wanted to address the *in vivo* selectivity of the current SPECT radioligands available for imaging of the DAT. As previously stated the *in vitro* selectivity for DAT compared to SERT is much higher for [^{123}I]PE2I than for i.e. [^{123}I]FP-CIT (10 fold, please see table 1).

However, it is well known in the radiopharmaceutical industry that *in vitro* selectivity and affinity is not always transferrable to *in vivo* settings, e.g. *in vitro* the β-CIT has similar affinity for DAT and SERT (Neumeyer *et al* 1991). In contrast SPECT imaging has shown midbrain activity closely associated with DAT levels in striatum (Laruelle *et al* 1993). The diagram of the study is shown in figure 18.

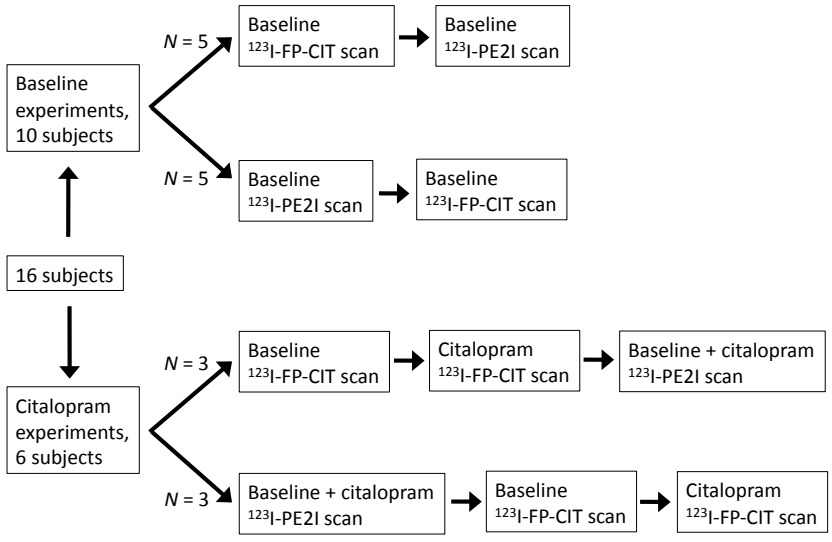

Figure 18. A total of sixteen healthy individuals were included; a diagram of the design of the study is shown in the figure (Ziebell *et al* 2010a).

Since [^{123}I]FP-CIT is administered as a bolus alone and [^{123}I]PE2I as a bolus followed by a constant infusion, binding parameters are not directly comparable in the baseline experiments (N=10). As the [^{123}I]FP-CIT measurements were made 3-4 hours post bolus injection a true steady state condition was not reached whereas with [^{123}I]PE2I, specific binding to non-

displaceable binding were measured at steady state conditions. In the [^{123}I]FP-CIT baseline experiments we therefore referred to the outcome as "binding ratios" (BR), and not BP_{ND}. The individual striatal- and thalamic-to-cerebellum BR/BP_{ND} is shown in figure 19.

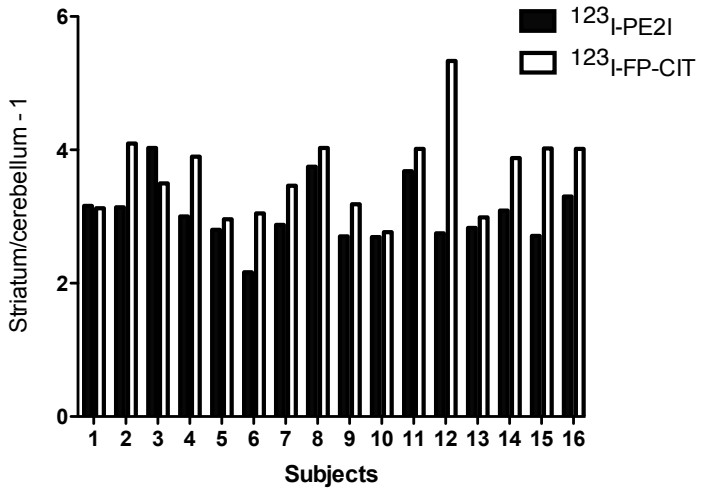

Figure 19. [^{123}I]FP-CIT BR is significantly higher than [^{123}I]PE2I BP_{ND} (t-test, $p<0.05$) (Ziebell *et al* 2010a).

Not surprisingly, the BR for [^{123}I]FP-CIT is significantly higher than BP_{ND} for [^{123}I]PE2I since according to our own data (Pinborg *et al* 2005) the transient equilibrium analysis tends to overestimate the true BP_{ND}. Interestingly, we found that the actual terminal plasma clearance rate was stable with an average of ~6% decline per hour and further more, that there was no difference between BP_{ND} calculated using SRTM and the binding ratio obtained as a mean from 180-240 min post [^{123}I]FP-CIT injection. Thus, in healthy individuals transient equilibrium analysis of [^{123}I]FP-CIT does not explain the higher [^{123}I]FP-CIT BR compared to BP_{ND} of [^{123}I]PE2I. This is probably because of the slower kinetics of [^{123}I]FP-CIT as compared to [^{123}I]PE2I so the SRTM do underestimate the transient equilibrium analysis for [^{123}I]FP-CIT as previously shown and discussed for [^{123}I]PE2I (Pinborg *et al* 2005). As a note of caution, altered plasma clearance may occur in patients suffering from e.g. renal diseases or where the metabolism of [^{123}I]FP-CIT is altered.

The average count rates in striatum were 3.0 ± 0.9 times higher for [^{123}I]FP-CIT as compared to [^{123}I]PE2I; 3.4 ± 0.9 times higher in thalamus and 2.7 ± 0.6 times higher in cerebellum. Thus, count statistics per injected MBq seem to be superior for [^{123}I]FP-CIT compared to [^{123}I]PE2I. This is particularly beneficial in patients with low DAT binding. The higher brain uptake of [^{123}I]FP-CIT is beneficial and compared to [^{123}I]PE2I it can be translated into a better determination of the target to background ratio, into a lower dose of radioactivity, or by shortening the scanning time.

To adres the *in vivo* SERT/DAT selectivity of [^{123}I]PE2I and [^{123}I]FP-CIT we first calculated the individual specific-to-nonspecific ratio in thalamus to the individual specific-to-nonspecific ratio in striatum (fig. 20). The ratio for [^{123}I]FP-CIT was significantly higher (43%) than for [^{123}I]PE2I (t-test, $p<0.005$, N=16), with a very high individual difference.

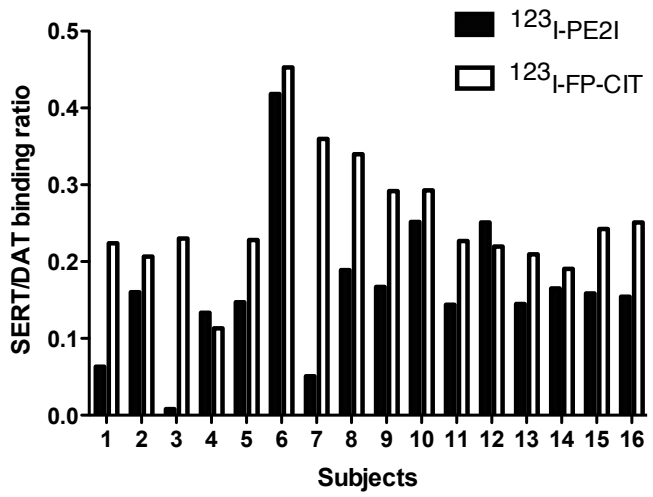

Figure 20. As a proxy for the *in vivo* SERT/DAT selectivity of [^{123}I]PE2I and [^{123}I]FP-CIT, the individual specific-to-nonspecific ratio in thalamus to the individual specific-to-nonspecific ratio in striatum is shown. The ratio for [^{123}I]FP-CIT is significantly higher than for [^{123}I]PE2I (t-test, $p<0.005$, N=16).

We needed to see if there could be any contribution to striatal binding of ratiotracer to SERT, therefore 6 additional healthy volunteers participated in a citalopram experiment. Citalopram

was given at a dose of 0.15 mg/kg bodyweight. For [^{123}I]FP-CIT complete TAC were obtained between 0-240 minutes so that we could fit the simplified reference tissue model (SRTM) and hence obtain true and comparable [^{123}I]FP-CIT BP_{ND} measurements to the true steady state obtained [^{123}I]PE2I BP_{ND} measurements. Citalopram infusion did not alter BP_{ND} for [^{123}I]PE2I in striatum (Wilcoxon : $p>0.1$) figure 21.

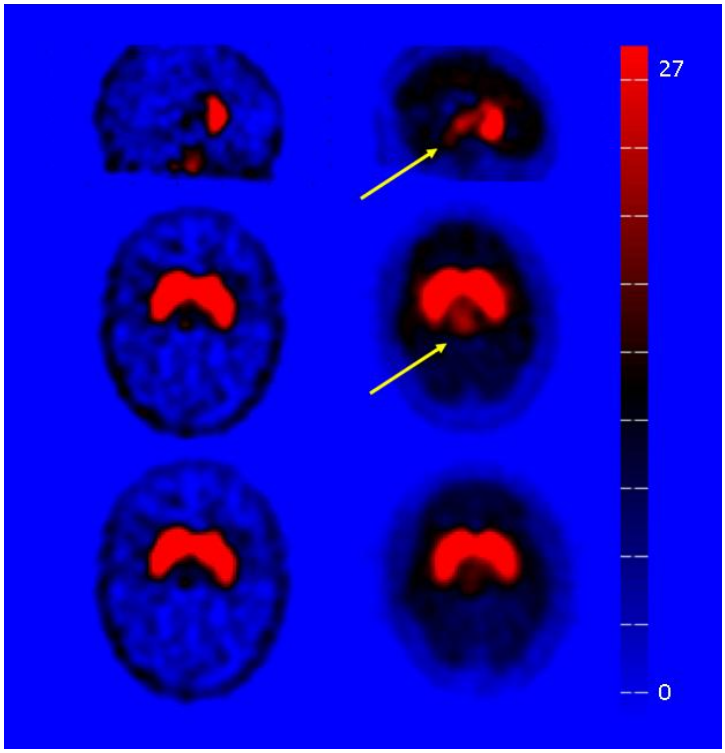

Figure 21. Example of a [^{123}I]PE2I (left column) and [^{123}I]FP-CIT (right column) image of the same individual. In the two first rows (sagittal and horizontal slices) the thalamus is clearly visualized in the [^{123}I]FP-CIT image (arrows). The bottom row shows the images after acute SERT blocking with citalopram (Ziebell *et al* 2010a).

The individual BP_{ND} of [^{123}I]FP-CIT in relation to the citalopram infusion is shown in figure 22. This illustrates how the individual striatal BP_{ND} obtained from [^{123}I]FP-CIT approximates the BP_{ND} obtained with [^{123}I]PE2I after citalopram infusion. After acute blocking of SERT with citalopram the 20% higher striatal specific to non-displaceable binding ratio of [^{123}I]FP-CIT than BP_{ND} of [^{123}I]PE2I now showed no significant difference.

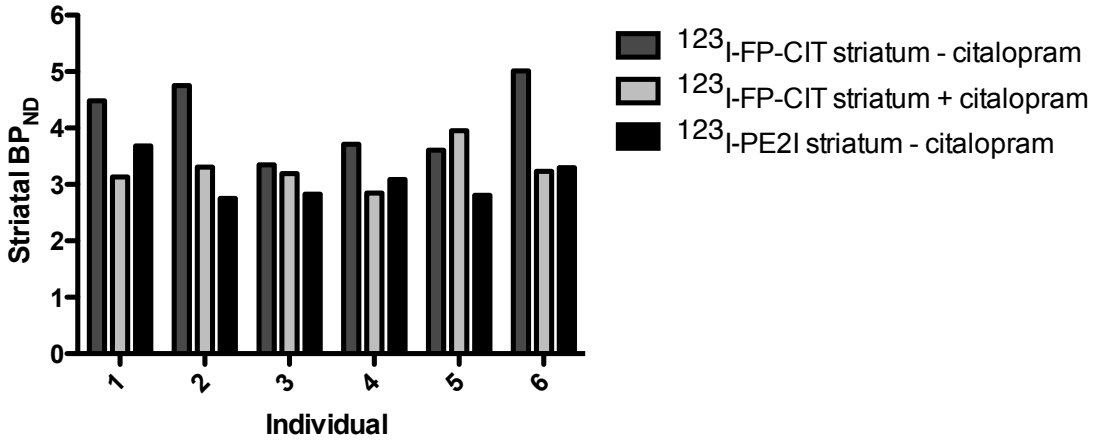

Figure 22. Demonstration of how that BP_{ND} for [^{123}I]FP-CIT approaches the BP_{ND} for [^{123}I]PE2I after SERT blocking by citalopram (Ziebell *et al* 2010a).

Based on the available *in vitro* data on [^{123}I]FP-CIT DAT versus SERT selectivity and affinity, the extent to which SERT blocking decreased striatal BP_{ND} was larger than expected and point towards [^{123}I]PE2I being even more selective *in vivo* than *in vitro* compared to [^{123}I]FP-CIT. This can be appreciated on a theoretically simulation we did (figure 23) based on the following equation:

$$\frac{SERTsignal}{TOTALsignal}\left(B_{avail,DAT}\right) = \frac{B_{avail,SERT}}{B_{avail,SERT} + \frac{K_{d,SERT}}{K_{d,DAT}} * B_{avail,DAT}}$$

SERTsignal = $B_{avail,SERT}/K_{d,SERT}$, TOTALsignal = $B_{avail,SERT}/K_{d,SERT} + B_{avail,DAT}/K_{d,DAT}$.

The binding of the radioligand to NET is neglected. Since K_d values are not available K_i are used instead and the ratio of K_i values are comparable to that of the K_d ratio.

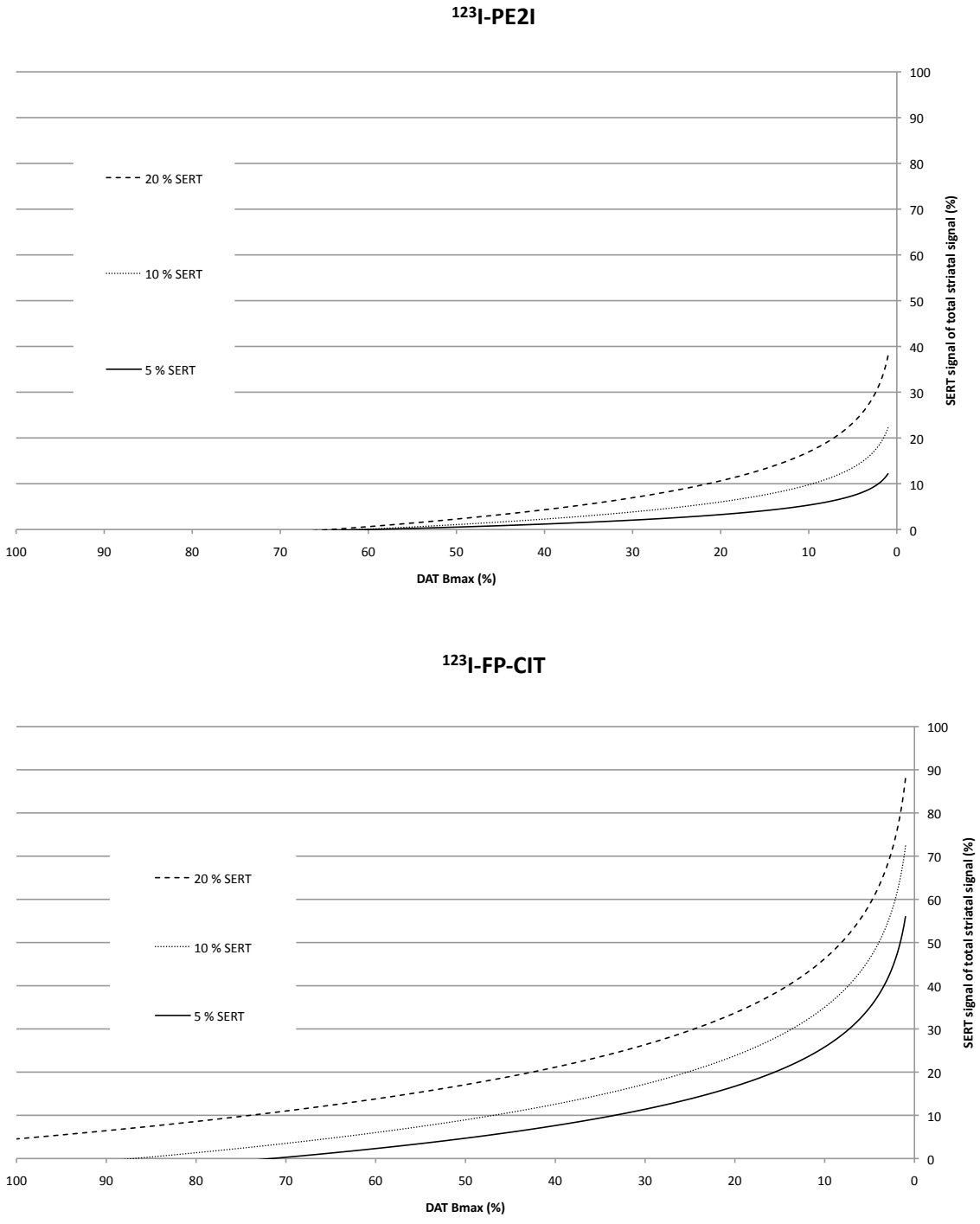

Figure 23. The figures show the theoretical proportion of SERT signal of total striatal signal in: [^{123}I]PE2I (top) and [^{123}I]FP-CIT (bottom) in a 20/1, 10/1 and 5/1 ratio of DAT/SERT distribution.

From the simulation it can be seen, that more than 20 % of the striatal transporters available should be SERT if the distribution of DAT and SERT should explain the decrease in striatal

BP_{ND} we observed for [^{123}I]FP-CIT. Human post-mortem brain studies point towards a $B_{avail, DAT}$: $B_{avail, SERT}$ ratio of 20:1 in putamen ~200:10 pmol/g (Madras *et al* 1998; Varnas *et al* 2004). This ratio could probably vary somewhat in healthy individuals and a large variation in BP_{ND} has indeed been reported in *in vivo* studies (standard deviation of BP_{ND} for SERT = 23 % of mean (Frankle *et al* 2006; Matsumoto *et al* 2009); DAT = 13% of mean (Booij *et al* 1998b; Ziebell *et al* 2007)). However, unlike [^{123}I]PE2I binding of [^{123}I]FP-CIT to SERT in striatum is not negligible.

Conclusions

The establishment of a B/I ratio (2.7h) for [^{123}I]PE2I was successful. Both in theory when simulated (maximum 10% difference in BP_{ND} with 2.2 fold increase in ratio), and in clinical practice in two independent populations of healthy volunteers (BP_{ND} stability 5%/h), the B/I was confirmed to provide stable steady state measurements in plasma and in brain tissue. The B/I design is more time consuming than a simple bolus injection, but is easily implemented for routine use in a SPECT laboratory and the number of acquisitions is not compromised.
The mode of administration of [^{123}I]FP-CIT makes it susceptible to interindividual variation in the terminal plasma clearance rate of the tracer, which may particularly be a problem in medicated patients, or patients with concomitant medical disorders. However, for healthy non-medicated individuals the influence of the terminal plasma clearance rate on the outcome parameter is not quantitatively important.

The reproducibility of the [^{123}I]PE2I binding to DAT using the B/I is comparable to other DAT SPECT tracers with a slightly higher reliability. There was a higher reproducibility in healthy volunteers with a higher [^{123}I]PE2I binding than in patients with low [^{123}I]PE2I binding ($\approx$ 3 fold) – as expected.

Anatomical precision of manual ROI delineation is compromised especially in patients with decreased striatal [^{123}I]PE2I binding, however co-registration with structural imaging (MRI) , even with external fiducial markers, does not increase accuracy, probably because of lack in precision of co-registration. In patients with a low binding the ROI delineation constituted no matter the method a 50 % of the overall reproducibility.

[^{123}I]PE2I showed a higher DAT/SERT *in vivo* selectivity than the widely and commercialized DAT radioligand [^{123}I]FP-CIT and the results were higher than expected from *in vitro* measurements. Even in high binding DAT regions, binding of [^{123}I]FP-CIT to SERT was significant and could be blocked by [^{123}I]FP-CIT preinjection with citalopram - oppositely [^{123}I]PE2I which was significantly unaffected. In clinical practice [^{123}I]FP-CIT is favourable regarding count statistics per injected MBq and administration of radioligand which is less troublesome as [^{123}I]PE2I. The easier administration of [^{123}I]FP-CIT is usable as long as the physician that interpret the scan result keep the possible confounders (terminal plasma clearance and SSRI medication) in mind, in research perspective, however, this is more critical.

Perspectives

For the first time SPECT neuroimaging has a very *in vivo* selective and reliable DAT radioligand that shows high reproducibility in both patients and healthy volunteers. In addition the B/I setup provides easy interpretation of pharmacological challenges. Thus, future studies based on the data included in this thesis would be interesting. [^{123}I]PE2I could be investigated in new studies or in replication of older studies where radioligands less DAT selective have been used. Interpretation of small differences in BP found in these studies could potentially be due to regulation in the SERT and not DAT; these are examples:

I) Depression in PD is common and has been the subject of research with SPECT, recently suggesting that DAT binding is lower in PD patients with depression than in PD without (Hesse *et al* 2009). Based on our results, replication of such a study would be interesting to see if the extend to which the decrease in striatal [^{123}I]FP-CIT binding is reflecting a decrease in SERT binding.

II) Correlation of trophic factors to the function of SPECT DAT imaging could also be potential research topics since evidence show an involvement of these factors in neurodegenerative disorders including PD (Zuccato and Cattaneo 2009). Likewise the choice of a selective DAT radiotracer would be important since trophic factors also have been shown to be involved in depression (Brunoni *et al* 2008) and hence the serotonin system.

III) SPECT imaging of the DAT is increasingly being used as an ancillary diagnostic tool in assessment of the diagnosis of movement disorders. The use of a selective DAT radioligand has not yet been explored. Several studies measuring the sensitivity and specificity of SPECT DAT with unselective radioligands have been carried out (Vlaar *et al* 2007). An unselective radioligand that is not measured at steady state

conditions would tend to overestimate binding, particularly in individuals with a high SERT binding and/or high terminal plasma clearance ratio. This would give rise to a higher number of false negative DAT SPECT scan results as compared to [^{123}I]PE2I SPECT scans. Whether this is also reflected in clinical practice remains unexplored. Within the last couple of years the term SWEDD has evolved. This is a phenomenon covering patients with Symptoms Without Evidence of Dopaminergic Deficits. The definition alone is so far not congruent. Originally SWEDD patients were introduced in intervention studies where 10-14 % of patients although clinically well defined, surprisingly had a normal dopaminergic scan. Although most of the patients recently have been shown to have another pathology not involving striatal neurodegeneration (Marshall *et al* 2009), this might not be the whole truth. Of course some of them could be suffering from a non-striatal neurodegenerative disease and initially misdiagnosed, however some could have an upregulated SERT and therefore a potential abnormal [^{123}I]PE2I scan despite of a normal [^{123}I]FP-CIT or [^{123}I]β-CIT scan.

Summary in Danish

Radioaktivt mærkede sporstoffer til afbildning af hjernens dopamintransporter (DAT) ved hjælp af Single Photon Emission Computer Tomography (SPECT) er i større og større omfang brugt som biomarkør for funktionen af den præsynaptiske dopaminerge nervecelle i hjernen. Iod-123 mærket N-(3-iodoprop-2E-enyl)-2-beta-carbomethoxy-3beta-(4-methylphenyl), kaldet PE2I er en sådan SPECT radioligand. [^{123}I]PE2I udmærker sig ved en 10 gange så høj selektivitet for DAT sammenlignet med serotonintransporteren (SERT) i forhold til [^{123}I]FP-CIT (DaTSCAN) der er en men kommercielt tilgængelig radioligand og derved meget udbredt. [^{123}I]PE2I har endvidere pga. dets lave affinitet for DAT meget hurtige farmakologisk kinetiske egenskaber i forhold til [^{123}I]FP-CIT med en striatal "peak time" omkring 30-60 min sammenholdt med 148 min for [^{123}I]FP-CIT. Pga. [^{123}I]PE2I's hurtige kinetiske egenskaber er det muligt af kvantificerer bindingen af [^{123}I]PE2I til DAT ved hjælp af kinetisk eller grafisk analyse efter bolusinjektion. Desuden tillader disse egenskaber at give [^{123}I]PE2I som en bolus efterfulgt af en infusion således at et konstant niveau af [^{123}I]PE2I opnås i plasma og hjernevæv hurtigt.

Et vigtigt element i kvantificeringen af DAT er en korrekt afgrænsning af "region of interest" (ROI) i SPECT-billedet. ROI-afgrænsningen kan have stor indflydelse på blandt andet den overordnede reproducerbarhed af metoden og er derfor vigtig.

Denne Ph.d.-afhandling omhandler undersøgelsen af SPECT DAT radioliganden [^{123}I]PE2I. Afhandlingen havde følgende 4 formål:

1) Etablering af en bolus/infusion (B/I) protokol for [^{123}I]PE2I, med henblik på opnåelse af "steady state" i plasma og hjerne.

2) Teste reproducerbarheden af B/I metoden hos raske og patienter med nedsat striatal binding af [^{123}I]PE2I.

3) Undersøge forskellige ROI afgrænsnings metoder mht. kvantificering af [^{123}I]PE2I.

4) Sammenligne bindingspotentiale og indflydelse af serotonin transporter binding ved [^{123}I]PE2I & [^{123}I]FP-CIT.

Baseret på præliminære bolus undersøgelser var det muligt af beregne den optimale B/I ratio for [^{123}I]PE2I. Denne ratio (2.7h) medførte "steady state" og en høj reproducerbarhed i både raske og patienter med reduceret [^{123}I]PE2I binding. Vi viste endvidere at manuel afgrænsning af ROI direkte på SPECT billeder var lige så præcist hvad angik intrasubjekt variabilitet målt som bindingspotentialet af DAT, som et automatisk ROI afgrænsende MRI-baseret "sandsynlighed" software program. Vi havde forventet at kunne se forskel på metoderne hos patienter med nedsat DAT binding. Dette var imidlertid ikke tilfældet, muligvis pga. usikkerheden involveret i co-registreringen mellem disse to billedemodaliteter, til trods for at vi brugte eksterne markører til hjælp ved co-registreringen. Endelig fandt vi at bidraget fra SERT til *in vivo* bindingen var betydeligt med [^{123}I]FP-CIT, men ikke påviseligt for [^{123}I]PE2I.

Afhandlingen konkluderer, at [^{123}I]PE2I er en superselektiv SPECT DAT radioligand med optimale kinetiske egenskaber der tillader præcis kvantificering af DAT i striatum. Dette medfører at [^{123}I]PE2I aktuelt er den mest pålidelige radioligand til brug for afbildning af DAT med SPECT i den menneskelige hjerne.

Summary in English

Imaging of the dopamine transporter (DAT) with Single Photon Emission Computer Tomography (SPECT) has increasingly been used as a biomarker for the integrity of presynaptic dopaminergic nerve cells in patients with movement disorders. 123-I-labelled N-(3-iodoprop-2E-enyl)-2-beta-carbomethoxy-3beta-(4-methylphenyl), named PE2I, has about 10-fold higher selectivity for the DAT than for the serotonin transporter (SERT) compared to the slightly older but very used and licensed radioligand [^{123}I]FP-CIT (DaTSCAN). Further because of its lower affinity to DAT, [^{123}I]PE2I has faster kinetics than [^{123}I]FP-CIT with a striatal peak time between 30-60 min compared to 148 minutes for [^{123}I]FP-CIT. Because of its fast kinetic properties, quantification of [^{123}I]PE2I binding to DAT is possible using kinetic or graphical analysis following bolus injection of tracer or as a combination of bolus and constant infusion where constant levels in plasma and brain tissue are achieved.

A particularly important step in the DAT quantification is a correct delineation of the region of interest (ROI) in the SPECT-image. The ROI delineation can have great impact on the overall reproducibility of the method and so should be considered in reproducibility studies.

This PhD-thesis covers the investigation of the SPECT DAT radioligand [^{123}I]PE2I which includes the following steps:

1) To establish a bolus/infusion (B/I) protocol for [^{123}I]PE2I that enable steady state conditions in plasma and brain.

2) To test the reproducibility of the B/I method in healthy subjects and patients with decreased striatal binding of [^{123}I]PE2I.

3) To examine different ROI delineation methods for [^{123}I]PE2I quantification.

4) To compare binding potential and contribution of serotonin transporter binding in [^{123}I]PE2I images as compared to [^{123}I]FP-CIT.

Based on preliminary bolus trials we were able to calculate a B/I ratio of [^{123}I]PE2I. This B/I ratio (2.7h) gave rise to steady state conditions and excellent reproducibility in both healthy volunteers and in patients with decreased [^{123}I]PE2I binding. Further we showed in healthy subjects that manual delineation of ROI directly on SPECT images perform equally well to a MRI-defined probability map based ROI delineation (MRD) in terms of intrasubject variability of binding potential of DAT. In patients the expected advantage of including MRI-based anatomical information for assessment of striatal DAT availability was not present. This was probably because of difficulties in co-registration between the two image modalities even though we used external fiducials. Finally the *in vivo* SERT binding in DAT images obtained with [^{123}I]FP-CIT was significant as compared to the [^{123}I]PE2I images.

In conclusion:

Even though the only licensed radioligand for DAT imaging ([^{123}I]FP-CIT) is selective for the DAT and easy to use, [^{123}I]PE2I seems to be a better alternative. [^{123}I]PE2I is a super selective SPECT DAT radioligand with optimal kinetic properties for accurate quantification of the DAT availability in striatum. Apart from the more laborious B/I design it is currently to be considered the best radioligand for imaging the DAT in the human brain with SPECT.

Articles

Paper 1

Quantification of ^{123}I-PE2I Binding to Dopamine Transporter with SPECT After Bolus and Bolus/Infusion

Lars H. Pinborg, MD[1]; Morten Ziebell, MD[1]; Vibe G. Frøkjær, MD[1]; Robin de Nijs, MS[1]; Claus Svarer, MS, PhD[1]; Steven Haugbøl, MD[1]; Stig Yndgaard, MD[2]; and Gitte M. Knudsen, MD, PhD[1]

[1]Neurobiology Research Unit, University Hospital Rigshospitalet, Copenhagen, Denmark; and [2]Department of Anesthesia, University Hospital Rigshospitalet, Copenhagen, Denmark

The aim of the present study was to describe a method combining easy implementation in a clinical setting with accuracy and precision in quantification of ^{123}I-labeled *N*-(3-iodoprop-(2E)-enyl)-2β-carboxymethoxy-3β-(4′-methylphenyl)nortropane (PE2I) binding to brain dopamine transporter. **Methods:** Five healthy subjects (mean age, 50 y; range, 40–68 y) were studied twice. In the first experiment, dynamic SPECT data and arterial plasma input curves obtained after ^{123}I-PE2I bolus injection were assessed using Logan, kinetic, transient equilibrium, and peak equilibrium analyses. Accurate and precise determination of BP_1 (binding potential times the free fraction in the metabolite-corrected plasma compartment) and BP_2 (binding potential times the free fraction in the intracerebral nonspecifically bound compartment) was achieved using Logan analysis and kinetic analysis, with a total study time of 90 min. In the second experiment, ^{123}I-PE2I was administrated as a combined bolus and constant infusion. The bolus was equivalent to 2.7 h of constant infusion. **Results:** The bolus-to-infusion ratio of 2.7 h was based on the average terminal clearance rate from plasma in the bolus experiments. Steady state was attained in brain and plasma within 2 h, and time–activity curves remained constant for another 2 h. Even when an average bolus-to-infusion ratio was used, the striatal BP_1 and BP_2 values calculated with kinetic analysis ($BP_1 = 21.1 \pm 1.1$; $BP_2 = 4.1 \pm 0.4$) did not significantly differ from those calculated with bolus/infusion analysis ($BP_1 = 21.0 \pm 1.2$; $BP_2 = 4.3 \pm 0.3$). Computer simulations confirmed that a 2-fold difference in terminal clearance rate from plasma translates into only a 10% difference in BP_1 and BP_2 calculated from 120 to 180 min after tracer administration. **Conclusion:** The bolus/infusion approach allows accurate and precise quantification of ^{123}I-PE2I binding to dopamine transporter and is easily implemented in a clinical setting.

Key Words: ^{123}I-PE2I; dopamine transporter; SPECT; kinetic analysis; Logan analysis; bolus/infusion analysis

J Nucl Med 2005; 46:1119–1127

Received Dec. 14, 2004; revision accepted Mar. 29, 2005.

For correspondence or reprints contact: Lars H. Pinborg, MD, Neurobiology Research Unit, Rigshospitalet, N9201, 9 Blegdamsvej, Copenhagen, DK-2100 Denmark.

E-mail: pinborg@nru.dk

The tropane analog *N*-(3-iodoprop-(2E)-enyl)-2β-carboxymethoxy-3β-(4′-methylphenyl)nortropane (PE2I) binds with high affinity to the neuronal dopamine transporter (DAT) (inhibition constant [K_i] = 17 nmol/L) and with much lower affinity to the serotonin transporter (29-fold) and the noradrenaline transporter (>58-fold) (*1*). In vivo, PET and SPECT studies on healthy subjects have demonstrated excellent kinetic properties for ^{11}C-PE2I (*2*) and ^{123}I-PE2I (*3–5*). Time–activity curves showed that striatum-specific binding peaked approximately 60 min after bolus injection and that, for PET, the striatum-to-cerebellum ratio was approximately 10 at peak time (*2*). The usefulness of the cerebellum and neocortex as reference regions has been demonstrated in monkeys, in which the striatal time–activity curves after ^{11}C-PE2I injection reached the level of the cerebellum and neocortex after injection of unlabeled 2β-carbomethoxy-3β-(4-iodophenyl)tropane (β-CIT). In addition, the cerebellar and neocortical time–activity curves were unchanged after injection of unlabeled β-CIT (*2*). This finding agrees with the very low ^{125}I-PE2I binding seen in the neocortex and cerebellum on human whole-hemisphere autoradiography (*6*). Only polar plasma metabolites of ^{11}C-PE2 (*2*) and ^{123}I-PE2I (*7*), unlikely to cross the blood–brain barrier to any significant extent, have been demonstrated. In baboons, in vivo striatal ^{11}C-PE2I B'_{max} values correlated with in vivo striatal 6-^{18}F-fluoro-L-dopa K_i values, with in vitro striatal ^{125}I-PE2I B_{max} values, and with the number of tyrosine hydroxylase–immunoreactive neurons in the substantia nigra (*8*). ^{123}I-PE2I has proven useful for preclinical and early diagnosis of Parkinson's disease in humans (*5*) and experimental Parkinson's disease in monkeys (*5,9*).

The aim of this study was to describe a method that provides a reliable quantitative estimate of receptor parameters and is easy to implement in a clinical setting. We present results from 5 healthy subjects who underwent SPECT twice: first after a bolus injection of ^{123}I-PE2I and then, days or weeks later, after a bolus injection plus a constant infusion of ^{123}I-PE2I. The ratio of the bolus size (MBq) to the infusion velocity (MBq/h) is defined as the

bolus-to-infusion ratio (h). The bolus-to-infusion ratio used in all bolus/infusion studies was determined from the average kinetic parameters of the initial bolus studies. The design of the study allowed direct comparison of binding potential (BP) after bolus and BP after bolus/infusion in each individual. The design also allowed comparison of use of the average bolus-to-infusion ratio and use of the theoretic optimal bolus-to-infusion ratio calculated from an individual's terminal clearance rate of ^{123}I-PE2I from plasma.

MATERIALS AND METHODS

Subjects

Five healthy subjects (mean age, 50 y; range, 40–68 y) were included in the study. All claimed to be alcohol and drug free, had no history of neurologic or psychiatric disorders, had normal results on physical examination and routine blood tests, and gave written informed consent. The study was performed in accordance with the ethical standards of the Declaration of Helsinki and was approved by the ethical committee of Copenhagen and Frederiksberg (KF 02-150/98).

Experimental Procedures

SPECT was performed using a triple-head IRIX SPECT scanner (Philips Medical Systems) fitted with general-purpose low-energy, parallel-hole collimators (spatial resolution, 8.5 mm at 10 cm). The imaging energy window was positioned at 143–175 keV. High-energy photons of ^{123}I penetrated through the lead of the collimator, and Compton scatter in the scintillation crystal caused erroneous counts in the imaging energy window. A second energy window positioned at 184–216 keV was used to correct for these high-energy photons in the imaging window. Projection data were recorded at 120 angles with an interval of 3°. Before reconstruction, the projection images of the 2 energy windows were subtracted. Reconstruction of the images was performed in MATLAB 6.5 (MathWorks) in 128 × 128 matrices (2.33-mm pixels and identical slice thickness) using standard filtered backprojection with a low-pass fourth-order Butterworth filter at 0.3 Nyquist (0.064/mm) and using uniform attenuation correction with an attenuation coefficient of 0.10/cm.

The system resolution at 10 cm from the collimator and 1 cm off center was 12 mm in full width at half maximum in the radial direction and 8 mm in full width at half maximum in the transverse and tangential directions. Figure 1 shows a representative SPECT image after bolus/infusion of ^{123}I-PE2I.

All subjects were studied twice, on 2 separate days. To block thyroidal uptake of free radioiodine, we gave 200 mg of potassium perchloride intravenously to all subjects 30 min before the ^{123}I-PE2I injection. In the first experiment, an average bolus of 138.3 MBq (range, 128.5–144.4 MBq) of ^{123}I-PE2I (MAP Medical Technologies) was administrated intravenously to all subjects. Tracer was delivered over a period of 10 s. Twenty-one sequential scan frames were acquired from 0 to 180 min after bolus injection. The frame durations were 6 × 5 min and 15 × 10 min. Great care was taken to ensure that each subject was aligned in the same position during the whole scan session by placing the subject's head within a support. A cannula was inserted into the radial artery for arterial blood sampling. Thirty-six arterial blood samples were collected from 0 to 180 min after bolus injection. During the first 2 min, 12 arterial blood samples were collected; from 2 to 35 min, 10 arterial blood samples were collected; and from 35 to 175 min, arterial blood samples were collected every 10 min. Octanol was extracted from the plasma to derive the lipophilic phase containing ^{123}I-PE2I (*7*). One milliliter of plasma and 2 mL of octanol were shaken for 2 min, and then 1 mL of the octanol phase was pipetted into another counting vial. The activity in the octanol phase, multiplied by 2, thus represented parent ^{123}I-PE2I. In the bolus-infusion experiments, conducted more than 3 wk later, an average bolus of 73.9 MBq (range, 63–93.8 MBq) of ^{123}I-PE2I was followed by a constant infusion of ^{123}I-PE2I for 3 h. The bolus-to-infusion ratio was 2.7 h (range, 2.6–2.8 h). In all experiments, the specific radioactivity was greater than 8.7 TBq/μmol. Eighteen sequential 10-min scan frames were collected from 60 to 240 min after tracer injection. Two cannulae were inserted into the cubital veins for tracer administration and venous blood sampling. Twenty-four venous blood samples were collected from 0 to 240 min after tracer injection. Metabolite correction was done. Plasma protein binding was not determined.

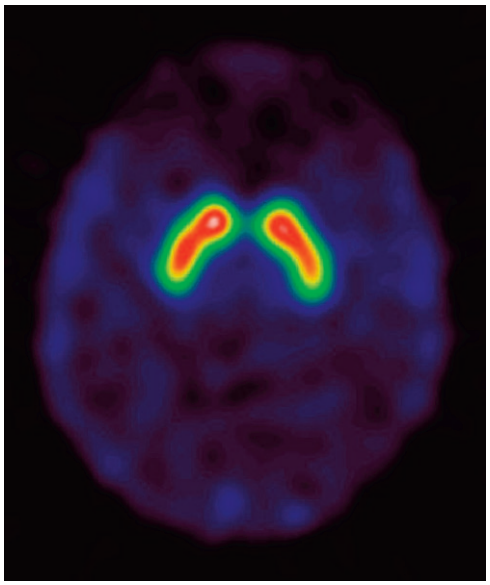

FIGURE 1. ^{123}I-PE2I SPECT image obtained from 2 to 3 h after tracer injection in healthy subject.

Regions of Interest (ROIs)

The individual bolus SPECT images and bolus/infusion SPECT images were manually aligned using software supplied with the scanner. Subsequently, the individual SPECT images were aligned on a voxel-by-voxel basis using a 3-dimensional automated 6-parameter rigid-body transformation (*10*). ROIs were drawn on the first frame of the bolus study and applied to all other frames, including the frames of the bolus/infusion study, thus generating time–activity curves for striatum and occipital cortex. ROIs were defined according to a standard anatomic atlas. To maximize the statistical quality of the SPECT data, we did not divide the striatum into smaller anatomic regions. The use of whole-striatum ROIs is not applicable in the study of Parkinson's disease and related

disorders because of the possibility of left/right and caudate/putamen asymmetry. In pathologic conditions, coregistration with MR images is beneficial for ROI delineation.

Derivation of Outcome Parameters

Derivation of outcome parameters was based on the 2-tissue-compartment model, which includes the metabolite-corrected plasma compartment (C_1, Bq/mL), the intracerebral nonspecifically bound compartment (C_2, Bq/mL), and the intracerebral specifically bound compartment (C_3, Bq/mL). K_1 (mL/mL/min) and k_2 (/min) denote the rate constants for transfer between C_1 and C_2; k_3 (/min) and k_4 (/min) denote the rate constants for transfer between C_2 and C_3; f_1 (unitless) is the fraction of C_1 free to transfer between C_1 and C_2; and f_2 (unitless) is the fraction of C_2 free to transfer between C_2 and C_1 or C_2 and C_3. Because of the overall physicochemical constancy of brain tissue, the concentration of tracer in C_2 is often assumed to equal the concentration of tracer in an ROI devoid of receptors (C_{ref}).

We defined 2 outcome parameters, BP_1 and BP_2. The transfer of tracer between compartments can be described by a set of 1-order differential equations. A similar set of equations can be written for the simple bimolecular association of a ligand with its receptor. Combining these sets of equations defines BP_1 (unitless) and BP_2 (unitless) in terms of steady-state concentrations of tracer in compartments, rate constants, and binding parameters:

$$BP_1 = \frac{C_3(\infty)}{C_1(\infty)} = \frac{K_1}{k_2}\frac{k_3}{k_4} = BP\ f_1, \qquad \text{Eq. 1}$$

$$BP_2 = \frac{C_3(\infty)}{C_2(\infty)} = \frac{k_3}{k_4} = BP\ f_2. \qquad \text{Eq. 2}$$

$C_1(\infty)$, $C_2(\infty)$, and $C_3(\infty)$ denote the steady-state radiotracer concentration in compartments. SPECT measures the total concentration of radiotracer in the brain (C_{tot}). Because of the overall physicochemical constancy of brain tissue, $C_2(\infty)$ is assumed to equal the concentration of tracer in an ROI devoid of receptors ($C_{ref}(\infty)$), and $C_3(\infty)$ is calculated as $C_{tot}(\infty) - C_{ref}(\infty)$.

The terms BP_1 and BP_2 are the BP of Mintun et al. (1984) (*11*) containing f_1 and f_2, respectively. Those authors used the non–protein-bound fraction of C_1 as a representation of f_1 and calculated f_2 from cerebellar data (assuming $C_{ref} = C_2$) and the measured value of f_1. BP is equal to the ratio of B'_{max} to K_d. B'_{max} (mmol/L) is the concentration of sites available for binding, and K_d (mmol/L) is the affinity constant of the tracer.

Bolus data were analyzed using graphical analysis (*12,13*), kinetic analysis (*14*) with the simplified reference tissue model (*15,16*), peak equilibrium analysis (*17*), and transient equilibrium analysis (*18*). Graphical analysis and kinetic analysis were performed using PMOD version 2.5 (PMOD Technologies). Striatal Logan plots were linear starting at 44 min (range, 30–60 min), and striatal Logan plots using occipital cortex as a representation of the input function were linear starting at 42 min (range, 40–50 min). The 2-tissue-compartment model (mean Akaike information criterion = 57 [range, 46–70]) gave better fits than did the 1-tissue-compartment model (mean Akaike information criterion = 86 [range, 77–96]). The full reference tissue model (*16*) and the simplified reference tissue model (*15*) provided practically identical Akaike information criterion values ($P > 0.12$, paired Student t test) and BP_2 values ($P > 0.26$, paired Student t test). Peak equilibrium analysis was done from 40 to 80 min. This period was based on the range of individual peak times for striatum-specific binding. For calculation of BP_1, the average ^{123}I-PE2I plasma concentration from 40 to 80 min was used. The transient equilibrium analysis was done from 90 to 180 min. The terminal elimination rate constant (a_3) associated with the slowest component of the bolus arterial input curve was determined for each subject. Linear regression analyses were done on logarithmic metabolite-corrected arterial input data from 105 to 175 min. Individual bolus-to-infusion ratios were calculated as $-1/a_3$ (in hours) as previously described (*19*).

RESULTS

Bolus Studies

Figure 2A shows the average time–activity curve for parent compound in arterial plasma. The individual bolus-to-infusion ratios ranged from 1.8 to 3.7 h (Table 1). The 95% confidence intervals for the individual a_3 values were large, and in subject 4 the SE of a_3 was comparable in size to a_3. The 95% confidence intervals of the individual bolus-to-infusion ratios (Table 1) were calculated from the 95% confidence intervals of a_3. An average bolus-to-infusion ratio of 2.5 h was calculated from average a_3 values. This bolus-to-infusion ratio is ideal for attaining a sustained steady state in plasma. We chose to increase the bolus-to-infusion ratio slightly—to 2.7 h—for faster steady-state attainment in the DAT-rich striatal ROI.

Figure 2B shows the average time–activity curves from striatum and occipital cortex. Striatal time–activity curves peaked between 15 and 21 min, and occipital cortex time–activity curves peaked between 3 and 9 min. Striatum-specific binding (striatum – occipital cortex) peaked between 45 and 75 min.

Figures 2C and 2D show the average ratio of striatum-specific binding to metabolite-corrected plasma and the average ratio of striatum-specific binding to occipital cortex, respectively, as a function of time. Starting approximately 90 min after bolus injection, the curves became horizontal.

Figure 3 shows the mean normalized BP_1 and BP_2 values as a function of time after bolus injection of tracer. For each subject, $BP_1(t)$ and $BP_2(t)$ were calculated by deleting a progressive number of frames from the end of the study. For each subject, $BP_1(t)$ and $BP_2(t)$ were normalized to the individual outcome measure calculated at 180 min (using the maximal number of data points). Except for the BP_1 value at 90 min, normalized BPs using kinetic analysis were greater than 90% of the final values from 65 min after ^{123}I-PE2I bolus injection. With the kinetic analysis, the SDs of normalized BP_1 were, however, larger than those obtained with the Logan analysis. The SDs of normalized BP_2, conversely, were comparable to those obtained with the Logan analysis except for the value at 65 min. In contrast to kinetic analysis, with Logan analysis the SDs of the average normalized BPs were less than 10% of the average normalized BP. However, for the Logan approach to be accurate, the acquisition time must be extended beyond 90 min for normalized BPs to be larger than 90% of the final values.

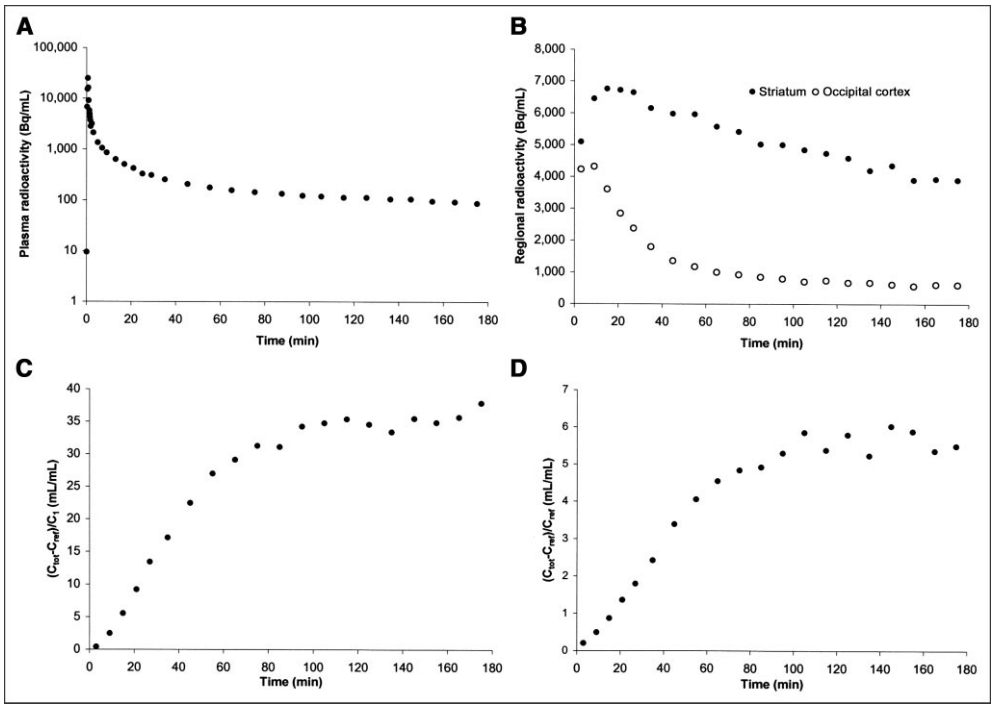

FIGURE 2. Average ^{123}I-PE2I bolus data: time course for metabolite-corrected plasma radioactivity (A), time course for striatum and occipital cortex radioactivity (B), time course for $(C_{tot} - C_{ref})/C_1$ (C), and time course for $(C_{tot} - C_{ref})/C_{ref}$ (D).

The individual and average outcome parameters are listed in Tables 2 and 3. Average striatal BP_1 and BP_2 values as calculated with kinetic analysis were 21.1 ± 1.1 and 4.1 ± 0.4, respectively. Compared with kinetic analyses, Logan analysis underestimated BP_1 by 11% ± 5% ($P < 0.02$, paired Student t test) and BP_2 by 3% ± 4% ($P < 0.18$, paired Student t test). Compared with kinetic analyses, transient equilibrium analyses overestimated BP_1 by 170% ± 20% ($P < 0.002$, paired Student t test) and BP_2 by 136% ± 8% ($P < 0.0002$, paired Student t test). Compared with kinetic analyses, peak equilibrium analyses overestimated BP_1 by 133% ± 21% ($P < 0.025$, paired Student t test) and BP_2 by 102% ± 7% ($P < 0.5$, paired Student t test). The distribution volume equaled the steady-state ratio of tissue

TABLE 1
Stability of Outcome Measures, Free Parent Compound, and Individual Optimal Bolus-to-Infusion Ratio

	Bolus/infusion experiments			Bolus experiments	
Subject no.	BP_1 (%/h)	BP_2 (%/h)	Plasma (%/h)	B/I ratio (h)	Confidence interval (h)
1	−0.1	−4.0	4.2	3.7	2.4–8.5
2	6.8*	2.2	−7.2*	2.4	1.3–12.8
3	−3.1	−6.6	−2.8	3.1	2.8–3.6
4	2.8	2.1	−3.4	2.6	1.3–214.0
5	−6.6	−3.1	−4.2	1.8	1.2–4.0
Average ± SD	−0.0 ± 5.2	−1.9 ± 3.9	−1.6 ± 4.9	2.7 ± 0.7	

*Slope of regression line calculated from 120 to 240 min is significantly different from zero ($P < 0.05$). BP_1, BP_2, and plasma stability measures were calculated from bolus/infusion data. Individual bolus-to-infusion ratios and corresponding 95% confidence intervals were calculated from terminal clearance rate from plasma after bolus injection of ^{123}I-PE2I.

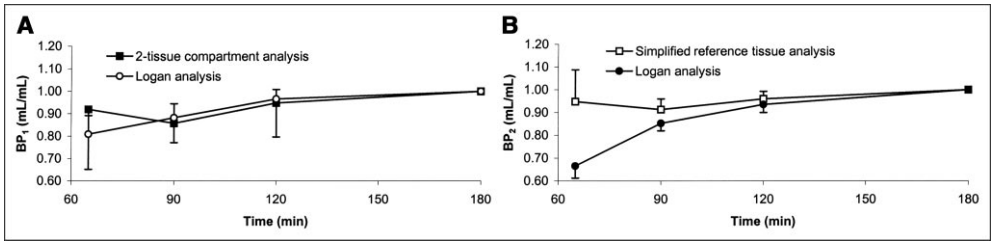

FIGURE 3. (A) Average (with SD) normalized $BP_1(t)$ in striatum calculated using 2-tissue-compartment analysis and Logan analysis with metabolite-corrected plasma as input function. (B) Average (with SD) normalized $BP_2(t)$ in striatum calculated using simplified reference tissue analysis and Logan analysis with occipital cortex as input function. Normalization was performed by dividing value at each time point by value at 180 min. For each method of analysis, average BP_1 and BP_2 were calculated by deleting a progressive number of frames from end of study.

to plasma parent activity and was calculated as $K_1/k_2(1 + k_3/k_4)$ using kinetic analysis. The average striatal distribution volume was 25.9 ± 1.4 mL/mL, and the average occipital cortex distribution volume was 5.0 ± 0.5 mL/mL. In subjects 1–5, the transfer rates from the tissue compartment to plasma (/min) were 0.016 ± 0.001, 0.009 ± 0.001, 0.014 ± 0.001, 0.009 ± 0.001, and 0.011 ± 0.001.

Bolus/Infusion Studies

In Figure 4, each data point represents the mean value of the 5 subjects studied with the average bolus-to-infusion ratio of 2.7 h (Table 1). The average time–activity curves (Figs. 4A and 4B) and outcome measures (Figs. 4C and 4D) plateaued approximately 100–120 min after tracer injection. The stability of the individual time–activity curves and outcome measures was calculated as the slope (linear regression analysis from 120 to 240 min) divided by the average value from 120 to 240 min multiplied by 100%. According to Table 1, individual BP_1, BP_2, and metabolite-corrected plasma radioactivity were stable from 120 to 240 min, with an hourly change of no more than 10%. Except for subject 2, the slopes of the plasma, BP_1, and BP_2 regression lines from 120 to 240 min were not significantly different from zero, but even in this subject, BP_1 and BP_2 were similar to values calculated using kinetic analysis. The individual and average outcome parameters are listed in Tables 2 and 3. Average striatal BP_1 and BP_2 values as calculated with bolus/infusion analysis were 21.0 ± 1.2 and 4.3 ± 0.3, respectively. There was no significant difference between BP_1 calculated using 2-tissue-compartment analysis compared with bolus/infusion analysis (paired Student *t* test, $P > 0.8$, Table 2) and BP_2 calculated using simplified reference tissue analysis compared with bolus/infusion analysis (paired Student *t* test, $P > 0.3$, Table 3). For bolus/infusion analysis, we tested time points ranging from 120 to 180 min and from 180 to 240 min. The average striatal distribution volume was 25.9 ± 1.3 mL/mL, and the average occipital cortex distribution volume was 4.9 ± 0.3 mL/mL.

DISCUSSION

So far, ^{123}I-PE2I has proven to be the ligand with the most favorable in vitro (*1*) and in vivo (*2*) characteristics for DAT quantification in humans using SPECT. The aim of the present study was to describe a method combining accurate, precise quantification of ^{123}I-PE2I binding to DAT and easy implementation in a clinical setting. By conducting the bolus and the bolus/infusion studies on the same subjects, we could eliminate the variation in DAT density that is due to genetic and environmental differences between subjects.

TABLE 2
BP_1 Values Calculated Using 5 Different Methods of Quantification

Subject no.	Bolus/infusion experiments (120–180 min)	Bolus experiments			
		Kinetic analysis (0–180 min)	Logan analysis (0–180 min)	Peak equilibrium (40–80 min)	Transient equilibrium (90–180 min)
1	22.9	21.8	20.4	26.4	31.5
2	20.7	19.8	18.3	31.7	34.0
3	20.6	20.9	19.2	26.0	34.0
4	21.3	20.7	18.1	30.9	41.1
5	19.6	22.6	18.2	24.4	39.0
Average ± SD	21.0 ± 1.2	21.1 ± 1.1	18.8 ± 1.0	27.9 ± 3.2	35.9 ± 4.0

BP_1 was calculated using Equation 1. Peak equilibrium and transient equilibrium were not calculated at tracer steady state.

TABLE 3
BP_2 Values Calculated Using 5 Different Methods of Quantification

Subject no.	Bolus/infusion experiments (120–180 min)	Bolus experiments			
		Reference tissue (0–180 min)	Logan analysis (0–180 min)	Peak equilibrium (40–80 min)	Transient equilibrium (90–180 min)
1	4.6	4.6	4.6	4.8	6.0
2	4.6	4.1	3.7	3.8	5.5
3	4.4	4.3	4.2	4.5	5.5
4	4.0	4.2	4.2	4.7	6.0
5	3.9	3.6	3.5	3.5	5.2
Average ± SD	4.3 ± 0.3	4.1 ± 0.4	4.0 ± 0.4	4.3 ± 0.6	5.6 ± 0.4

BP_2 was calculated using Equation 2. Peak equilibrium and transient equilibrium were not calculated at tracer steady state.

Transient Equilibrium Analysis and Peak Equilibrium Analysis

We found that striatum and occipital cortex time–activity curves peaked within 30 min and that the ratio of striatum-specific binding to nonspecific binding stabilized at an average value of 5.6 ± 0.5 approximately 90 min after ^{123}I-PE2I bolus injection. For comparison, the ratio of striatum-specific binding to nonspecific binding of ^{123}I-FP-CIT, an *N*-fluoropropyl analogue of β-CIT, stabilizes at a value of 2.5 ± 0.6 after approximately 180 min (*20,21*). However, our findings suggest that if transient equilibrium analysis is to be used to calculate DAT density after bolus injection of tracer, ^{123}I-PE2I is preferable to ^{123}I-FP-CIT in terms of both total study time and

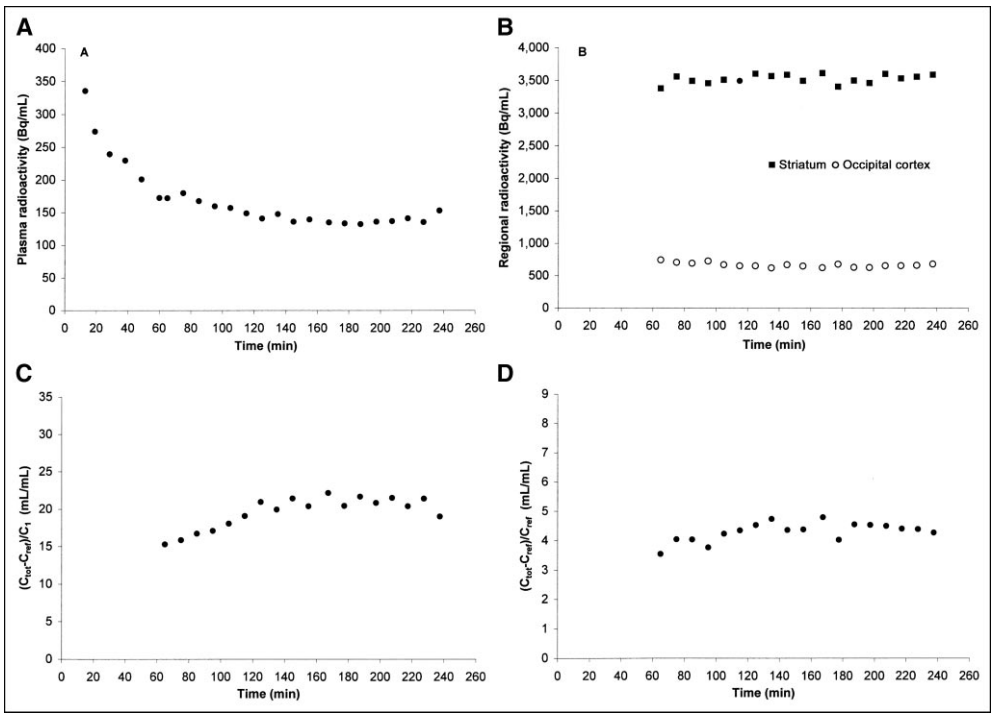

FIGURE 4. Average ^{123}I-PE2I bolus/infusion data: time course for metabolite-corrected plasma radioactivity (A), time course for striatum and occipital cortex radioactivity (B), time course for $(C_{tot} - C_{ref})/C_1$ (C), and time course for $(C_{tot} - C_{ref})/C_{ref}$ (D).

target-to-background ratio. In addition, PE2I has the advantage of being selective for DAT.

In a clinical context, transient equilibrium analysis is easy with respect to tracer administration, data acquisition, and data analysis. However, in addition to transporter/receptor BP, simple tissue-to-blood ratios and tissue-to-tissue ratios calculated at transient equilibrium will reflect the terminal clearance rate from plasma (*18*). According to Table 1, the interindividual variability in the bolus-to-infusion ratios is not negligible (2.7 ± 0.7 h). Furthermore, the terminal clearance rate of ^{123}I-PE2I from plasma is comparable to the transfer rate from the tissue compartment to plasma. Thus, transient equilibrium analysis of ^{123}I-PE2I bolus data overestimates BP_1 and BP_2 values significantly, and BP_1 SEM is large compared with the outcome of a kinetic analysis. In such cases, distinguishing between a normal and a pathologic DAT BP will be more difficult, thus reducing the usefulness of DAT scanning as a clinical tool.

There is no statistical difference between BP_2 calculated using peak equilibrium analysis (40–80 min) and BP_2 calculated using simplified reference tissue analysis, and the SEMs are also comparable. According to Figures 2C and 2D, outcome parameters using peak equilibrium analysis increase rapidly from 0 to 70–80 min, making identification of the correct acquisition period important. In theory, the correct acquisition time must be identified individually around the individual peak time of striatum-specific binding. In practice, a predefined experimentally determined acquisition period is often used. However, striatum-specific time–activity curves will peak earlier in subjects with low BPs than in subjects with high BPs. Thus, applying to Parkinson's disease patients an acquisition time defined in healthy volunteers is likely to overestimate the true BP. Therefore, dynamic acquisition is a sine qua non of peak equilibrium analysis if one is to obtain reliable and comparable BP estimates.

Kinetic Analysis and Logan Analysis

Kinetic analysis and Logan analysis of bolus data are considered gold standards for quantification of radioligand binding to synaptic molecules. Compared with kinetic modeling, Logan analysis is well known to underestimate BP because of the statistical bias associated with linear transformation of binding data (Tables 1 and 2) (*22*). The use of Logan analysis or kinetic analysis in clinical studies is hampered by the need for long study times and arterial blood sampling in case a suitable reference tissue does not exist. Figure 3 addresses the study time needed for accurate and precise quantification of ^{123}I-PE2I binding to DAT using kinetic analysis and Logan analysis. Kinetic analyses (simplified reference tissue analysis in particular) accurately quantify ^{123}I-PE2I binding to DAT starting approximately 60 min after bolus injection. However, for precise quantification of BP_2 using kinetic analysis, the acquisition time must be extended to 90 min. In contrast, Logan analysis precisely quantifies BP_1 and BP_2 starting approximately 60 min after bolus injection. However, for accurate quantification of ^{123}I-PE2I binding to DAT using Logan analysis, the total acquisition time must be at least 90 min after bolus injection. A 90-min total acquisition time after bolus injection of ^{123}I-PE2I is shorter than previously found (120 min) (*3*)—a fact that probably reflects the improved statistical quality of SPECT data using state-of-the-art hardware.

Bolus/Infusion Analysis

The limitations of the transient and peak equilibrium approaches related to nonsteady-state conditions in brain and plasma are overcome in bolus/infusion studies by administration of the tracer as a bolus followed by a constant infusion. As tracer steady state is attained in brain and plasma, the net flux of tracer between compartments becomes zero and the size of the compartments becomes constant, allowing the outcome parameters to be calculated as simple ratios. Several advantages with the bolus/infusion approach deserve consideration: Quantification of binding parameters is insensitive to changes in cerebral blood flow. For tracers without a suitable reference region, venous blood sampling replaces the more invasive arterial blood sampling. For drugs administered as a bolus plus constant infusion at pharmacologic doses, the acute effect on binding parameters may be calculated within a single scan session after a single radioligand synthesis. If scanning has to be aborted before the scheduled time because of patient discomfort or other causes, quantification of binding parameters may still be possible despite the reduced statistical quality of the data.

The bolus/infusion approach also has some disadvantages: To hasten steady state, a bolus of radiolabeled ligand must be administered, but the optimal bolus-to-infusion ratio required to hasten steady state may vary considerably because of differences in tracer clearance and receptor binding between individuals. In this study, individual bolus-to-infusion ratios ranged from 1.8 to 3.7 h (Table 1), and a bolus-to-infusion ratio of 2.7 h was used in all subsequent bolus/infusion studies. For fast attainment of steady state in plasma, a bolus-to-infusion ratio of 2.5 h ($-1/\text{average}(a_3)$) would have been ideal. To hasten attainment of steady state in striatum, we increased the bolus-to-infusion ratio from 2.5 to 2.7 h. Post hoc computer simulations based on the bolus data suggested that a bolus-to-infusion ratio of 2.9 h would have more rapidly attained stable striatal BP_1 and BP_2 values. However, the average experimental data imply that a bolus-to-infusion ratio of 2.7 h quickly attains stable striatal ^{123}I-PE2I concentrations (Fig. 4B), with a modest overshoot in the plasma (Fig. 4A) and occipital cortex (Fig. 4B) ^{123}I-PE2I concentrations. Further increasing the bolus-to-infusion ratio and, thus, the overshoot in occipital cortex and plasma is likely to slow the attainment of stable values for BP_1 (Fig. 4C) and BP_2 (Fig. 4D). The size and sign of the percentage change in plasma ^{123}I-PE2I concentrations per hour were in agreement with the individual bolus-determined optimal bolus-to-infusion ratios. For BP_1 and BP_2, the percentage change per hour, compared with the individual bolus-determined optimal bolus-to-infusion ratio, was

less consistent with expectations. However, in all subjects, individual BP_1, BP_2, and metabolite-corrected plasma radioactivity were stable (defined as a change of no more than 10%/h) from 120 to 240 min after bolus/infusion of ^{123}I-PE2I, and BP_1 and BP_2 values calculated using bolus/infusion analysis were not significantly different from values calculated using kinetic analysis. This finding is remarkable considering the range of individual bolus-to-infusion ratios. However, as discussed in the Appendix, computer simulations demonstrate that a 2-fold variation in terminal clearance rate from plasma translates into only a 10% variation in the BPs calculated from 120 to 180 min. Furthermore, estimated a_3 values are calculated from the noisy terminal part of the metabolite-corrected plasma time–activity curve, and the 95% confidence intervals are large. Thus, the individual "true" a_3 values may be more similar than is indicated by the estimated a_3 values. Comparing the individual size of BP_1 calculated using transient equilibrium analysis ($K_1/(k_2 + a_3)$) (*18*) with the individual size of BP_1 calculated using kinetic analysis (K_1/k_2) supports this idea.

CONCLUSION

Graphical analysis and kinetic analysis quantify ^{123}I-PE2I-bolus data both accurately and precisely. However, in a clinical setting, a total scan time of 90 min may be too inconvenient. With respect to experimental simplicity, transient equilibrium analysis is an attractive and widely used method in nuclear medicine. However, for PE2I and many other ligands with terminal clearance rates from plasma comparable to the transfer rates from the tissue compartment, clinical feasibility is hampered by low accuracy and significantly reduced precision. According to our data from healthy volunteers, peak equilibrium analysis allows accurate, precise calculation of BP_2. However, accuracy and precision depend on precise identification of the peak time of specific binding, because the apparent BP_2 value doubles from 40 to 80 min. Thus, in patients with changes in DAT density, total time spent in the scanner must be increased to identify individual peak times. The bolus/infusion approach quantifies ^{123}I-PE2I bolus/infusion data both accurately and precisely. According to experimental data and computer simulations, individual differences in terminal clearance rates from plasma do not affect outcome parameters after 120 min of constant ^{123}I-PE2I infusion. Some may consider the need for a constant infusion of tracer to be an important limitation for clinical studies. In our experience, the increase in experimental complexity is small compared with the advantages of the bolus/infusion approach. We have implemented the bolus/infusion approach for clinical studies of DAT using ^{123}I-PE2I SPECT.

APPENDIX

It is possible to simulate the outcome of a bolus/infusion study using the kinetic parameters calculated from a bolus-

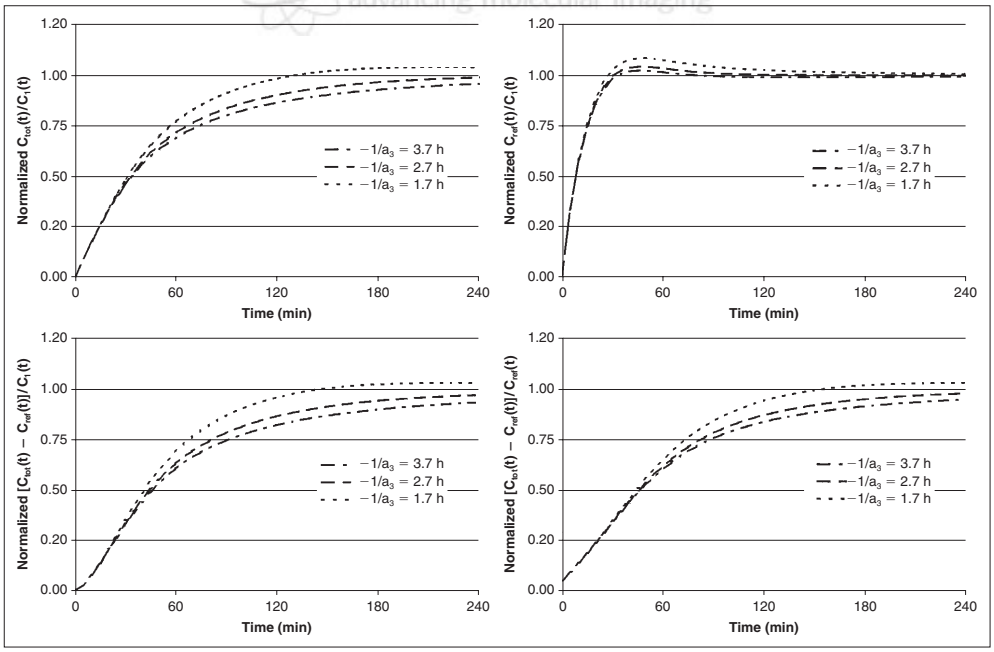

FIGURE 1A. Computer simulations of outcome parameters after bolus plus constant infusion of radiotracer. See text for details.

alone study (*23*). The bolus input function is approximated to a sum of 3 exponential functions ($\sum_{i=1}^{3} A_i e^{a_i t}$), and in the 1-tissue-compartment situation, K_1 and k_2 values are calculated using kinetic analysis:

$$C_1(t) = \sum_{i=1}^{3} A_1\left(\left(B/I - \frac{1}{-a_i}\right)e^{a_i t} + \frac{1}{-a_i}\right), \quad \text{Eq. 1A}$$

$$C_{tot}(t) = \sum_{i=1}^{3} A_i\left(\left(B/I - \frac{1}{-a_i}\right)\frac{K_1}{k_2 + a_i}(e^{a_i t} - e^{-k_2 t}) + \frac{1}{-a_i}\frac{K_1}{k_2}(1 - e^{-k_2 t})\right), \quad \text{Eq. 2A}$$

$$C_{ref}(t) = \sum_{i=1}^{3} A_i\left(\left(B/I - \frac{1}{-a_i}\right)\frac{K_1^{ref}}{k_2^{ref} + a_i}(e^{a_i t} - e^{-k_2^{ref} t}) + \frac{1}{-a_i}\frac{K_1^{ref}}{k_2^{ref}}(1 - e^{-k_2^{ref} t})\right), \quad \text{Eq. 3A}$$

where B/I (h) is the bolus-to-infusion ratio, A_i (unitless) is the relative zero intercept of each exponential, and a_i (/min) is the elimination rate constant associated with each exponential. Figure 1A shows simulated outcome parameters from 0 to 240 min. Outcome parameters are calculated using Equations 1A–3A. Total distribution volume = $C_{tot}(t)/C_1(t)$, reference distribution volume = $C_{ref}(t)/C_1(t)$, $BP_1(t) = (C_{tot}(t) - C_{ref}(t))/C_1(t)$, and $BP_2(t) = (C_{tot}(t) - C_{ref}(t))/C_{ref}(t)$. Values have been normalized with the individual steady-state values. In all situations, B/I = 2.7 h, $a_1 = -0.6$/min, $a_2 = -0.06$/min, $K_1 = 0.42$ mL/mL/min, $k_2 = 0.016$/min, $K_1^{ref} = 0.35$ mL/mL/min, and $k_2^{ref} = 0.068$/min. Individual curves represent situations with different terminal clearance rates from plasma (a_3). In the keys, the individual a_3 value is expressed as $-1/a_3$ (h), representing the individual optimal bolus-to-infusion ratio. The simulations demonstrate 2 important points on the use of the bolus/infusion approach. First, calculations of BP_1 and BP_2 using a population-based average bolus-to-infusion ratio are clearly vulnerable to individual differences in terminal clearance rate from plasma. However, the vulnerability decreases with time. From 120 to 180 min, the average normalized BP_1 values are 1.01 ($-1/a_3$ = 1.7 h), 0.92 ($-1/a_3$ = 2.7 h), and 0.87 ($-1/a_3$ = 3.7 h) and the average normalized BP_2 values are 0.99 ($-1/a_3$ = 1.7 h), 0.92 ($-1/a_3$ = 2.7 h), and 0.88 ($-1/a_3$ = 3.7 h). Thus, a 2.2-fold variation in terminal clearance rate from plasma translates into only a 10% variation in the calculated BPs. Second, to hasten attainment of steady-state BPs, it is beneficial to increase the bolus-to-infusion ratio beyond the value calculated from the average a_3 value.

ACKNOWLEDGMENTS

We thank Gerda Thomsen, Karin Stahr, Inge Møller, and Anja Pedersen for expert technical assistance. This work was supported by the Danish Health Research Council, the 1991 Pharmacy Foundation Health Insurance Fund, the Lundbeck Foundation, the Elsass Foundation, and the University of Copenhagen.

REFERENCES

1. Emond P, Garreau L, Chalon S, et al. Synthesis and ligand binding of nortropane derivatives: N-substituted 2beta-carbomethoxy-3beta-(4′-iodophenyl)nortropane and N-(3-iodoprop-(2E)-enyl)-2beta-carbomethoxy-3beta-(3′,4′-disubstituted phenyl)nortropane—new high-affinity and selective compounds for the dopamine transporter. *J Med Chem.* 1997;40:1366–1372.
2. Halldin C, Erixon-Lindroth N, Pauli S, et al. [(11)C]PE2I: a highly selective radioligand for PET examination of the dopamine transporter in monkey and human brain. *Eur J Nucl Med Mol Imaging.* 2003;30:1220–1230.
3. Kuikka JT, Baulieu JL, Hiltunen J, et al. Pharmacokinetics and dosimetry of iodine-123 labelled PE2I in humans, a radioligand for dopamine transporter imaging. *Eur J Nucl Med.* 1998;25:531–534.
4. Pinborg LH, Videbaek C, Svarer C, Yndgaard S, Paulson OB, Knudsen GM. Quantification of [(123)I]PE2I binding to dopamine transporters with SPET. *Eur J Nucl Med Mol Imaging.* 2002;29:623–631.
5. Prunier C, Payoux P, Guilloteau D, et al. Quantification of dopamine transporter by ^{123}I-PE2I SPECT and the noninvasive Logan graphical method in Parkinson's disease. *J Nucl Med.* 2003;44:663–670.
6. Hall H, Halldin C, Guilloteau D, et al. Visualization of the dopamine transporter in the human brain postmortem with the new selective ligand [^{125}I]PE2I. *Neuroimage.* 1999;9:108–116.
7. Videbaek C, Knudsen GM, Bergstrom K, et al. Octanol extraction yields similar results as HPLC for quantitation of [^{123}I]PE2I metabolism [abstract]. *Eur J Nucl Med.* 1999;26:1139.
8. Poyot T, Conde F, Gregoire MC, et al. Anatomic and biochemical correlates of the dopamine transporter ligand ^{11}C-PE2I in normal and parkinsonian primates: comparison with 6-[^{18}F]fluoro-L-dopa. *J Cereb Blood Flow Metab.* 2001;21:782–792.
9. Prunier C, Bezard E, Montharu J, et al. Presymptomatic diagnosis of experimental Parkinsonism with ^{123}I-PE2I SPECT. *Neuroimage.* 2003;19:810–816.
10. Woods RP, Cherry SR, Mazziotta JC. Rapid automated algorithm for aligning and reslicing PET images. *J Comput Assist Tomogr.* 1992;16:620–633.
11. Mintun MA, Raichle ME, Kilbourn MR, Wooten GF, Welch MJ. A quantitative model for the in vivo assessment of drug binding sites with positron emission tomography. *Ann Neurol.* 1984;15:217–227.
12. Logan J, Fowler JS, Volkow ND, et al. Graphical analysis of reversible radioligand binding from time-activity measurements applied to [N-^{11}C-methyl]-(−)-cocaine PET studies in human subjects. *J Cereb Blood Flow Metab.* 1990;10:740–747.
13. Logan J, Fowler JS, Volkow ND, Wang GJ, Ding YS, Alexoff DL. Distribution volume ratios without blood sampling from graphical analysis of PET data. *J Cereb Blood Flow Metab.* 1996;16:834–840.
14. Koeppe RA, Holthoff VA, Frey KA, Kilbourn MR, Kuhl DE. Compartmental analysis of [^{11}C]flumazenil kinetics for the estimation of ligand transport rate and receptor distribution using positron emission tomography. *J Cereb Blood Flow Metab.* 1991;11:735–744.
15. Lammertsma AA, Hume SP. Simplified reference tissue model for PET receptor studies. *Neuroimage.* 1996;4:153–158.
16. Hume SP, Myers R, Bloomfield PM, et al. Quantitation of carbon-11-labeled raclopride in rat striatum using positron emission tomography. *Synapse.* 1992;12:47–54.
17. Farde L, Eriksson L, Blomquist G, Halldin C. Kinetic analysis of central [^{11}C]raclopride binding to D_2-dopamine receptors studied by PET: a comparison to the equilibrium analysis. *J Cereb Blood Flow Metab.* 1989;9:696–708.
18. Carson RE, Channing MA, Blasberg RG, et al. Comparison of bolus and infusion methods for receptor quantitation: application to [^{18}F]cyclofoxy and positron emission tomography. *J Cereb Blood Flow Metab.* 1993;13:24–42.
19. Pinborg LH, Adams KH, Svarer C, et al. Quantification of 5-HT2A receptors in the human brain using [^{18}F]altanserin-PET and the bolus/infusion approach. *J Cereb Blood Flow Metab.* 2003;23:985–996.
20. Booij J, Bergmans P, Winogrodzka A, Speelman JD, Wolters EC. Imaging of dopamine transporters with [^{123}I]FP-CIT SPECT does not suggest a significant effect of age on the symptomatic threshold of disease in Parkinson's disease. *Synapse.* 2001;39:101–108.
21. Booij J, Hemelaar TG, Speelman JD, de Bruin K, Janssen AG, van Royen EA. One-day protocol for imaging of the nigrostriatal dopaminergic pathway in Parkinson's disease by [^{123}I]FPCIT SPECT. *J Nucl Med.* 1999;40:753–761.
22. Slifstein M, Laruelle M. Effects of statistical noise on graphic analysis of PET neuroreceptor studies. *J Nucl Med.* 2000;41:2083–2088.
23. Pinborg LH, Videbaek C, Knudsen GM, et al. Dopamine D(2) receptor quantification in extrastriatal brain regions using [(123)I]epidepride with bolus/infusion. *Synapse.* 2000;36:322–329.

Original article

Reproducibility of [^{123}I]PE2I binding to dopamine transporters with SPECT

Morten Ziebell[1], Gerda Thomsen[1], Gitte M. Knudsen[1], Robin de Nijs[1], Claus Svarer[1], Aase Wagner[2], Lars H. Pinborg[1]

[1] Neurobiology Research Unit, Rigshospitalet, N9201, 9 Blegdamsvej, Copenhagen, 2100, Denmark
[2] Diagnostic Radiology, University Hospital Rigshospitalet, Copenhagen, Denmark

Received: 1 November 2005 / Revised: 11 April 2006 / Accepted: 30 April 2006 / Published online: 29 July 2006

Abstract. *Purpose:* The iodinated cocaine derivative [^{123}I]PE2I is a new selective ligand for in vivo studies of the dopamine transporter (DAT) with SPECT. Recently, a bolus/infusion (B/I) protocol for [^{123}I]PE2I measurements of DAT density was established [Pinborg LH et al. *J Nucl Med* 2005;46:1119–271]. The aims of this study were, firstly, to evaluate the test–retest variability using the B/I protocol and, secondly, to evaluate the B/I approach in a new group of healthy subjects using two outcome parameters, BP_1 (C_{ROI}/C_{plasma}) and BP_2 (C_{ROI}/C_{REF}).
Methods: Seven healthy subjects were subjected to [^{123}I]PE2I SPECT scanning twice. For both studies, the two outcome parameters BP_1 and BP_2 were calculated based on two different methods for region of interest (ROI) delineation, namely manual delineation and probability map-based automatic delineation with MRI co-registration.
Results: With manual delineation, striatal test–retest variability (absolute difference between first and second scan as a percentage of the mean) of BP_1 and BP_2 was 13.9% (range 1.8–35.7%) and 4.1% (range 0.5–9.7%) respectively. The probability map-based automatic delineation resulted in striatal test–retest variability of 17.2% (range 4.3–40.5%) and 5.2% (range 0.1–10.9%) respectively. The B/I approach provided stable brain activity from 120 to 180 min post injection in both high- and low-count regions with a mean % change/hour in striatal BP_2 of 10.6.
Conclusion: [^{123}I]PE2I SPECT with the B/I approach yields a highly reproducible measure of striatal dopamine transporter binding. The appropriateness of a B/I protocol with a B/I ratio of 2.7 h (i.e. with a bolus worth 2.7 h of infusion) was confirmed in an independent sample of healthy subjects.

Morten Ziebell (✉)
Neurobiology Research Unit,
Rigshospitalet,
N9201, 9 Blegdamsvej,,
Copenhagen, 2100, Denmark
e-mail: ziebell@nru.dk
Tel.: +45-354-56713

Keywords: [^{123}I]PE2I – Dopamine transporters – SPECT – Reproducibility – Bolus/infusion

Eur J Nucl Med Mol Imaging (2007) 34:101–109
DOI 10.1007/s00259-006-0161-z

Introduction

The clinical features of idiopathic Parkinson's disease (IPD)—rigidity, tremor and bradykinesia—may also be present in other neurodegenerative diseases, and clinico-pathological correlations in patients diagnosed with IPD show that 10–20% have other diagnoses, e.g. Alzheimer's disease, vascular parkinsonism (vPD), drug-induced parkinsonism (dPD), essential tremor (ET), progressive supranuclear palsy (PSP) or multiple system atrophy (MSA) [2].

During the past decade, imaging of the dopamine transporter (DAT) has increasingly been used as a biomarker for the integrity of presynaptic dopaminergic nerve cells in patients with movement disorders [2–8]. In clinical practice, DAT imaging with SPECT is an important tool to assist in the clinical diagnosis of IPD and other neurodegenerative diseases. In IPD, DAT imaging has consistently shown: (1) low striatal DAT density [5, 6, 9]; (2) side-to-side asymmetry, with greater losses in DAT density in the striatum contralateral to the clinically most affected side [5]; and (3) earlier onset of decline in DAT density in the putamen as compared with the caudate nucleus [5]. In patients with MSA and PSP, by contrast, the side-to-side asymmetry is less pronounced, and a more homogeneous loss of DAT binding takes place in the caudate nucleus and putamen [4, 9, 10].

PE2I is a cocaine derivative that is structurally related to other DAT tracers for SPECT, such as FP-CIT and β-CIT [11, 12]. PE2I is a highly selective ligand with fast kinetics and a high target to background ratio [1]. In a recent study, we compared in the same subjects different methods for quantification of [^{123}I]PE2I DAT binding [1], both following bolus alone and following bolus plus constant

tracer infusion. We concluded that the bolus/infusion (B/I) approach is superior to a bolus alone study since it allows for accurate quantification of [^{123}I]PE2I binding and is easily implemented in a clinical setting [1].

The aims of the present study were to test the reproducibility and reliability of the B/I approach for quantification of [^{123}I]PE2I binding to DAT using BP_1 (C_{ROI}/C_{plasma}) and BP_2 (C_{ROI}/C_{REF}) as outcome parameters and, secondly, to test the feasibility of the previously described B/I protocol in a new sample.

Materials and methods

Subjects

For the reproducibility study, seven healthy subjects (age range 41–71 years, three males and four females) were studied twice, at intervals lasting from 7 to 21 days. The subjects were recruited from a local newspaper advertisement and were asked to complete a questionnaire before entering the study. None of the subjects had any history of neurological or psychiatric disorders, and they all claimed to be alcohol- and drug-free. Physical examinations and routine blood tests were normal in all subjects.

All subjects provided informed written consent. The study was performed in accordance with the ethical standards of the Declaration of Helsinki and was approved by the ethical committee of Copenhagen and Frederiksberg (KF 12–009/04).

Experimental procedures

Procedures were done according to Pinborg et al. [1], except that instead of taking 24 venous blood samples between time 0 and 240 min, only two samples were taken 150 min after injection. Cannulas were inserted into both cubital veins for tracer administration and blood sampling respectively. To block thyroidal uptake of free radioiodine, all subjects received 200 mg potassium perchloride intravenously 30 min before [^{123}I]PE2I injection. In all experiments an average bolus of 73.9 MBq (range 63–93.8 MBq) [^{123}I]PE2I was administered, immediately followed by a constant infusion of [^{123}I]PE2I for 3 h. The B/I protocol was similar in both studies, with a bolus worth 2.7 h (range 2.6–2.8 h) of infusion (the B/I ratio). As already mentioned, two separate venous blood samples were drawn at 150 min. Plasma was sampled from the blood, followed by octanol extraction to derive the lipophilic phase containing [^{123}I]PE2I [13]. One ml of plasma and 2 ml of octanol was shaken for 2 min, and then 1 ml of the octanol phase was pipetted into another counting vial. Finally the octanol fraction was counted in a γ-counter (Cobra II, Packard Instrument Company). The activity in the octanol phase multiplied by 2 thus represents parent [^{123}I]PE2I. Cross-calibration with a phantom containing a well-known concentration of [^{123}I]PE2I was done in order to enable comparison of activity measurements between the SPECT scanner and the γ-counter.

SPECT imaging was performed with a triple-head IRIX camera (Philips Medical, Cleveland, USA) fitted with low-energy, general-purpose, parallel-hole collimators (spatial resolution 8.5 mm at 10 cm). The mean radius of rotation was 13.9 cm. Each camera covered 120° of the circular orbit. Scans were performed in continuous mode with an angular step of 3° and 40 steps. Six SPECT acquisitions each of 10 min duration were obtained between 120 and 180 min post injection. Reconstruction of the images was performed with a MATLAB 6.5 (Mathworks)-based program in 128^2 matrices (2.33-mm pixels and identical slice thickness) using standard filtered back projection with a low-pass fourth-order Butterworth filter at 0.3 Nyquist (0.064 mm^{-1}). The images were subsequently corrected with an attenuation algorithm fitted to the individual head area using an attenuation coefficient with an empirical value of 0.10 cm_{-1}.

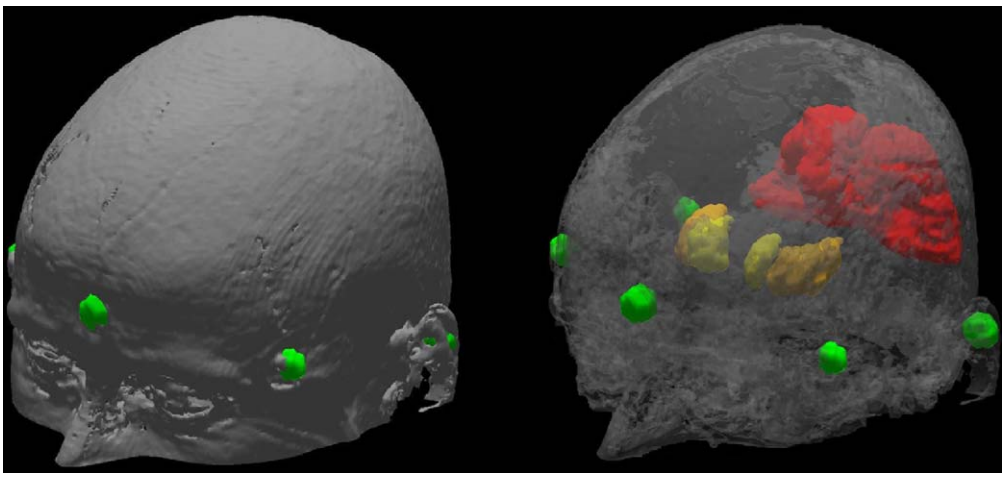

Fig. 1. 3D view of the semi-automatic co-registration. The *left side of the panel* shows the alignment of a subject's MR skull and the fiducial markers (green ROIs), visualised from a threshold SPECT image. In the *right panel*, the skull is visualised transparently, thus showing the volumes of interest [caudate nucleus (*yellow*), putamen (*orange*) and occipital cortex (*red*)] and the five external fiducials from the threshold SPECT image

Magnetic resonance imaging

All subjects underwent two structural magnetic resonance imaging (MRI) scans with a 1.5-T Vision scanner (Siemens, Erlangen, Germany) using the 3D MPRAGE sequence (TI/TD/TE/TR=300/300/4.4/11.4 ms, flip angle 12°) acquired as sagittal plane scans with a spatial resolution of 1.50×1.13×1.02 mm^3. There were 130 planes and the in-plane matrix was 230×256. MRI and SPECT scans were acquired on the same days. Co-registration of the MRI to the SPECT images was facilitated by the use of five external fiducials glued to the skin (a single one over the glabella, and one over the temple bone and one behind the ear, bilaterally). The fiducials were made of 5-mm-diameter plastic containers filled with olive oil and ^{99}Tc, thereby being visible on both MRI and SPECT (Fig. 1).

Regions of interest

The ROIs were applied to the SPECT images in two different ways: manually or probability map based. With the manual method, ROIs were manually delineated directly on the reconstructed SPECT images guided by the use of Kretschmann and Weinrich's Neuro-anatomical atlas [14]. The direct adaptation of ROI coordinates from the atlas required a reorientation of the reconstructed images to the canthomeatally oriented plane. ROIs were delineated on five consecutive slices (7 mm/slice) in a summed image from all six SPECT frames acquired from 120 to 180 min post injection. In order to mimic the SPECT DAT quantification used in daily clinical practice, a new set of ROIs were drawn for each scan event. With the second method the probability map-based automatic delineation approach developed by Svarer et al. [15] was used: Co-registration of MR and SPECT images was performed using a semi-automatic Matlab (Mathworks Inc., Natick, MA, USA) based method [16]. The corresponding external fiducial markers were manually identified and defined on the MR and SPECT images. A rigid transformation between the images was then estimated automatically by minimising the sum of squared errors between the defined points. This method was chosen as it has been demonstrated that automatic approaches such as the AIR and SPM99 methods [16, 17] are less optimal for alignment of MR and SPECT images with tracer binding confined to selected brain regions [16, 18], as is the case for [^{123}I]PE2I imaging. ROIs were subsequently identified automatically on the MR image and directly transferred to the co-registered SPECT image, as described by Svarer et al. [15]; with this probability map-based delineation approach, the putamen and caudate are identified separately. The probability map-based method includes ROIs covering the volume of the entire region whereas with the manually delineated method, striatal ROIs are calculated on the basis of two-

Table 1. Individual outcome parameters of the two tests. ROIs were manually delineated on SPECT acquisition (summed image from six consecutive frames from 120 to 180 min post injection)

Subject	1	2	3	4	5	6	7	Mean	SD	Reliability
Striatum BP_2										
Study 1	2.3	3.4	4.2	3.5	3.3	4.3	3.6	3.6	0.7	
Study 2	2.3	3.3	4.5	3.5	3.2	4.5	4.0	3.7	0.8	
Variability (%)	0.5	3.7	−7.0	−1.9	2.6	−3.3	−9.7	−2.2	5.4	0.96
ABS variability (%)	0.5	3.7	7.0	1.9	2.6	3.3	9.7	4.1	3.2	
Caudate nucleus BP_2										
Study 1	2.6	3.8	4.3	3.4	3.7	4.5	3.8	3.8	0.7	
Study 2	2.5	3.6	4.6	3.7	3.3	4.9	4.1	3.9	0.8	
Variability (%)	1.4	5.1	−6.4	−9.2	12.6	−6.5	−6.1	−1.3	8.0	0.95
ABS variability (%)	1.4	5.1	6.4	9.2	12.6	6.5	6.1	6.8	3.5	
Putamen BP_2										
Study 1	2.5	3.5	4.5	3.8	3.6	4.7	3.8	3.8	0.7	
Study 2	2.5	3.4	4.8	3.7	3.7	4.6	4.3	3.8	0.8	
Variability (%)	0.8	3.4	−7.1	4.2	−2.9	0.6	−11.9	−1.9	5.9	0.95
ABS variability (%)	0.8	3.4	7.1	4.2	2.9	0.6	11.9	4.4	4.0	
Striatum BP_1										
Study 1	14.5	13.9	19.9	16.3	18.8	23.8	–	18.6	4.0	
Study 2	15.4	19.9	20.3	18.9	23.0	24.9	–	21.9	3.8	
Variability (%)	−6.0	−35.7	−1.8	−14.7	−20.1	−4.8	–	−13.9	16.1	0.56
ABS variability (%)	6.0	35.7	1.8	14.7	20.1	4.8	–	13.9		
Caudate nucleus BP_1										
Study 1	16.1	15.5	19.5	18.6	19.7	25.1	–	19.1	3.4	
Study 2	17.0	21.9	21.4	21.0	24.9	25.4	–	21.9	3.0	
Variability (%)	−5.1	−34.3	−9.2	−12.3	−23.3	−1.2	–	−14.2	14.3	0.47
ABS variability (%)	5.1	34.3	9.2	12.3	23.3	1.2	–	14.2	13.2	
Putamen BP_1										
Study 1	15.6	14.3	22.0	16.4	20.2	24.8	–	18.9	4.1	
Study 2	16.5	20.6	21.1	18.4	23.8	26.7	–	21.2	3.7	
Variability (%)	−5.8	−35.9	4.2	−12.0	−16.2	−7.1	–	−12.1	13.5	0.69
ABS variability (%)	5.8	35.9	4.2	12.0	16.2	7.1	–	13.5	11.8	

ABS absolute

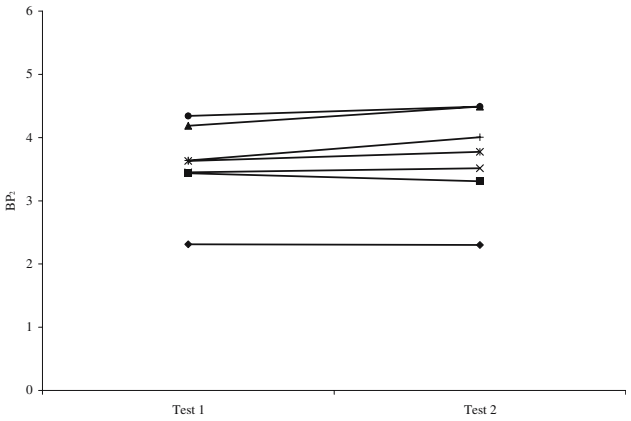

Fig. 2. Striatal BP_2 values from the first to the second scan showing inter-subject and intra-subject variation from the two experiments using manual delineation. No significant variation was found in BP_2 ($p>0.1$) from the first to the second scan using Student's paired *t* test

Table 2. Individual outcome parameters of the two tests. ROIs were delineated by a probability map-based semi-automatic approach on SPECT acquisition (summed image from six consecutive frames from 120 to 180 min post injection)

Subject	1	2	3	4	5	6	7	Mean	SD	Reliability
Striatum[a] BP_1										
Study 1	12.6	11.8	17.1	13.1	17.0	21.4	–	15.5	3.4	
Study 2	13.8	17.8	18.1	16.1	21.6	22.3	–	18.3	3.0	
Variability (%)	−8.9	−40.5	−5.2	−20.5	−23.6	−4.3	–	−17.2	12.7	0.58
ABS variability (%)	8.9	40.5	5.2	20.5	23.6	4.3		17.2	12.7	
Caudate nucleus BP_1										
Study 1	14.4	13.1	16.5	15.7	16.9	19.8	–	16.1	2.1	
Study 2	12.7	18.5	19.3	16.5	25.7	19.0	–	18.6	3.9	
Variability (%)	12.0	−33.8	−15.5	−4.5	−41.0	4.1	–	−13.1	19.2	0.23
ABS variability (%)	12.0	33.8	15.5	4.5	41.0	4.1		18.5	14.1	
Putamen BP_1										
Study 1	11.8	11.2	17.5	11.9	17.1	21.9	–	15.2	3.9	
Study 2	14.2	17.5	17.4	15.9	20.2	23.6	–	18.1	3.0	
Variability (%)	−18.8	−43.6	0.3	−28.2	−16.7	−7.2	–	−19.0	14.2	0.63
ABS variability (%)	18.8	43.6	0.3	28.2	16.7	7.2		19.2	14.0	
Striatum[a] BP_2										
Study 1	2.1	2.6	3.7	2.7	2.9	3.1	3.7	3.0	0.5	
Study 2	2.1	2.8	3.3	2.8	3.2	3.1	3.8	3.0	0.5	
Variability (%)	−0.1	−9.4	10.4	−2.5	−10.9	0.8	−2.1	−2.0	6.6	0.92
ABS variability (%)	0.1	9.4	10.4	2.5	10.9	0.8	2.1	5.2	4.5	
Caudate nucleus BP_2										
Study 1	2.4	2.9	3.8	2.6	3.5	3.1	3.5	3.1	0.5	
Study 2	2.0	2.9	3.9	3.0	3.3	3.7	3.2	3.1	0.6	
Variability (%)	20.8	−2.6	−1.3	−12.9	5.1	−17.0	6.3	−0.2	11.7	0.83
ABS variability (%)	20.8	2.6	1.3	12.9	5.1	17.0	6.3	9.4	7.0	
Putamen BP_2										
Study 1	2.0	2.5	3.6	2.8	2.6	3.1	3.8	2.9	0.6	
Study 2	2.2	2.8	3.1	2.7	3.2	2.9	4.0	3.0	0.5	
Variability (%)	−10.1	−12.6	15.1	3.1	−18.7	7.7	−5.0	−2.9	11.1	0.84
ABS variability (%)	10.1	12.6	15.1	3.1	18.7	7.7	5.0	10.3	5.1	

ABS absolute

[a]Striatum: Caudate nucleus (counts×ml^{-1}) ×Caudate nucleus (ml)/(Caudate nucleus (ml)+Putamen (ml)) + Putamen (counts×ml^{-1}) ×Putamen (ml)/(Putamen (ml)+Caudate nucleus (ml))

dimensional delineations times the slice distance. The occipital cortex was used as a region representing non-specific binding only.

Derivation of binding parameters

Two different outcome parameters, BP_1 and BP_2 [1], were calculated according to:

$$BP_1 = \frac{C_3(\infty)}{C_1(\infty)} = BP \times f_1 \quad (1)$$

$$BP_2 = \frac{C_3(\infty)}{C_2(\infty)} = BP \times f_2 \quad (2)$$

where $C_1(\infty)$ denotes the constant tracer concentration in the metabolite-corrected plasma compartment, in this instance the mean of two blood samples drawn at 150 min post injection, and $C_2(\infty)$ and $C_3(\infty)$ denote the constant radiotracer concentration in the non-specific and specific compartments, respectively. In practice this concentration is computed by SPECT ROIs (counts/ml) from the summed SPECT acquisitions. Emission tomography measures the total concentration of radiotracer in the striatum (C_{tot}). Due to the overall physicochemical constancy of brain tissue, $C_2(\infty)$ is assumed to equal the concentration of tracer in an ROI devoid of receptors [$C_{ref}(\infty)$] and $C_3(\infty)$ is calculated as $C_{tot}(\infty)-C_{ref}(\infty)$.

The free fraction of tracer in plasma, f_1, and the free tracer fraction in brain tissue, f_2, were not measured and, accordingly, the binding potential (BP) equal to the ratio of the density of available transporters, B'_{max}, to the affinity constant of the tracer [1], K_d, was not directly determined.

Statistical analysis

The *stability* of the individual time-activity curves and outcome measures was calculated as the slope (linear regression analysis from 120 to 180 min) divided by the average value from 120 to 180 min times 100%.

$$Stability\ (\%change/hour) = \frac{slope(\alpha = BP/m)}{Mean\ BP2(from\ 120-180\,\mathrm{min})/60\,\mathrm{min}} \quad (3)$$

The *variability* of measurements was computed as the numerical difference between the two measurements, expressed as a percentage of the mean value of both measurements:

$$Variability(\%) = \frac{|BP2_{test1} - BP2_{test2}|}{Mean(BP2_{test1}, BP2_{test2})} \quad (4)$$

The *reliability* of the measures was further assessed relative to the between- and within-subject variance by the intraclass correlation coefficient, r_1, calculated as [5]:

$$Reliability = \frac{MS_B - MS_W}{MS_B + (n-1) \times MS_W} \quad (5)$$

where MS_B=mean sum of squares between subjects; MS_W=mean sum of squares within subjects; n=number of within-subject measurements. MS_B and MS_W were derived by use of the ANOVA test.

The reliability is a measure of the variability that is due to similarities in individual transporter concentrations. A low variability could be due to a low inter-individual variability of DAT density (B'_{max}). It is not possible to establish a level of significance for reliability and therefore this variable is only useful for comparison of different studies of reproducibility (non-statistically).

Results

Table 1 shows the individual BP_1 and BP_2 values and variability measures using manual delineation of ROIs.

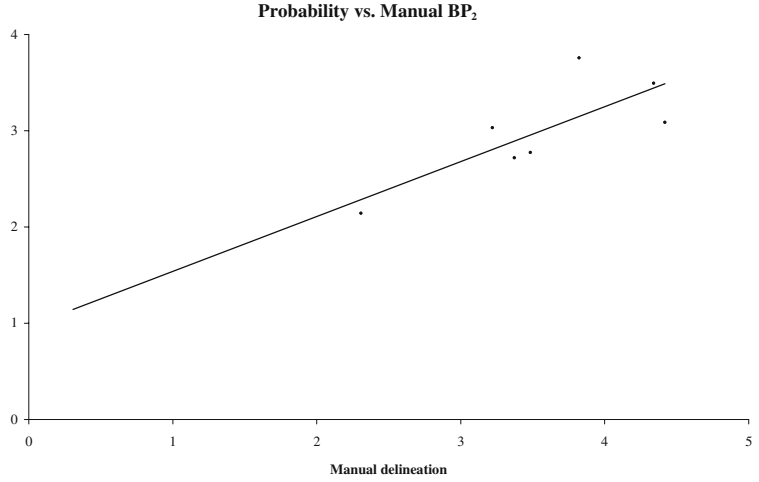

Fig. 3. Individual probability map-based BP_2 vs manual BP_2. Slope 0.6

Figure 2 presents the BP_2 inter- and intra-individual variability. The reliability of BP_2 was significantly higher (0.95–0.96) than that of BP_1 (0.47–0.69). Table 2 shows individual BP_1 and BP_2 values and variability measures using probability map-based ROI delineation. Both BP_1 and BP_2 values were significantly lower with the probability map-based ROI delineation than with manual delineation (paired t test: p=0.02, Fig. 3). By contrast, non-specific binding as defined from the occipital region was similar with the two ROI delineation methods. A high variability in free parent compound in the two blood samples drawn at each experiment was found. First experiment: primary blood output, mean 164 Bq/ml; secondary blood output, 168 Bq/ml; individual difference, range 0.1–12.7%, mean 2.3%. Second experiment: primary blood output, mean 142 Bq/ml; secondary blood output, 148 Bq/ml; individual difference, range 0.7–12.2%, mean 4.1%. In subject 7, blood sampling failed owing to technical problems. Figure 4 shows individual striatal BP_2 values from manual delineation at different time points

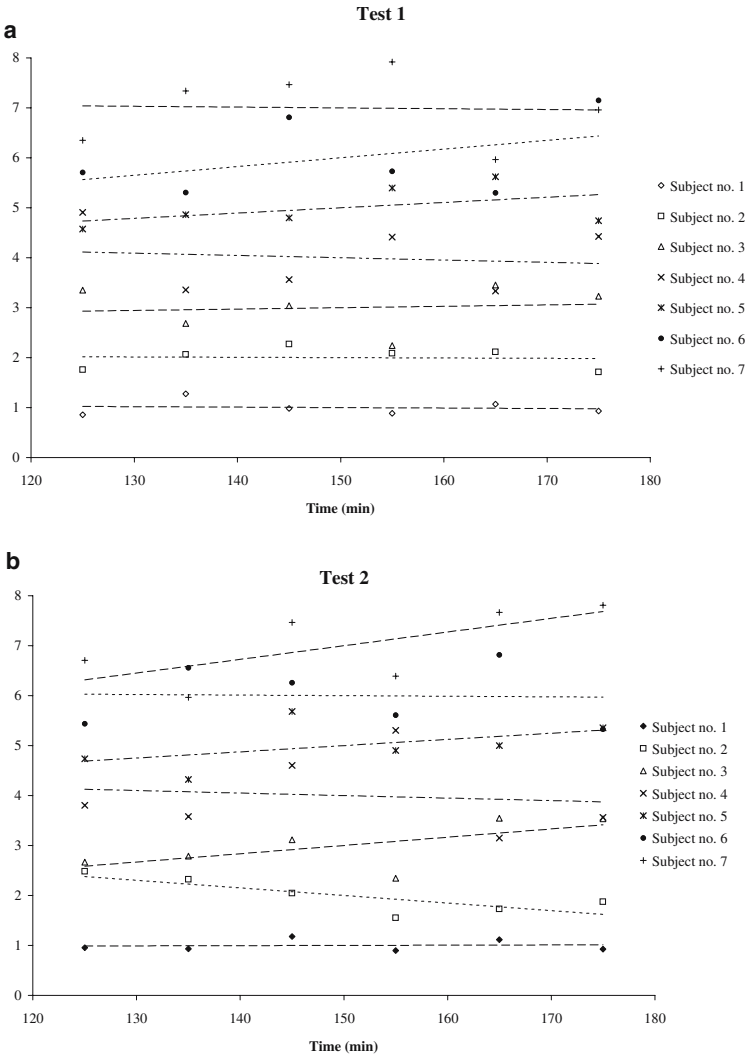

Fig. 4. a, **b** Individual striatal time-activity curves from the first and second experiments, with manual delineation. Each individual was normalised to the mean value within the scanning time from 120 to 180 min and added by the subject number from 1 to 7 to separate individual time-activity curves

from 120 to 180 min at the first and second measurements. Each time point represents the BP_2 value normalised with the individual's mean BP_2 value from 120 to 180 min.

Table 3 shows the % change per hour in time-activity curves and BP_2 values. The stability measures were calculated from the slope of the regression lines shown in Fig. 4a and b. No correlation was found between the relative difference in stability measures for the first and the second measurement and the relative difference in BP_2 values. There was a significant difference in individual BP_2 stability between the first and second scans ($p \leq 0.03$). Table 4 shows the percent difference in ROI volumes depending on the delineation method; the manual delineation resulted in significantly smaller ROIs ($p<0.009$). Simple regression analysis showed no correlation between the volumes of individual ROIs as determined by either method and variability in caudate nucleus or putamen.

Reproducibility of ROI volumes was significantly higher for the probability map-based method (1%) than for the manual delineation method (8%) ($p<<0.001$).

Table 4. ROI volumes (mean, studies 1 and 2) and percent difference in individual ROI volumes based on manual delineation or probability map-based methods

Manual delineation				
Individual	Caudate		Putamen	
	ml	%	ml	%
1	2.3	14.7	3.0	2.1
2	2.0	1.5	2.8	2.3
3	1.4	11.2	1.8	14.5
4	1.4	4.2	1.8	7.7
5	1.9	6.6	2.7	4.7
6	1.8	6.7	2.5	12.9
7	1.5	14.7	2.2	7.7
Mean	1.8	8.5	2.4	7.4
Semi-automatic delineation (probability map-based method)				
Individual	Caudate		Putamen	
	ml	%	ml	%
1	2.4	1.3	5.9	0
2	2.6	0.2	5.8	0
3	3.0	2.1	5.5	1.3
4	2.2	1.1	5.8	0
5	1.8	1.4	5.2	3.2
6	2.6	0.5	5.9	0.8
7	2.6	0.5	5.9	0.8
Mean	2.5	1.0	5.7	0.9

Discussion

In this study we have shown that [^{123}I]PE2I SPECT measurements of DAT with the B/I approach are highly reproducible, particularly with BP_2 as the outcome parameter. Manual ROI delineation on the functional image was associated with significantly lower reproducibility of volume determination and also resulted in significantly smaller volumes as compared with automatic delineations based on MR probability maps. Nevertheless, the latter approach resulted in a slightly higher variability of BP_2 as compared with manual delineation. Finally, in an independent sample of healthy controls we confirmed that a B/I protocol of 2.7 h resulted in stable plasma and brain tissue levels of parent compound.

The reproducibility of [^{123}I]PE2I SPECT measurements of DAT with the B/I approach will depend upon both

Table 3. Stability (% change/h) after administration of a B/I ratio of 2.7 h following manual delineation

	Study 1			Study 2		
Subject	Striatum	Occipital	BP_2	Striatum	Occipital	BP_2
1	−2.5	−2.0	−5.7	2.8	1.3	2.4
2	−8.4	−7.3	−2.1	1.4	27.1	−26.8
3	−6.2	−8.8	5.3	1.8	−23.4	33.3
4	−5.1	−0.1	−7.0	−6.6	2.5	−7.7
5	−10.0	−13.9	12.6	−9.7	−21.9	14.9
6	0.4	−1.6	−4.0	3.6	5.1	−1.2
7	−7.0	−4.9	−1.5	0.1	−17.7	23.4
Mean	−5.6	−5.5	−0.3	−0.9	−3.9	5.5
SD	3.5	4.9	7.0	5.1	18.3	20.2
ABS mean	5.7	5.5	5.6	3.7	14.2	15.7

SD standard deviation, *ABS* absolute

Stability of striatal and occipital volumes: slope of time-activity curve (120–180 min)×60 min divided by mean values from 120 to 180 min in percent.

Stability of BP_2: slope of time-activity curve (estimated by striatum/occipital −1) from 120 to 180 min×60 min divided by mean values from 120 to 180 min in percent.

methodological and biological variability. In our study it was not possible to assess the relative contribution of each of these factors, but methodological variability is determined by variations in, for example, SPECT acquisition, movement artefacts, the reconstruction process and delineation of ROIs. Whereas the former variability potentially can be minimised, we attempted to assess the contribution from variations in ROI delineations by comparing two different methods. In most clinical settings, manual ROI delineations are done directly on the SPECT images, not least because the corresponding structural images are often not available. With this approach, an ROI set is defined from an anatomical atlas and delineated on the individual SPECT scans. Interestingly, although the manual approach was both less precise and less reproducible in terms of volume assessment, it provided a functional reproducibility measure that was better than the probability map-based one. For both delineation methods, BP_2 test–retest variability was considerably lower than has been reported in similar studies using other DAT ligands (FP-CIT: range 5–16%; β-CIT: range 7–16%) [19–22]. With the probability map-based approach, test–retest variability was slightly higher and BP_2 values were significantly lower than with the manual approach. The latter is probably primarily a partial volume effect related to a larger ROI volume using the probability map- based approach compared with the manual "hot spot" delineation approach, where ROIs are delineated on a few slices only (no attempts were made to manually move the MR-defined volumes to the "hot spots" on the SPECT image). Although the volumes were highly reproducible, the outcome measures showed a much larger variability with the probability map-based approach that was unrelated to the volume of the ROI. This was most likely caused by difficulties in the MR/SPECT co-registration. It is likely that in patients with striatal DAT pathology, the probability map-based approach is superior to manual delineation, simply because the striatal tracer concentration is closer to the non-specific tracer concentration, thereby hampering correct adjustment of ROIs. In this study only two venous blood samples were drawn. If a suitable reference region does not exist, we recommend drawing at least six venous blood samples [1] for reproducible metabolite correction of the input curve.

Analysis of test–retest steady state conditions

At constant tracer levels, quantification of DAT density is both experimentally and analytically simple. Outcome parameters are calculated as simple tissue to venous blood ratios (BP_1) or, if a suitable reference region exists, as simple tissue to reference tissue ratios (BP_2).

In this study, where the stability of the striatal and occipital time-activity curves was evaluated in a separate group of healthy subjects, we found that in the first and second examinations the percent change in plasma activity varied somewhat over time. The time-activity curves (Fig. 4) and the fact that the stability measures were lower in the high count striatal ROIs than in the low count occipital cortex ROI imply that the variability was primarily due to random noise. This is also supported by the fact that, although the stability was significantly different from the first to the second scan, no difference was found in the reproducibility. In our recent study, we were able to demonstrate both experimentally and through computer simulations that a twofold variation in the terminal plasma clearance rate only translates into a 10% difference in BP_1 and BP_2 calculated from 120 to 180 min after tracer administration and that outcome parameters were stable in all subjects in the same time period [1]. Accordingly, in spite of variations in plasma levels, the outcome parameters for dopamine transporter binding were highly reproducible.

Conclusion

In this study we have demonstrated that [^{123}I]PE2I SPECT with the bolus/infusion approach yields highly reproducible and reliable values for striatal dopamine transporter binding. Both the manual delineation and the probability map-based method yielded highly reproducible BP_2 quantification in healthy subjects. Further, the generalisability of the applied bolus/infusion protocol was confirmed in an independent group of healthy volunteers, and this approach allows the study of three or more subjects within a normal working day.

[^{123}I]PE2I is a highly selective ligand for the dopamine transporter site that provides highly reproducible measures of striatal binding and allows for imaging within 2 h after injection. Future studies must assess the reproducibility of dopamine transporter binding with PE2I SPECT in patients with basal ganglia pathology.

Acknowledgements. The authors thank Karin Stahr for expert technical assistance. This work was supported by the Danish Medical Research Council, the Toyota Foundation, the Elsass Foundation, the University of Copenhagen and H:S Hovedstadens Sygehusfællesskab.

References

1. Pinborg LH, Ziebell M, Frokjaer VG, de Nijs R, Svarer C, Haugbol S, et al. Quantification of ^{123}I-PE2I binding to dopamine transporter with SPECT after bolus and bolus/infusion. J Nucl Med 2005;46(7):1119–1127
2. Allard PO, Rinne J, Marcusson JO. Dopamine uptake sites in Parkinson's disease and in dementia of the Alzheimer type. Brain Res 1994;637(1–2):262–266
3. Bao SY, Wu JC, Luo WF, Fang P, Liu ZL, Tang J. Imaging of dopamine transporters with technetium-99m TRODAT-1 and single photon emission computed tomography. J Neuroimaging 2000;10(4):200–203
4. Brucke T, Asenbaum S, Pirker W, Djamshidian S, Wenger S, Wober C, et al. Measurement of the dopaminergic degeneration in Parkinson's disease with [^{123}I] beta-CIT and SPECT. Correlation with clinical findings and comparison with multiple system atrophy and progressive supranuclear palsy. J Neural Transm Suppl 1997;50:9–24

5. Innis RB, Seibyl JP, Scanley BE, Laruelle M, Abi-Dargham A, Wallace E, et al. Single photon emission computed tomographic imaging demonstrates loss of striatal dopamine transporters in Parkinson disease. Proc Natl Acad Sci USA 1993;90(24):11965–11969
6. Lee CS, Samii A, Sossi V, Ruth TJ, Schulzer M, Holden JE, et al. In vivo positron emission tomographic evidence for compensatory changes in presynaptic dopaminergic nerve terminals in Parkinson's disease. Ann Neurol 2000;47(4): 493–503
7. Marshall V, Grosset DG. Role of dopamine transporter imaging in the diagnosis of atypical tremor disorders. Mov Disord 2003;18(Suppl 7):S22–S27
8. Prunier C, Bezard E, Montharu J, Mantzarides M, Besnard JC, Baulieu JL, et al. Presymptomatic diagnosis of experimental parkinsonism with ^{123}I-PE2I SPECT. Neuroimage 2003;19 (3):810–816
9. Knudsen GM, Karlsborg M, Thomsen G, Krabbe K, Regeur L, Nygaard T, et al. Imaging of dopamine transporters and D2 receptors in patients with Parkinson's disease and multiple system atrophy. Eur J Nucl Med Mol Imaging 2004;31 (12):1631–1638
10. Varrone A, Marek KL, Jennings D, Innis RB, Seibyl JP. [^{123}I] beta-CIT SPECT imaging demonstrates reduced density of striatal dopamine transporters in Parkinson's disease and multiple system atrophy. Mov Disord 2001;16(6):1023–1032
11. Carroll FI, Rahman MA, Philip A, Lewin AH, Boja JW, Kuhar MJ. Synthesis and receptor binding of cocaine analogs. NIDA Res Monogr 1991;105:147–153
12. Emond P, Garreau L, Chalon S, Boazi M, Caillet M, Bricard J, et al. Synthesis and ligand binding of nortropane derivatives: N-substituted 2beta-carbomethoxy-3beta-(4′-iodophenyl)nortropane and *N*-(3-iodoprop-(2*E*)-enyl)-2beta-carbomethoxy-3beta-(3′,4′-disubstituted phenyl)nortropane. New high-affinity and selective compounds for the dopamine transporter. J Med Chem 1997;40(9):1366–1372
13. Videbaek C, Knudsen GM, Bergstrom KA, Hiltunen J, Pinborg LH, Kuikka JT, et al. Octanol extraction yields similar results as HPLC for quantification of [^{123}I]PE2I metabolism. Eur J Nucl Med 1999;26:1139
14. Kretschmann H-J, Weinrich W. Neuroanatomy and cranial computed tomography. Stuttgart: Thieme; 1986
15. Svarer C, Madsen K, Hasselbalch SG, Pinborg LH, Haugbol S, Frokjaer VG, et al. MR-based automatic delineation of volumes of interest in human brain PET images using probability maps. Neuroimage 2005;24(4):969–979
16. Ashburner J, Friston K. Multimodal image coregistration and partitioning—a unified framework. Neuroimage 1997;6 (3):209–217
17. Woods RP, Cherry SR, Mazziotta JC. Rapid automated algorithm for aligning and reslicing PET images. J Comput Assist Tomogr 1992;16(4):620–633
18. Pietrzyk U, Herholz K, Fink G, Jacobs A, Mielke R, Slansky I, et al. An interactive technique for three-dimensional image registration: validation for PET, SPECT, MRI and CT brain studies. J Nucl Med 1994;35(12):2011–2018
19. Booij J, Habraken JB, Bergmans P, Tissingh G, Winogrodzka A, Wolters EC, et al. Imaging of dopamine transporters with iodine-123-FP-CIT SPECT in healthy controls and patients with Parkinson's disease. J Nucl Med 1998;39(11):1879–1884
20. Morrish PK. How valid is dopamine transporter imaging as a surrogate marker in research trials in Parkinson's disease? Mov Disord 2003;18(Suppl 7):S63–S70
21. Pirker W, Djamshidian S, Asenbaum S, Gerschlager W, Tribl G, Hoffmann M, et al. Progression of dopaminergic degeneration in Parkinson's disease and atypical parkinsonism: a longitudinal beta-CIT SPECT study. Mov Disord 2002;17 (1):45–53
22. Seibyl JP, Marek K, Sheff K, Baldwin RM, Zoghbi S, Zea-Ponce Y, et al. Test/retest reproducibility of iodine-123-betaCIT SPECT brain measurement of dopamine transporters in Parkinson's patients. J Nucl Med 1997;38(9):1453–1459

Paper 3

Volume 38 | Number 2 | June 2010 The Official Publication of SNMTS

JNMT

Journal of Nuclear Medicine Technology

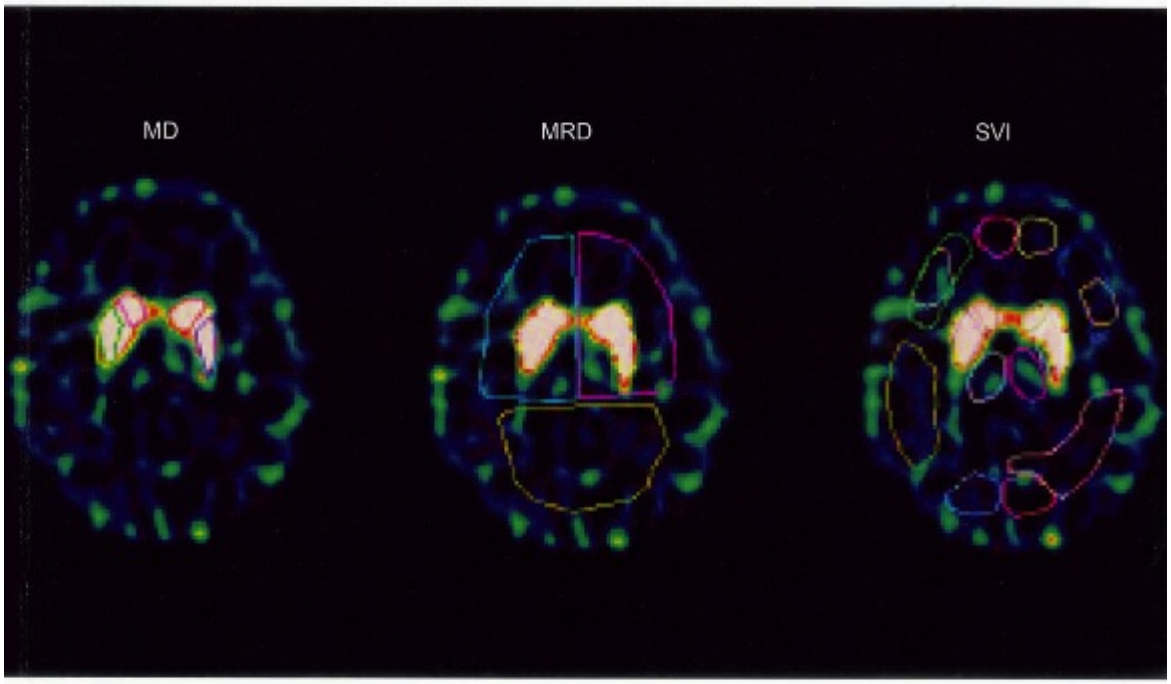

Three different methods of ROI delineation on SPECT images of the same brain slice in the same individual.

See page 63.

SNMTS
Advancing Molecular Imaging and Therapy

MRI-Guided Region-of-Interest Delineation Is Comparable to Manual Delineation in Dopamine Transporter SPECT Quantification in Patients: A Reproducibility Study

Morten Ziebell[1], Lars H. Pinborg[1,2], Gerda Thomsen[1], Robin de Nijs[3], Claus Svarer[1], Aase Wagner[4], and Gitte M. Knudsen[1]

[1]Neurobiology Research Unit and Cimbi, University of Copenhagen, Rigshospitalet, Copenhagen, Denmark; [2]Epilepsy Clinic, Department of Neurology, University of Copenhagen, Rigshospitalet, Copenhagen, Denmark; [3]Department of Clinical Physiology and Nuclear Medicine, University of Copenhagen, Rigshospitalet, Copenhagen, Denmark; and [4]Department of Diagnostic Radiology, University of Copenhagen, Rigshospitalet, Copenhagen, Denmark

A particularly sensitive step in the quantification of SPECT images of the dopamine transporter (DAT) is a correct delineation of the region of interest (ROI). In this study, we primarily compared the reproducibility of the following different approaches for ROI delineation in SPECT images of the DAT: the use of manual delineation (MD) on high-count striatal slides directly on the SPECT image, ROI delineation based on individual MR images (MRD), and oversized striatal ROIs—that is, the striatal volume of interest (SVI), as described previously. We also assessed the ability of the different approaches to identify striatal pathology in patients with parkinsonism. **Methods:** Eight patients with highly variable reductions in cerebral DAT availability were SPECT-scanned twice with ^{123}I-labeled *N*-(3-iodoprop-(2E)-enyl)-2β-carboxymethoxy-3β-(4′-methylphenyl) nortropane bolus infusion setup and once with an MRI scanner. For SPECT/MRI coregistration, we used external fiducial markers visible on both MRI and SPECT. With the MD and MRD methods, the outcome parameters for DAT availability were the binding potentials and the ratio at equilibrium of specifically bound radioligand to nondisplaceable radioligand in tissue (BP_{ND}). For the SVI method, the outcome parameter was the specific binding ratio (SBR). **Results:** No statistically significant difference in striatal BP_{ND} intraobserver reproducibility was seen among any of the 3 methods. The intraobserver reproducibility average ± SD for MD was 7.0% ± 4.1%; for MRD, 5.7% ± 5.4%; and for SVI, 6.7% ± 6.0%. Mean intrasubject variability, as determined from the test–retest scans, did not differ with the 3 delineation methods used. The average (±SD) intrasubject variability of striatal BP_{ND} was 11.9% ± 10.0% with MD and 14.6% ± 15.3% with MRD. With the SVI method, the intrasubject variability of striatal specific binding ratio was 10.0% ± 10.2%. BP_{ND} values obtained with the MD and MRD methods were similar (paired *t* test, $P > 0.4$). **Conclusion:** In patients with reduced striatal DAT binding, the reproducibility of the outcome from ROI MD is comparable to both that obtained by delineation of ROI on individual MR images, followed by coregistration to the SPECT image, and that obtained with the SVI-based approach.

Key Words: ^{123}I-PE2I; dopamine transporters; SPECT; reproducibility; ROI delineation

J Nucl Med Technol 2010; 38:61–68
DOI: 10.2967/jnmt.109.072801

Imaging of cerebral dopamine transporter (DAT) binding is increasingly used as a surrogate marker for the integrity of dopaminergic nerve cells (*1–9*). Brain imaging of DAT with SPECT constitutes an important adjunct to neurologists' clinical evaluations of patients with movement disorders, particularly in the early stages of the disease (*10*). For routine clinical purposes, visual inspection and qualitative assessment of the images by an experienced reader may suffice. For research purposes, however, and particularly for longitudinal studies that are designed to evaluate treatment efficacies (*11*), quantitative estimates of DAT availability are required (*12,13*).

A particularly important step in DAT quantification is a correct delineation of the region of interest (ROI) in the SPECT image. Overall, there are 3 principally different ways of delineating ROIs on the SPECT image: manual delineation (MD) directly on the SPECT image, template-guided delineation, and delineation based on coregistration with another brain image that provides structural information, such as MRI. In theory, there is only a limited difference between the MD and the adjustable template–based delineation. Compared with MD, the largest advantage of template-based delineation is that it is less time-consuming and is operator-independent (*14*). An alternative to an anatomically correct ROI was described by Tossici-Bolt et al. in 2006—the so-called striatal volume-of-interest (SVI) method (*15*). This method requires no structural

Received Nov. 12, 2009; revision accepted Mar. 10, 2010.
For correspondence contact: Morten Ziebell, Neurobiology Research Unit, Rigshospitalet, N9201, 9 Blegdamsvej, Copenhagen, DK-2100, Denmark.
E-mail: ziebell@nru.dk

information on the individual patient's brain but involves a template of oversized ROIs involving all striatal slices. The calculated volume of interest (VOI), the total counts within this volume, the count concentration in a reference region, and a population-based estimate of the average striatal volume are then used to calculate a striatal binding ratio (SBR) equivalent to the ratio of the specific-to-nondisplaceable uptake.

Various studies have attempted to assess different delineation methods by comparing them to a qualitative visual assessment (*14*). In the absence of a gold standard, however, the most viable way to evaluate the different ROI delineation methods against each other is to perform reproducibility studies. The reproducibility of a method is important not only to the identification of the most suitable method for quantification but also to the appropriate design of studies in terms of, for example, sample size. Reproducibility studies of brain SPECT outcomes of DAT binding have been conducted in both healthy volunteers (*16,17*) and patients with affected striatal DAT availability (*18–21*). Intrasubject variability results from both biologic and methodologic variation. In the absence of subject-specific anatomic information (e.g., cerebral MRI), the ROI delineation is anticipated to be particularly prone to observer bias, but this bias has, to our knowledge, never been formally assessed in SPECT studies of patients with reduced DAT availability.

In healthy volunteers, we showed previously that in terms of the intrasubject variability of the binding potential of DAT, MD of ROIs directly on SPECT images was equally as effective as MRI-defined probability map–based ROI delineation (MRD) (*17*). The advantage of including MRI-based anatomic information for the assessment of striatal DAT availability in patients with decreased binding is, however, unknown. It is expected that the test–retest variability is greater in patients with reduced DAT availability, because the concentration of tracer in patients' striatal regions is closer to the nonspecific tracer concentrations. In this context, the method for ROI delineation without anatomic information is even more difficult and prone to more observer bias.

The aim of this present study was to compare 3 different methods of ROI delineation on SPECT images of the DAT in patients with reduced DAT availability. The outcome measure was the reproducibility of the delineation (the intraobserver reproducibility) and how large an impact it would have on the overall individual scan-to-scan variability (the intrasubject variability).

MATERIALS AND METHODS

Patients

Eight patients with parkinsonism (average age, 69 y; age range, 57–80 y; 6 men) were studied twice, at intervals between 14 and 21 d. The patients were included on the day of their assignment for diagnostic ^{123}I-labeled *N*-(3-iodoprop-(2E)-enyl)-2β-carboxymethoxy-3β-(4′-methylphenyl) nortropane (^{123}I-PE2I) SPECT and asked to enroll in the study if their ^{123}I-PE2I SPECT scan was compatible with decreased DAT density. The patients had an average history of 35 mo of neurologic symptoms (range, 12–72 mo). The average scores were 46 (range, 19–72) on the Unified Parkinson Disease Rating Scale, 2.1 (range, 1–3) on the Hoehn and Yahr (H&Y) scale, and 28.5 (range, 25–30) on the Mini-Mental State Examination. Routine blood test results were normal in all patients. Brain MRIs were unremarkable in all patients. None of the patients was taking antiparkinson drugs before or at the time of the examination. Two patients were taking antidepressant medication (selective serotonin reuptake inhibitors), and their medication was kept unchanged during the test–retest period.

All patients gave informed written consent. The study was performed in accordance with the ethical standards of the Declaration of Helsinki and was approved by the ethical committee of Copenhagen and Frederiksberg (KF 12–009/04).

Experimental Procedures

As a DAT radiotracer we used ^{123}I-PE2I, which is a highly selective DAT ligand with fast kinetics and high target-to-background ratio (*4*). Pinborg et al. demonstrated the feasibility of a bolus–plus–constant infusion (B/I) approach for ^{123}I-PE2I administration (*22*). The B/I approach is superior to a bolus-alone approach because the former allows for the simple and accurate quantification of ^{123}I-PE2I binding to DAT. Procedures were performed according to the method of Ziebell et al. (*17*). Cannulas were inserted into both cubital veins for tracer administration and blood sampling. To block thyroidal uptake of free radioiodine, all patients received 200 mg of potassium perchloride intravenously 30 min before ^{123}I-PE2I injection. An average intravenous bolus of 74.3 MBq (range, 65.8–79.9 MBq) of ^{123}I-PE2I was given, immediately followed by a constant infusion (mean, 96.5 MBq; range, 88.6–100.1 MBq) of ^{123}I-PE2I for 3 h. The B/I protocol was similar in both studies, with a bolus equal to 2.7 h (range, 2.6–2.8 h) of infusion (the B/I ratio).

SPECT was performed with a triple-head IRIX camera (Philips Medical) fitted with low-energy, general-purpose parallel-hole collimators (spatial resolution, 8.5 mm at 10 cm). The mean radius of rotation was 13.9 cm. Each head covered 120° of the circular orbit. Scans were obtained and stored at fixed angles, with an angular interval of 3°. Six SPECT scans (duration, 10 min) were acquired between 120 and 180 min after injection. The images were reconstructed with a MATLAB 6.5 (The MathWorks)–based program in 128 × 128 matrices (2.33-mm pixels and identical slice thickness) using standard filtered backprojection with a low-pass fourth-order Butterworth filter at 0.3 Nyquist (0.64 cm^{-1}).

High-energy photons of ^{123}I penetrated through the lead of the collimator, and Compton scatter in the scintillation crystal caused erroneous counts in the imaging energy window. Therefore, a second energy window positioned at 184–216 keV was used to correct for these downscattered photons in the imaging window (*23*) (positioned at 143–175 keV). Before reconstruction, the projection images of the second energy window were subtracted from the imaging energy window using a weight of 1.1 (*24*).

MRI

All patients underwent 1 structural MRI scan with a 1.5-T Vision scanner (Siemens) using the 3-dimensional magnetization-prepared rapid acquisition gradient-echo sequence (inversion time/delay time/echo time/repetition time = 300/300/4.4/11.4 ms; flip angle, 12) acquired as sagittal-plane scans with a spatial resolution

of 1.50 × 1.13 × 1.02 mm. There were 130 planes, and the in-plane matrix was 230 × 256. The MRI scan and the first SPECT scan were acquired on the same day.

ROIs

The ROIs were applied to the SPECT images in 3 different ways; the first 2 have already been discussed (*17*).

MD. The ROIs and reference region (cerebellum) were manually delineated directly on the reconstructed SPECT images, guided by the use of Kretschmann and Weinrich's neuroanatomic atlas (*25*). The direct adaptation of ROI coordinates from the atlas required a reorientation of the reconstructed images to the canthomeatal plane (using, for instance, MATLAB [The MathWorks] or any other program capable of reorienting the reconstructed SPECT images). ROIs were delineated on 5 consecutive slices (2.3 mm/slice) in a summed image from all 6 SPECT frames acquired from 120 to 180 min after injection. All delineations were performed by the same operator with 5 y of experience in ROI delineation on DAT SPECT images.

MRD. The ROIs were delineated on the patient's individual MR image and transferred via a coregistration procedure to the individual SPECT image. The actual delineation of the ROIs was computed using a probability map–based method developed by Svarer et al. (*26*), and cerebellum was used as the reference region. MR and SPECT images were coregistered also using a semiautomatic MATLAB-based method with visual quality inspection, as previously described (*17*). Corresponding external fiducial markers (5 on each image) were manually identified on the MR and SPECT images. A rigid transformation between the images was then estimated automatically by minimizing the sum of squared errors between the defined points. The MRD software program does not define an overall striatal ROI but delineates only caudate nucleus and putamen as separate ROIs. Because we wanted to compare the reproducibility of striatal specifically bound radioligand to nondisplaceable radioligand in brain tissue (BP_{ND}) between the MRD method and the other ROI-delineating methods, we calculated a volume-weighted striatal ROI for the MRD:

$$\text{Striatum (MRD)} = \frac{(\text{caudate [mL]} \times BP_{ND,\text{Caudate}}) + (\text{putamen [mL]}) \times BP_{ND,\text{Putamen}})}{(\text{caudate [mL]} + \text{putamen [mL]})}$$

For those with special interest, a detailed illustration of the method is available in Svarer et al. (*26*).

SVI. The original method uses template ROIs large enough to contain all striatal counts, partial volume included, that the operator is required to position (not to delineate) on each side. A 3-dimensional slab (rather than a single slice) ensures the visualization and inclusion of partial-volume counts in the VOIs (*15*). We adapted this method with the following modifications: instead of constructing a slab—that is, a summed image of all slices with striatal activity and using a template for ROI delineation—we manually delineated the ROIs on the slice with the highest striatal counts and copied these ROIs to all slices with striatal radioactivity. Next, the cerebellum was manually delineated and used as a reference region instead of using the whole brain minus the ROI. And finally, rather than using an average population-based striatal volume (based on postmortem studies) and applying this volume to all individuals, we calculated the striatal volume using each patient's MR image with the MRD method. For those with special interest, a detailed illustration of the method is available in Tossici-Bolt et al. (*15*).

Figure 1 illustrates the 3 different methods of ROI delineation on SPECT images of the same individual.

Derivation of Binding Parameters and Reproducibility

The outcome parameter BP_{ND} was calculated according to a consensus established by Innis et al. in 2007 (*27*). At steady state, BP_{ND} = specifically bound radioligand/nondisplaceable radioligand in brain tissue.

The SBR was calculated according to the method of Tossici-Bolt et al. (*15*):

$$SBR = \frac{Ct_{VOI}/c_r - V_{VOI}}{V_S}, \qquad \text{Eq. 1}$$

where V_S is the anatomic volume of striatum, Ct_{VOI} the total counts in striatal VOI, c_r the count concentration in a reference region devoid of receptors or transporters, and V_{VOI} the volume of the SVI (which is unitless, like the binding potential).

Because the MRI delineation is semiautomatic, the software provides caudate and putamen regions separately and the striatal binding potential was computed as a volume-weighted average of the caudate nucleus and putamen.

Figure 2 illustrates the study setup. ^{123}I-PE2I SPECT scans were delineated for each individual and striatal DAT availability quantified, and the process was repeated 4 wk later. This process was performed on both the first and the second ^{123}I-PE2I SPECT

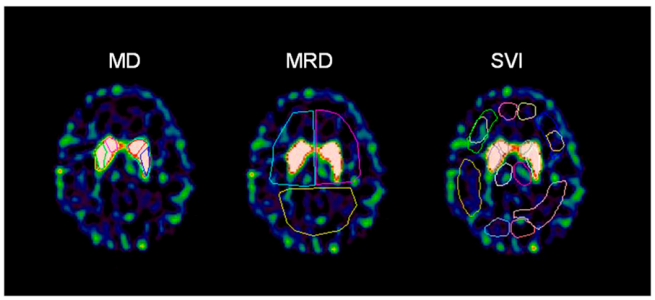

FIGURE 1. Three different methods of ROI delineation on SPECT images of same brain slice in same individual.

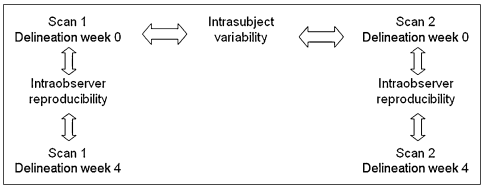

FIGURE 2. Flowchart of study. Eight individuals were scanned twice. Every SPECT (n = 16) image was delineated at week 0, and process was repeated 4 wk later. From these data, intraobserver reproducibility could be calculated according to Equation 2. For every individual, there were 14–21 d between first scan and rescan; from these data (n = 8), intrasubject variability was calculated according to Equation 3.

scan, producing 2 datasets for each region (Fig. 2, left to right, striatum, caudate nucleus, and putamen), 96 total.

The intraobserver reproducibility as a measure of how reproducible the method for ROI delineation is in the same SPECT image was calculated as:

$$\text{Intraobserver reproducibility} = \frac{|\text{BP}(\text{week 0}) - \text{BP}(\text{week 4})|}{(\text{BP}(\text{week 0}) + \text{BP}(\text{week 4}))/2}. \quad \text{Eq. 2}$$

SBR was used instead of binding potential for the SVI method in Equations 2, 3, and 5. As mentioned, both scan 1 and scan 2 were used to calculate the intraobserver reproducibility.

Reproducibility of the ROI volumes within each method was calculated in the same manner as for Equation 2, using the volumes instead of the binding potential.

The intrasubject variability as a measure of the individual ^{123}I-PE2I SPECT scan-to-scan variability was calculated in the same way:

$$\text{Intrasubject variability} = \frac{|\text{BP}_{\text{Scan1}} - \text{BP}_{\text{Scan2}}|}{(\text{BP}_{\text{Scan1}} + \text{BP}_{\text{Scan2}})/2}, \quad \text{Eq. 3}$$

where BP_{Scan1} is the binding potential from the first scan (test) and BP_{Scan2} is the binding potential from the second scan (retest).

The reliability of the measures was assessed relative to the between- and within-patient variance by the intraclass correlation coefficient, calculated as in the study by Ichise et al. (*28*):

$$\text{Reliability} = \frac{(\text{MS}_\text{B} - \text{MS}_\text{W})}{(\text{MS}_\text{B} + \text{MS}_\text{W})}, \quad \text{Eq. 4}$$

where MS_B is the mean sum of squares between patients and MS_W the mean sum of squares within patients (*17*).

The availability of DAT for each patient was also compared with a group of healthy patients. Binding potentials from 25 healthy volunteers, previously scanned with ^{123}I-PE2I SPECT, were age-corrected to match the age of the patients, and a 6.6% reduction per decade was used (*29*). The age-adjusted binding potential from the 8 patients was then inserted in the following formula:

$$\text{DAT availability} = \frac{\text{Binding potential (patient)}}{\text{Binding potential (age-adjusted normal value)}} \times 100\%. \quad \text{Eq. 5}$$

Statistical Analysis

Linear regression analyses were performed on the intraobserver reproducibility. The slope of linear equations was forced through (0.0). When tested using a Student t test, P values below 0.05 were considered statistically significant. Unless otherwise stated, all values are given as mean ± SD. Because of the small sample size regarding the intrasubject variability (n = 8), we used the nonparametric Wilcoxon matched-pairs signed rank sum test. All statistical analyses were performed with GraphPad Prism (version 5.00v; GraphPad Software Inc.).

RESULTS

BP_{ND} values in the most affected striatal ROI (of the 2 sides), compared with BP_{ND} values from our database of 25 age-matched healthy volunteers (*17,22*), were 8%−82% for MD, 3%−96% for MRD, and 26%−100% for SVI.

Intraobserver Reproducibility

The intraobserver reproducibility for each method is shown in Figure 3—that is, the calculated BP_{ND} from the first ROI delineation is plotted against the BP_{ND} from the second ROI delineation. Table 1 summarizes the intraobserver reproducibility of either BP_{ND} or SBR for all 3 methods; the intraobserver reproducibility was not significantly different among any of the 3 ROI delineation methods (paired t test, $P > 0.1$).

The intraobserver reproducibility of the mean ROI volumes for MD was 12.3% ± 9.3% in the striatum, 19.6% ± 13.3% in the caudate nucleus, and 18.3% ± 14.2% in the putamen. For MRD, the reproducibility was 1.3% ± 1.2% for the caudate nucleus and 0.9% ± 0.6% for the putamen.

There was no statistically significant difference (paired t test, $P > 0.4$) in BP_{ND} values between the MD and MRD methods (Fig. 4), and a linear regression analysis showed an excellent correlation with a slope of 0.99 (R^2 = 0.98). However, the delineated putaminal volumes with the MD method were statistically significantly smaller (4.7 vs. 6.1 mL) ($P < 0.001$) than those delineated with the MRD method. However, the volumes of the caudate nuclei showed no significant difference (3.1 vs. 3.0 mL) ($P > 0.4$).

Intrasubject Variability

Table 2 shows the individual and average striatal intrasubject variability with the 3 different methods, and Table 3 summarizes the sample-based average results for all ROIs. There was no statistically significant difference in the striatal intrasubject variability with the 3 methods (Wilcoxon matched-pairs signed rank sum test, $P > 0.2$).

We also compared the 3 ROI delineation methods in terms of reproducibility for the single individual—that is, whether all 3 methods provided a consistent picture of a patient's intrasubject variability. A statistically significant

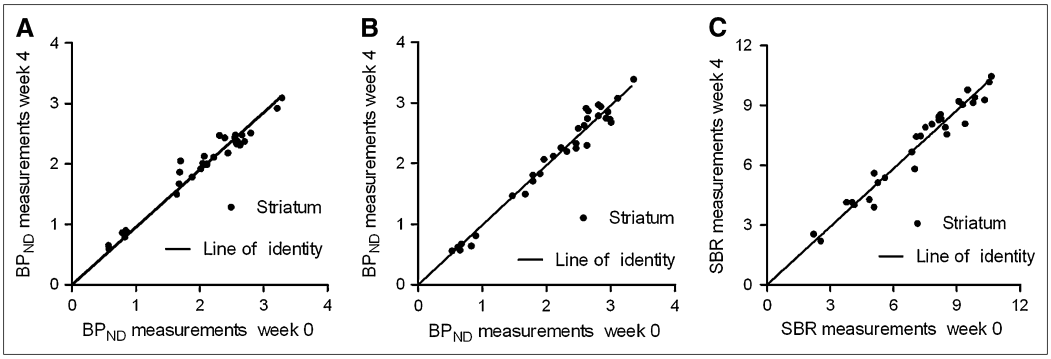

FIGURE 3. Intraobserver reproducibility of BP_{ND} in striatum for different delineation methods. MD (A), probability map–based delineation (B), and SVI (C). For all 3 methods, both test and retest scans were quantified (32 data points).

correlation was found only between the MRD and the SVI methods (Wilcoxon matched-pairs signed rank sum test, $P < 0.01$).

To conduct an absolute quantification using the SVI method, the exact size of the individual striatum volume is needed. We wanted to investigate the actual difference in striatal volume in this small sample of patients. The actual average striatal size, computed using the individual MRI scans, was 9.0 mL (range, 7.2–10.4 mL).

DISCUSSION

The aim of the present study was to compare 3 different types of ROI application methods on SPECT images of the DAT. Outcome measures were reproducibility of the delineation and how reproducibility might affect scan-to-scan variability in patients with reduced DAT density. Our patients, compared with the healthy population, had a DAT availability reduced between 5% and 85%.

The intraobserver reproducibility ranged from 5.7% to 7%, and there was no significant difference among any of the methods. The number of patients in this study is low, however, with 2 scannings per subject the number of ROIs reaches 16. The performance of the intraobserver reproducibility is considerable; thus, for all 3 methods approximately 50% contribution of the overall intrasubject variability in patients with decreased DAT availability stems from the intraobserver reproducibility. The MD method is obviously operator-dependent and dependent on experience. We did not attempt to address the interobserver reproducibility in this study, but assessment of interobserver reproducibility in the individual SPECT centers is recommended if MD is the chosen method.

In theory, the SVI approach and other template methods facilitate the delineation of ROIs, are automated and thereby independent of experienced readers, and are more objective and less sensitive to partial-volume effects than MD. Our results show that the SVI method did not result in a significantly better intraobserver reproducibility than the 2 other methods. We implemented modifications using a different reference region and the individually determined striatal volumes (based on MRIs) and using ROI MD instead of a template. As can be seen from Equation 1, exchanging a population-based average striatal volume with the MRI-determined individual striatal volume did not affect the reproducibility. By contrast, the absolute value of SBR is linearly related to the actual volume and we found a quite high interindividual variation in the MRI-determined striatal volumes, ranging from 7.2 to 10.4 mL, suggesting that the outcome parameter SBR is determined

TABLE 1
Summed Intraobserver Reproducibility of 3 Different Methods

Method	Caudate nucleus	Putamen	Striatum	ICC
MD (BP_{ND})	10.2% ± 9.2%	9.7% ± 5.4%	7.0% ± 4.1%	0.97
MRD (BP_{ND})	14.2% ± 12.3%	8.1% ± 7.5%	5.7% ± 5.4%*	0.98
SVI (SBR)			6.7% ± 6.0%	0.98

*Calculated striatum = volume-weighted (caudate nucleus+ putamen).
ICC = intraclass correlation coefficient.
No statistically significant better intraobserver reproducibility was observed for any method (MD vs. MRD, MD vs. SVI, MRD vs. SVI; $P > 0.1$), and all performed equally for intraclass correlation coefficient ($n = 16$).

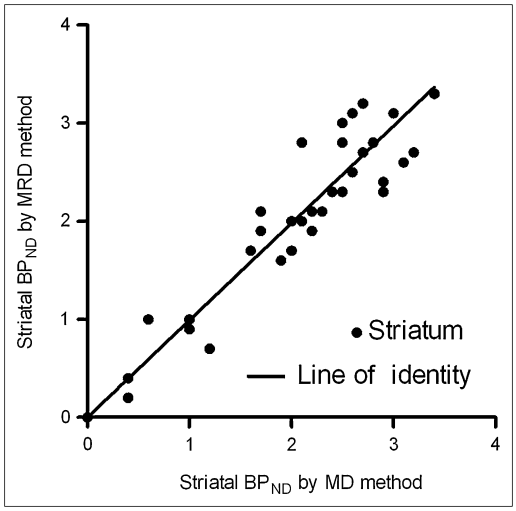

FIGURE 4. BP_{ND} values for caudate nucleus and putamen by ROI application with MD vs. probability map–based automatic delineation method. Linear regression analysis showed excellent correlation, $R^2 = 0.96$.

with some uncertainty. Our SBR values are much higher than the BP_{ND} values found. This is because SBR = BP_{ND} + 1, and because our striatal volumes on average are 20% smaller than the average striatal size of 11.2 mL, because the semiautomatic MRI ROI delineation program does not include the caudate nucleus and putamen as a whole striatum but as 2 separate regions.

The intrasubject variability, depending on the chosen method, was between 11% and 15%. Data from previous test–retest DAT SPECT studies are reviewed in Table 4; the intrasubject variability and reliability (equivalent to the intraclass correlation coefficient) from the present study fall within the same range.

Not surprisingly, in all studies, except for one, the intrasubject variability was lower in healthy volunteers than in patients with reduced DAT availability.

As previously mentioned, the difference between MD and adjustable-template delineation is limited. Not surprisingly, the similar intraobserver reproducibility of the MD and the SVI methods, compared with the other 2 methods, did not result in a significantly smaller intrasubject variability, even though this method has higher absolute quantification values. A serious limitation with the SVI method as it is currently implemented is that it does not allow for the calculation of a posterior–anterior ratio.

The intrasubject variability of the MRI-defined ROI delineation—the MRD method—yielded an outcome similar to that of the MD method, despite the fact that MRD is most likely better able to determine the exact VOI (*17*), which could be of particular importance in patients with reduced DAT availability. The volumes with the MRD method were, however, highly reproducible, suggesting that it is because SPECT/MRI coregistration represents a vulnerable step that MRI-template–based delineation lacks a clear benefit (*30*). Although this coregistration should be similar in patients and in healthy volunteers when using external fiducials, this is apparently not the case. A small misalignment probably has a greater effect on the mean count in a ROI in patients than in healthy volunteers because of the lower striatal radiotracer concentration that can easily move the ROI out of the hot spot. The intrasubject variability of the MD method was almost twice as high in patients as in healthy controls. This is not surprising because it is more difficult to delineate a missing putamen on a SPECT image that is without anatomic information.

TABLE 2
Individual Striatal Intrasubject Variability of Most Affected Side

Method	Subject 1	2	3	4	5	6	7	8	Mean ± SD
MD									
Striatal BP_{ND} test	2.06	0.87	2.07	3.21	2.11	0.57	2.58	1.64	1.9
Striatal BP_{ND} retest	1.88	0.87	2.55	2.66	2.63	0.58	2.56	2.05	2.0
Reproducibility (%)	9.3	0.1	20.5	18.8	21.6	1.8	0.5	22.2	11.9 ± 10.0
MRD									
Striatal* BP_{ND} test	1.90	0.67	2.46	2.64	2.99	0.65	2.46	1.47	1.9
Striatal* BP_{ND} retest	1.67	0.53	2.63	2.65	2.96	0.62	3.11	2.32	2.1
Reproducibility (%)	12.9	23.3	6.6	0.7	1.1	4.1	23.3	45.0	14.6 ± 15.3
SVI									
Striatal SBR test	7.51	2.21	8.46	10.33	8.23	4.13	8.53	5.08	6.8
Striatal SBR retest	7.08	2.54	8.15	9.85	9.09	4.03	9.78	7.01	7.2
Reproducibility (%)	5.8	14.0	3.7	4.8	9.9	2.5	13.7	32.0	10.8 ± 10.2

*Calculated striatum = volume-weighted (caudate nucleus + putamen).

No significant difference in intrasubject variability was observed for any method (*t* test, $P > 0.5$). BP_{ND} outcome measurements were not significant different using MD vs. MRD method (*t* test, $P > 0.5$; $n = 8$).

TABLE 3
Summed Intrasubject Variability from 3 Different ROI Application Methods (n = 8)

Method	Caudate nucleus	Putamen	Striatum	ICC
MD (BP_{ND})	19.4% ± 14.3%	14.8% ± 6.0%	11.9% ± 10.0%	0.88
MRD (BP_{ND})	16.4% ± 11.9%	15.8% ± 11.7%	14.6% ± 15.3%*	0.90
SVI (SBR)			10.8% ± 10.2%	0.90

*Calculated striatum = volume-weighted (caudate nucleus + putamen).
ICC = intraclass correlation coefficient.

Unfortunately, we have no data on the SVI method, but the strength of this method is exactly that it requires no anatomic information and, as such, should be independent of the DAT availability.

There was an excellent correlation between BP_{ND} values obtained from MD and MRD (Fig. 4). So even though MD of a low-count putamen on the SPECT images is difficult without additional anatomic information, MRI coregistration offers no significant advantage in accuracy when it comes to DAT quantification with SPECT.

Finally, we also compared the 3 ROI delineation methods in terms of variability for the single individual. We found a highly statistically significant correlation between the individual MRD- and SVI-determined intrasubject variability but not with these 2 methods and the MD method. This suggests that compared with the MD, the MRD and the SVI methods are less observer-dependent by either increasing the reproducibility of the ROI volumes (MRD) or simply by bypassing the reproducibility (SVI). With the reduced delineator variation and the strict correlation in the individual patient test–retest variability in these 2 methods, a substantial part of the scan-to-scan variability must be due to changes in DAT availability in the current 2- to 3-wk scanning interval and not to methodologic issues.

A limitation of this study was that the sample size was small; however, it was within the general size of data in test–retest studies for SPECT/PET.

CONCLUSION

We find that in patients with reduced striatal DAT binding, MD by an experienced reader provides BP_{ND} measurements that are in complete correspondence to MRI-based delineations. Further, the MD and the MRD methods performed equally well in terms of intraobserver reproducibility, despite the fact that the reproducibility of the ROI volumes was superior in the MRI-based method. Thus, the advantage of the ROI volume reproducibility is lost in the coregistration between MR and DAT images. Trying to overcome accurate striatal ROI delineations using template-based oversized ROIs was not more effective than using MD in terms of intraobserver reproducibility or intrasubject variability.

ACKNOWLEDGMENTS

We thank Glenna Skouboe for expert technical assistance. This work was supported by Rigshospitalet; the Lundbeck Foundation; the EC-FP6-project DiMI, LSHB-CT-2005-

TABLE 4
Intrasubject Variability of Various DAT Radioligands for SPECT

Study	Ligand	Total patients (n)	Delineation	Intrasubject variability*		Reliability ICC
				Healthy volunteers	Patients	
Ziebell et al. (*17*)	PE2I	7	MD HC	4.1 ± 3.2		0.96
Seibyl et al. (*20*)	β-CIT	7	Template WS	12.8 ± 8.9†		0.82
Booij et al. (*18*)	FP-CIT	6	Template HC	7.3 ± 3.2		0.92†
Tsuchida et al. (*21*)	FP-CIT	10	Template HC	11.1 ± 10.4		0.59
Pirker et al. (*31*)	β-CIT	9	MD HC	8.2 ± 7.2		0.70
Ziebell et al., current study	PE2I	8	MD HC		11.9 ± 10.0	0.88
Seibyl et al. (*20*)	β-CIT	7	Template WS		16.8 ± 13.3†	0.82
Booij et al. (*18*)	FP-CIT	6	Template HC		7.9 ± 6.9	0.72†
Tsuchida et al. (*21*)	FP-CIT	6	Template HC		7.8 ± 8.9	0.95
Hwang et al. (*19*)	Trodat	20	MD HC		10.2 ± 6.2	0.95

*Mean outcome for either BP_{ND} or SBR (±SD).
†Data extracted from publication.
ICC = intraclass correlation coefficient; HC = high-count slides; WS = whole striatum.

512146; the Toyota Foundation; the University of Copenhagen; and H:S (The Capital Region of Denmark).

REFERENCES

1. Bao SY, Wu JC, Luo WF, Fang P, Liu ZL, Tang J. Imaging of dopamine transporters with technetium-99m TRODAT-1 and single photon emission computed tomography. *J Neuroimaging.* 2000;10:200–203.
2. Brucke T, Asenbaum S, Pirker W, et al. Measurement of the dopaminergic degeneration in Parkinson's disease with [^{123}I] β-CIT and SPECT: correlation with clinical findings and comparison with multiple system atrophy and progressive supranuclear palsy. *J Neural Transm Suppl.* 1997;50:9–24.
3. Prunier C, Bezard E, Montharu J, et al. Presymptomatic diagnosis of experimental parkinsonism with ^{123}I-PE2I SPECT. *Neuroimage.* 2003;19:810–816.
4. Emond P, Guilloteau D, Chalon S. PE2I: a radiopharmaceutical for in vivo exploration of the dopamine transporter. *CNS Neurosci Ther.* 2008;14:47–64.
5. Marshall V, Grosset D. Role of dopamine transporter imaging in routine clinical practice. *Mov Disord.* 2003;18:1415–1423.
6. Scherfler C, Schwarz J, Antonini A, et al. Role of DAT-SPECT in the diagnostic work up of parkinsonism. *Mov Disord.* 2007;22:1229–1238.
7. Morrish PK. How valid is dopamine transporter imaging as a surrogate marker in research trials in Parkinson's disease? *Mov Disord.* 2003;18(suppl 7):S63–S70.
8. Poewe W, Scherfler C. Role of dopamine transporter imaging in investigation of parkinsonian syndromes in routine clinical practice. *Mov Disord.* 2003;18(suppl 7):S16–S21.
9. Knudsen GM, Karlsborg M, Thomsen G, et al. Imaging of dopamine transporters and D_2 receptors in patients with Parkinson's disease and multiple system atrophy. *Eur J Nucl Med Mol Imaging.* 2004;31:1631–1638.
10. Innis RB, Seibyl JP, Scanley BE, et al. Single photon emission computed tomographic imaging demonstrates loss of striatal dopamine transporters in Parkinson disease. *Proc Natl Acad Sci USA.* 1993;90:11965–11969.
11. Marek K, Jennings D, Seibyl J. Do dopamine agonists or levodopa modify Parkinson's disease progression? *Eur J Neurol.* 2002;9(suppl 3):15–22.
12. Zaidi H, El Fakhri G. Is absolute quantification of dopaminergic neurotransmission studies with ^{123}I SPECT ready for clinical use? *Eur J Nucl Med Mol Imaging.* 2008;35:1330–1333.
13. Delorenzo C, Kumar JD, Zanderigo F, Mann JJ, Parsey RV. Modeling considerations for in vivo quantification of the dopamine transporter using [^{11}C]PE2I and positron emission tomography. *J Cereb Blood Flow Metab.* 2009;29:1332–1345.
14. Koch W, Radau PE, Hamann C, Tatsch K. Clinical testing of an optimized software solution for an automated, observer-independent evaluation of dopamine transporter SPECT studies. *J Nucl Med.* 2005;46:1109–1118.
15. Tossici-Bolt L, Hoffmann SM, Kemp PM, Mehta RL, Fleming JS. Quantification of [^{123}I]FP-CIT SPECT brain images: an accurate technique for measurement of the specific binding ratio. *Eur J Nucl Med Mol Imaging.* 2006;33:1491–1499.
16. Seibyl JP, Laruelle M, van Dyck CH, et al. Reproducibility of iodine-123-β-CIT SPECT brain measurement of dopamine transporters. *J Nucl Med.* 1996;37:222–228.
17. Ziebell M, Thomsen G, Knudsen GM, et al. Reproducibility of [^{123}I]PE2I binding to dopamine transporters with SPECT. *Eur J Nucl Med Mol Imaging.* 2007;34:101–109.
18. Booij J, Habraken JB, Bergmans P, et al. Imaging of dopamine transporters with iodine-123-FP-CIT SPECT in healthy controls and patients with Parkinson's disease. *J Nucl Med.* 1998;39:1879–1884.
19. Hwang WJ, Yao WJ, Wey SP, Ting G. Reproducibility of ^{99m}Tc-TRODAT-1 SPECT measurement of dopamine transporters in Parkinson's disease. *J Nucl Med.* 2004;45:207–213.
20. Seibyl JP, Marek K, Sheff K, et al. Test/retest reproducibility of iodine-123-βCIT SPECT brain measurement of dopamine transporters in Parkinson's patients. *J Nucl Med.* 1997;38:1453–1459.
21. Tsuchida T, Ballinger JR, Vines D, et al. Reproducibility of dopamine transporter density measured with ^{123}I-FPCIT SPECT in normal control and Parkinson's disease patients. *Ann Nucl Med.* 2004;18:609–616.
22. Pinborg LH, Ziebell M, Frokjaer VG, et al. Quantification of ^{123}I-PE2I binding to dopamine transporter with SPECT after bolus and bolus/infusion. *J Nucl Med.* 2005;46:1119–1127.
23. Small AD, Prosser J, Motherwell DW, McCurrach GM, Fletcher AM, Martin W. Downscatter correction and choice of collimator in ^{123}I imaging. *Phys Med Biol.* 2006;51:N307–N311.
24. de Nijs R, Svarer C, Holm S. Correction for high energy photons and scatter for dynamic SPECT studies with I-123 [abstract]. *Eur J Nucl Med Mol Imaging.* 2004;31(suppl 2):402.
25. Kretschmann H-J, Weinrich W. *Neuroanatomy and Cranial Computed Tomography.* Stuttgart, Germany: Thieme; 1986.
26. Svarer C, Madsen K, Hasselbalch SG, et al. MR-based automatic delineation of volumes of interest in human brain PET images using probability maps. *Neuroimage.* 2005;24:969–979.
27. Innis RB, Cunningham VJ, Delforge J, et al. Consensus nomenclature for in vivo imaging of reversibly binding radioligands. *J Cereb Blood Flow Metab.* 2007;27:1533–1539.
28. Ichise M, Ballinger JR, Vines D, Tsai S, Kung HF. Simplified quantification and reproducibility studies of dopamine D2-receptor binding with iodine-123-IBF SPECT in healthy subjects. *J Nucl Med.* 1997;38:31–37.
29. van Dyck CH, Seibyl JP, Malison RT, et al. Age-related decline in dopamine transporters: analysis of striatal subregions, nonlinear effects, and hemispheric asymmetries. *Am J Geriatr Psychiatry.* 2002;10:36–43.
30. Marner L, Knudsen GM, Haugbol S, Holm S, Baare W, Hasselbalch SG. Longitudinal assessment of cerebral 5-HT_{2A} receptors in healthy elderly volunteers: an [^{18}F]-altanserin PET study. *Eur J Nucl Med Mol Imaging.* 2008;35:1–4.
31. Pirker W, Djamshidian S, Asenbaum S, et al. Progression of dopaminergic degeneration in Parkinson's disease and atypical parkinsonism: a longitudinal β-CIT SPECT study. *Mov Disord.* 2002;17:45–53.

Paper 4

Serotonin Transporters in Dopamine Transporter Imaging: A Head-to-Head Comparison of Dopamine Transporter SPECT Radioligands ^{123}I-FP-CIT and ^{123}I-PE2I

Morten Ziebell[1], Signe Holm-Hansen[1], Gerda Thomsen[1], Aase Wagner[2], Peter Jensen[1], Lars H. Pinborg[1,3], and Gitte Moos Knudsen[1]

[1]Neurobiology Research Unit and Cimbi, Rigshospitalet and University of Copenhagen, Copenhagen, Denmark; [2]Diagnostic Radiology, Rigshospitalet and University of Copenhagen, Copenhagen, Denmark; and [3]Department of Neurology, Epilepsy Clinic, Rigshospitalet and University of Copenhagen, Copenhagen, Denmark

Current SPECT radioligands available for in vivo imaging of the dopamine transporter (DAT) also show affinity for monoamine transporters other than DAT, especially the serotonin transporter (SERT). The effect of this lack of selectivity for in vivo imaging is unknown. In this study, we compared the SPECT radioligands ^{123}I-2-β-carbomethoxy-3β-(4-iodophenyl)-*N*-(3-fluoropropyl)nortropane (^{123}I-FP-CIT) and ^{123}I-*N*-(3-iodoprop-2E-enyl)-2-β-carbomethoxy-3β-(4-methylphenyl) (^{123}I-PE2I). ^{123}I-FP-CIT has a 10-fold higher selectivity than ^{123}I-FP-CIT for DAT versus SERT. **Methods:** Sixteen healthy individuals were scanned in random order with both radioligands. The radioligands were administered according to standard recommendations: ^{123}I-FP-CIT was given as a bolus injection, and the ratio between the striatum and reference tissue was measured after 3 h. ^{123}I-PE2I was administered in a bolus–infusion setup, and the nondisplaceable binding potential (BP_{ND}) was measured after 2 h. To assess the contribution of SERT to the overall SPECT signal, SERT was blocked by intravenous citalopram in 6 of the individuals. **Results:** The striatum-to-reference ratio − 1 of ^{123}I-FP-CIT was on average 18% higher than the striatal BP_{ND} of ^{123}I-PE2I. Equal doses of radioactivity resulted in 3 times higher counting rates for ^{123}I-FP-CIT than for ^{123}I-PE2I, both in target and in reference brain regions. Citalopram infusion led to significant reductions in both striatal (22.8% ± 20.4%, $P < 0.05$) and thalamic (63.0% ± 47.9%, $P < 0.05$) ^{123}I-FP-CIT binding ratios, whereas BP_{ND} of ^{123}I-PE2I was unaltered. Likewise, blocking of SERT led to increased (21% ± 30.1%, $P < 0.001$) plasma ^{123}I-FP-CIT, probably as a result of significant blocking of peripheral SERT binding sites. By contrast, plasma ^{123}I-PE2I remained stable. **Conclusion:** ^{123}I-FP-CIT and ^{123}I-PE2I had approximately the same target-to-background ratios, but per injected megabecquerel, ^{123}I-FP-CIT gave rise to 3-fold higher cerebral counting rates. We found that ^{123}I-FP-CIT, but not ^{123}I-PE2I, brain images have a highly interindividual but significant signal contribution from SERT. Whether the SERT signal contribution is of clinical importance needs to be established in future patient studies.

Key Words: ^{123}I-FP-CIT (DaTSCAN); ^{123}I-PE2I; SPECT

J Nucl Med 2010; 51:1885–1891
DOI: 10.2967/jnumed.110.078337

Cocaine labeled with ^{11}C was the first radioligand to be used for imaging the cerebral dopamine transporter (DAT) in vivo (*1*), but several other radioligands have subsequently been developed and tested as PET or SPECT ligands. With the introduction of 2-β-carbomethoxy-3β-(4-iodophenyl)-tropane (^{123}I-β-CIT) in 1991 (*2*), brain imaging of the DAT became a clinically useful method for supplementary diagnosis of movement disorders. A couple of serious drawbacks with ^{123}I-β-CIT are that the radioligand has equal affinity for DATs and serotonin transporters (SERT) and that the slow kinetics of the ligand require imaging to be conducted 24 h after bolus injection.

2-β-carbomethoxy-3β-(4-iodophenyl)-*N*-(3-fluoropropyl)-nortropane (FP-CIT) was synthesized in 1994 (*3*); its cerebral distribution and dosimetry in healthy volunteers was subsequently reported by Booij et al. in 1998 (*4*). ^{123}I-FP-CIT, compared with ^{123}I-β-CIT, has an improved selectivity for DAT versus SERT (Table 1), and because of its lower DAT affinity ^{123}I-FP-CIT has much faster kinetic properties, with a striatal peak time at 148 min after intravenous injection. Faster kinetic properties mean that with ^{123}I-FP-CIT, the time between tracer injection and SPECT could be reduced to 3 h, making it more feasible for use in the scanning of outpatients (*5*). With a bolus injection and without measurements of the arterial input function, the outcome parameter (usually the binding ratio between a target and a reference region) does, however, become sensitive to intersubject variation in the plasma clearance rate of the radioligand (*6*). ^{123}I-FP-CIT was licensed as DaTSCAN (Amersham Health) in Europe in 2000, and since then it has become a frequently used SPECT radioligand, particularly as an ancillary tool to diagnose patients with movement disorders. In 2006, more than 500 European SPECT

Received Apr. 19, 2010; revision accepted Sep. 7, 2010.
For correspondence contact: Gitte Moos Knudsen, Neurobiology Research Unit, Rigshospitalet, N9201, 9 Blegdamsvej, Copenhagen, DK-2100 Denmark.
E-mail: gmk@nru.dk

centers were using ^{123}I-FP-CIT for clinical purposes (*7*). The radioligand has also been widely used in both preclinical and clinical studies; a PubMed search in January 2010 shows that ^{123}I-FP-CIT currently is mentioned in over 275 scientific papers.

^{123}I-labeled *N*-(3-iodoprop-2E-enyl)-2-β-carbomethoxy-3β-(4-methylphenyl), named PE2I (MAP Medical Technologies), was synthesized in 1997 (*8*), and a dosimetry study in humans was published in 1998 (*9*). The ligand has about a 30-fold higher affinity for DAT than for SERT (Table 1), and because of its lower affinity to DAT ^{123}I-PE2I has faster kinetics than ^{123}I-FP-CIT, with a striatal peak time between 30 and 60 min. Quantification of ^{123}I-PE2I binding to DAT is possible using kinetic or graphical analysis after bolus injection of the tracer and SPECT for 90 min or as a combination of bolus and constant infusion, for which unvarying levels in plasma and brain tissue are achieved after approximately 2 h (*10,11*). PE2I has also proven suitable as an ^{11}C-labeled PET probe (*12*). In ^{123}I-labeled form, neither PE2I nor FP-CIT gives rise to radiolabeled metabolites that can permeate the blood–brain barrier (*13,14*). Despite its favorable properties, ^{123}I-PE2I is currently not licensed as a SPECT radioligand for clinical use.

The aim of this study was to compare ^{123}I-PE2I and ^{123}I-FP-CIT in a head-to-head design in terms of their binding parameters in various brain regions of interest (ROIs) and examine the significance of the SERT contribution to the total signal. The contribution was addressed by blocking the SERT with acute citalopram (Seropram; Lundbeck A/S) infusion.

MATERIALS AND METHODS

Sixteen healthy individuals (mean age ± SD, 43.1 ± 16.7 y; age range, 21–69 y; 10 men) were included; a diagram of the study design is shown in Figure 1. All subjects gave written informed consent. The study was performed in accordance with the ethical standards of the Declaration of Helsinki and was approved by the ethical committee of Copenhagen Capital Region (protocol H-B-2008-024).

The healthy volunteers were recruited through advertising on the Internet or in newspapers. None of the subjects had any history of neurologic or psychiatric disorders, and they all claimed no drug or alcohol abuse. None smoked, nor were any taking medication. Cerebral MRI scans were obtained before the first SPECT scan, to exclude structural abnormalities and signs of vascular pathology. The results of routine urine drug tests and routine blood tests were normal in all subjects.

TABLE 1
SERT and DAT Binding Affinity of Inhibitor (K_i), as Measured in Rat Brain Homogenates

Ligand	K_i DAT (nM), ^{3}H-GBR-12935	K_i SERT (nM), ^{3}H-paroxetine	SERT-to-DAT ratio
^{123}I-β-CIT*	27	3	0.1
^{123}I-FP-CIT†	3.5	9.7	2.8
^{123}I-PE2I*	17	500	29.4

*According to study of Abi-Dargham et al. (*5*).
†According to study of Emond et al. (*8*).

Experimental Procedures

Radioligand Administration. Cannulas were inserted into both cubital veins for radioligand administration and blood sampling. To block thyroidal uptake of free radioiodine, all subjects received 200 mg of potassium perchloride intravenously 30 min before either ^{123}I-PE2I or ^{123}I-FP-CIT injection.

Baseline Experiments. In 10 subjects, the radioligands were administered according to standardized protocols, adapted to the differences in the kinetic properties (*5,10*).

^{123}I-PE2I. A bolus–infusion protocol of 2.7 (i.e., the bolus is worth 2.7 h of infusion) was used (*10,11*). An average intravenous bolus of 2.0 ± 0.1 mL (mean, 77.1 MBq [range, 65.3–91.7 MBq]) of ^{123}I-PE2I was administered. The intravenous bolus was immediately followed by a constant infusion (for a total of 3 h) of 3 ± 0.1 mL (mean, 103.7 MBq [range, 92.3–124.2 MBq]) of ^{123}I-PE2I dissolved in 43 mL of saline. The mean injected mass of PE2I was 1×10^{-3} μg/mL. Six SPECT acquisitions, each lasting 10 min, were obtained between 120 and 180 min after ^{123}I-PE2I injection.

^{123}I-FP-CIT. An average intravenous bolus of 2.0 ± 0.1 mL (mean, 190.2 MBq [range, 184.3–202.2 MBq]) of ^{123}I-FP-CIT was administered. The mean injected mass of FP-CIT was 0.1 μg/mL. Six SPECT acquisitions, each lasting 10 min, were obtained between 180 and 240 min after ^{123}I-FP-CIT injection.

There was an average of 10 d (range, 7 to 14 d) between the ^{123}I-FP-CIT and ^{123}I-PE2I scan; scans were acquired in randomized order.

Citalopram Experiments. Six additional subjects participated in a citalopram experiment. Citalopram (40 mg/mL) was given at a dose of 0.15 mg/kg of body weight. The infusion lasted 30 min and was administered using an infusion pump.

For ^{123}I-FP-CIT, the subjects underwent 2 SPECT scannings (1 d apart): a baseline scan and second scan that was immediately preceded by citalopram injection before the SPECT acquisition. For both scans, 24 × 10-min acquisitions (complete time–activity curves) were obtained between 0 and 240 min.

For ^{123}I-PE2I, the subjects underwent only 1 SPECT scanning. The acquisition was extended to 1 h, with a maintained bolus-to-infusion ratio. One hundred minutes after ^{123}I-PE2I injection, a 40-min baseline scan was obtained, and then citalopram infusion was started and scanning data were acquired for an additional 100 min. Frames from 100 to 140 and from 140 to 240 min (8 × 5 and 10 × 10 min, respectively) were obtained.

All subjects were monitored with standard electrocardiogram and blood pressure measurements.

Blood Sampling. Venous blood was collected every 10 min at the SPECT frame mid time. The sample was centrifuged, plasma was collected, and octanol was added to derive the lipophilic phase containing the radioligand parent compound (*14*). The sample was shaken and centrifuged, the octanol phase was pipetted into a counting vial, and, finally, radioactivity was measured in a γ-counter (Cobra II; Packard Instrument Co.).

Citalopram concentrations in blood were measured at 30 and 90 min after citalopram injection.

SPECT Acquisition and Image Reconstruction. SPECT images were acquired with a triple-head IRIX camera (Philips Medical) fitted with low-energy, general all-purpose, parallel-hole collimators (spatial resolution, 8.5 mm at 10 cm). The mean radius of

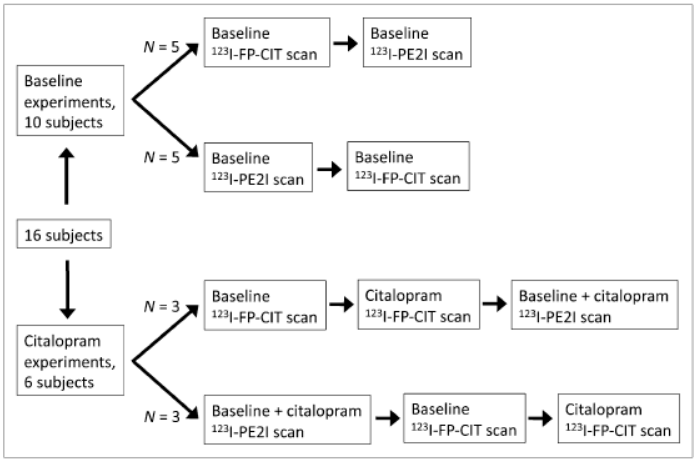

FIGURE 1. Flowchart of study design. Ten subjects were randomized to receive either ^{123}I-PE2I or ^{123}I-FP-CIT for first scan. Six additional subjects were randomized to receive either ^{123}I-PE2I or ^{123}I-FP-CIT for baseline scan before corresponding citalopram challenge scan. To use all baseline experiments for head-to-head comparison of ^{123}I-PE2I or ^{123}I-FP-CIT, we also included baseline (i.e., without drug) experiments from citalopram experiments, so that total number of individuals with baseline and no-drug experiments was 16.

rotation was 15.2 cm. Each head covered 120° of the circular orbit. Scans were obtained and stored at fixed angles, with an angular interval of 3°.

The images were reconstructed with a MATLAB 6.5 (The MathWorks)–based program in 128 × 128 matrices (2.33-mm pixels and identical slice thickness) using standard filtered backprojection with a low-pass fourth-order Butterworth filter at 0.3 Nyquist (0.64 cm^{-1}). This method is discussed in further detail in the study by Ziebell et al. (*15*).

ROIs

ROIs were manually delineated because we previously have shown that manually derived delineation is comparable to MRI-guided ROI delineation in DAT SPECT quantification (*15*). This comparability is probably because these small ROIs can move easily out of the hot spot, despite the use of external fiducial markers, which should improve coregistration accuracy. Therefore, delineation of ROIs in DAT SPECT images is only a close estimate but never a 100% exact anatomic ROI with regard to the size, shape, and positioning, no matter the method used (manual delineation directly on the SPECT image, population-based template-guided delineation, delineation based on coregistration with another brain image that provides structural information, such as MRI) (*15*).

The ROIs were outlined by 1 delineator with more than 5 y of experience; in the case of the ^{123}I-FP-CIT scans, the delineator was unaware of whether citalopram had been administered. ROIs were delineated directly on the reconstructed SPECT images, guided by the use of Kretschmann and Weinrich's neuroanatomic atlas (*16*). Direct adaptation of ROI coordinates from the atlas required the use of a MATLAB program (The MathWorks) adapted in-house to reorient the reconstructed images to the cantho-meatally oriented plane. ROIs were delineated on 5 consecutive slices (2.3 mm/slice) in a summed image from all SPECT frames acquired from the scanning.

The ROIs were first randomly delineated either on the ^{123}I-FP-CIT image or on the ^{123}I-PE2I image. Then the 2 images were coregistered using visual assessment, and the ROI was transferred to the image of the other radioligand. Finally, the placement of the ROIs was adjusted to get the maximum counts per ROI, without changing the size or shape of the ROI. ROIs were optimized to eliminate coregistration errors.

Derivation of Binding Parameters

Because ^{123}I-FP-CIT is administered as a bolus alone and ^{123}I-PE2I as a bolus followed by a constant infusion, binding parameters are not directly comparable in the baseline experiments (n = 10). In these experiments, ^{123}I-FP-CIT was measured from 3 to 4 h after bolus injection, and ^{123}I-FP-CIT was therefore not in a true steady-state condition. With ^{123}I-PE2I, however, specific binding to nondisplaceable binding is measured at steady-state conditions, which are reached between 100 and 180 min (*10*).

It is only at true steady-state conditions that the ratio of specific to nondisplaceable binding is equal to the binding potential of the nondisplaceable radioligand (BP_{ND}) (*17*). Therefore, in the ^{123}I-FP-CIT baseline experiments we refer to the outcome as binding ratios and not BP_{ND}.

BP_{ND} was calculated as:

$$BP_{ND} = \frac{\text{Total radioligand}}{\text{Nondisplaceable radioligand}} - 1,$$

where nondisplaceable equals the sum of the free and nonspecific bound radioligand concentration represented by the cerebellum, which is assumed to be devoid of DAT.

To do an exact comparison of BP_{ND} between the 2 radioligands in the citalopram experiments (n = 6), we had to calculate true ^{123}I-FP-CIT BP_{ND}, which is done by obtaining full ^{123}I-FP-CIT time–activity curves and applying simplified reference tissue modeling (SRTM) (*18*). ^{123}I-PE2I is in true a steady-state condition; thus, we could conduct a within-scan pharmacologic SERT displacement with citalopram while continuing to acquire the time–activity curves. SRTM was performed with PMOD software (version 3.0; PMOD Technologies).

Changes in the plasma concentrations of the radioligand after citalopram administration were calculated differently for the 2 radiotracers. For ^{123}I-FP-CIT, we used the plasma time–activity data to calculate the area under the curve, and for ^{123}I-PE2I we

took advantage of ^{123}I-PE2I attaining tracer steady state and simply compared plasma concentration before, during, and after the pharmacologic challenge.

Statistical Analysis

All statistical analyses were performed with GraphPad Prism (version 5.00; GraphPad Software Inc.). Unless otherwise stated, all values are given as mean ± SD.

A 2-tailed paired *t* test was used to compare binding ratios and BP_{ND} values obtained with the 2 radioligands. *P* values below 0.05 were considered statistically significant. All values are given with 95% confidence interval. Because of the small sample size in the citalopram experiments ($n = 6$), we used a nonparametric Wilcoxon matched-pairs signed rank sum test.

RESULTS

Counting Rates and Binding

Compared with ^{123}I-PE2I, for ^{123}I-FP-CIT the average counting rates were 3.0 ± 0.9 (range, 1.7–4.8) times higher in the striatum, 3.4 ± 0.9 (range, 2.1–5.6) times higher in the thalamus, and 2.7 ± 0.6 (range, 1.7–4.0) times higher in the cerebellum. The individual striatal- and thalamic-to-cerebellum binding ratios or BP_{ND}s are shown in Figure 2. The average binding ratio was 3.6 ± 0.7 for ^{123}I-FP-CIT, which was significantly higher than the BP_{ND} of 3.0 ± 0.5 for ^{123}I-PE2I (*t* test, $P < 0.005$). One individual had an ^{123}I-FP-CIT binding ratio lower than the ^{123}I-PE2I BP_{ND}; the remaining 15 individuals had between 0% and 30% higher ^{123}I-FP-CIT binding ratios. The average thalamus–to–cerebellum binding ratio was 0.9 ± 0.3 for ^{123}I-FP-CIT—significantly higher than the BP_{ND} of 0.5 ± 0.2 for ^{123}I-PE2I (*t* test, $P < 0.001$). Seen consistently in all individuals, the individual thalamus binding ratio was between 10% and 800% higher for ^{123}I-FP-CIT than the BP_{ND} was for ^{123}I-PE2I. Because the thalamus has 20 times more SERT than DAT binding sites and the proportions are opposite in the striatum (*19–21*), we calculated the thalamic-to-striatal ratio as proxy for in vivo DAT selectivity (Fig. 3). This ratio was 46% higher for ^{123}I-FP-CIT than for ^{123}I-PE2I

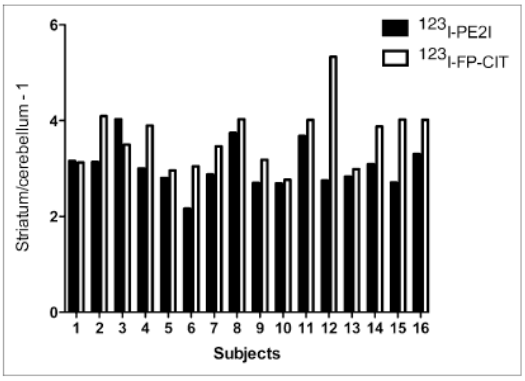

FIGURE 2. Individual ratios of specific to nonspecific striatal binding ($n = 16$). ^{123}I-FP-CIT binding ratio is significantly higher than ^{123}I-PE2I BP_{ND} (*t* test, $P < 0.05$).

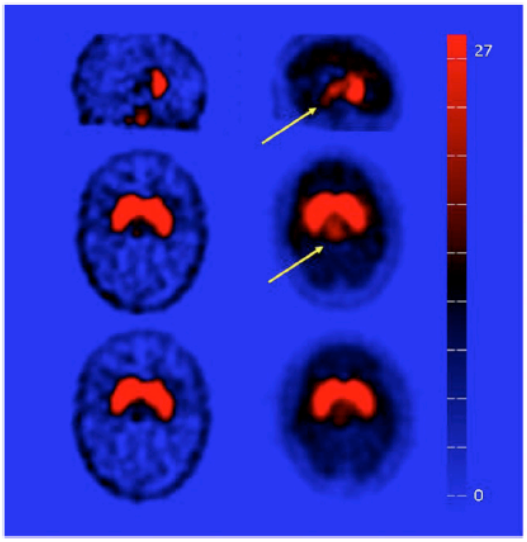

FIGURE 3. ^{123}I-PE2I image (left) and ^{123}I-FP-CIT image (right) of same individual. In first 2 rows (sagittal and horizontal slices), thalamus is clearly visualized in ^{123}I-FP-CIT image (arrows). Bottom row shows images after acute SERT blocking with citalopram.

(*t* test, $P < 0.005$). For both radioligands, the ratio of caudate to putamen binding was not significantly different from 1 (*t* test, $P > 0.1$). Finally, the standard reference regions were compared; there was no statistically significant difference for either radioligand between mean counts in occipital cortex and cerebellum (*t* test, $P > 0.5$).

Citalopram Experiments

All subjects, except for 1, received the planned dose of 0.15 mg of citalopram per kilogram of body weight. One volunteer experienced nausea and vomiting 15 min after citalopram administration was initiated; therefore, the infusion was stopped (at the current dose of 0.11 mg/kg) and symptoms disappeared within a few minutes. For the second scan, 0.11 mg of citalopram per kilogram was administered over 30 min (as in the first scan), and this time the subject did not experience any side effects. One subject had a mild drop in blood pressure, from 110 to 95 mm Hg, lasting for 2 h. The other 5 volunteers felt slightly lightheaded for a few minutes toward the end of the infusion, but this effect disappeared a few minutes after citalopram infusion was terminated. The mean plasma citalopram concentration at 30 and 90 min after radiotracer injection was 52.2 ± 11.4 and 47.3 ± 9.6 nmol/L, respectively. No difference in mean plasma citalopram concentrations between the 2 radioligands was observed: ^{123}I-FP-CIT, 47.0 ± 10.0 nmol/L, and ^{123}I-PE2I, 52.4 ± 11.0 nmol/L. After administration of citalopram, compared with the unblocked condition, the area under the curve of the venous blood samples for ^{123}I-FP-CIT (from 0 to 240 min) increased by 21.2% (range, 1.6%–82.0%) (Wilcoxon, $P < 0.05$). By

contrast, citalopram infusion did not alter ^{123}I-PE2I plasma radioactivity. Acute citalopram treatment resulted in an average decrease in ^{123}I-FP-CIT BP_{ND} values of 22.8% (range, −9.0%–43.2%) in the striatum (Wilcoxon, $P < 0.05$) and of 63.0% (range, 19.0%–131.3%) in the thalamus (Wilcoxon, $P < 0.05$). When the ratio method (based on 180–240 min) was used instead, these numbers were 15.6% (range, 0.5%–38.0%) and 86.3% (range, 25.2%–125.7%). There was no correlation between the relative decrease in BP_{ND} in the striatum and thalamus within the single individual.

For ^{123}I-PE2I, citalopram infusion did not alter BP_{ND} in the striatum or thalamus (Wilcoxon, $P > 0.1$). Figure 4 shows ^{123}I-PE2I and ^{123}I-FP-CIT images retrieved for the same individual; binding in the thalamus is easily appreciated in the ^{123}I-FP-CIT image, disappearing after citalopram infusion. The individual BP_{ND} in relation to the citalopram infusion is shown in Figures 5A and 5B. Figure 5C illustrates how the individual striatal BP_{ND} obtained from ^{123}I-FP-CIT approximates the BP_{ND} obtained with ^{123}I-PE2I after citalopram infusion. For ^{123}I-FP-CIT, the SRTM fitted the time–activity curve from 0 to 240 min. We estimated the distribution volume in the cerebellum—that is, the ratio of the total concentration of radioligand in the cerebellum to the total concentration of radioligand in plasma, using the venous blood samples from 0 to 240 min. This distribution volume was 1.5 ± 0.6 Bq/mL (brain)/Bq/mL (blood) for ^{123}I-PE2I and 5.5 ± 2.0 for ^{123}I-FP-CIT. In all 6 individuals, the SRTM-determined BP_{ND} obtained with ^{123}I-FP-CIT at baseline was significantly higher than BP_{ND} for ^{123}I-PE2I: ^{123}I-FP-CIT, 4.2 ± 0.7, and ^{123}I-PE2I, 3.1 ± 0.4 (Wilcoxon, $P < 0.05$). This difference was, however, highly variable among the individuals, ranging from 5% to 93%. The difference between ^{123}I-PE2I BP_{ND} and

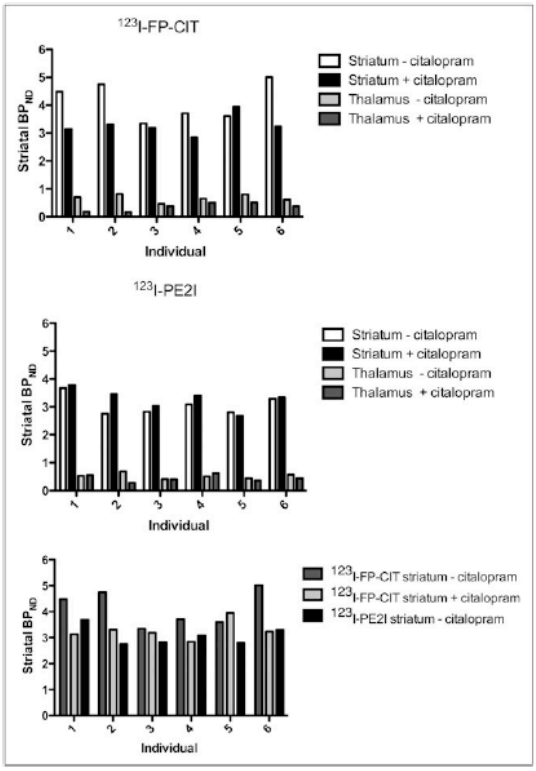

FIGURE 5. Response to citalopram infusion, expressed as change in BP_{ND} in striatum and thalamus. BP_{ND} for ^{123}I-FP-CIT was calculated with SRTM; BP_{ND} for ^{123}I-PE2I was calculated as ratio between steady-state tissue levels. (C) BP_{ND} for ^{123}I-FP-CIT approaches BP_{ND} for ^{123}I-PE2I after SERT blocking. Same subject was used for all experiments.

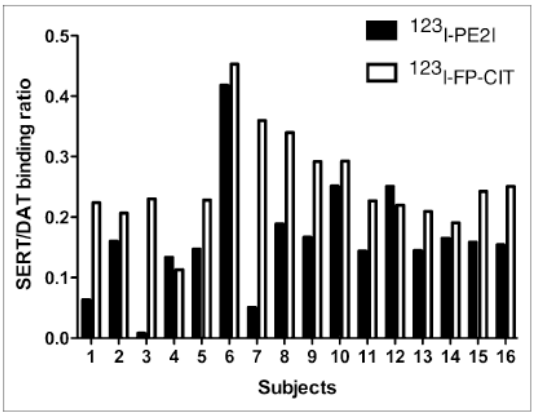

FIGURE 4. As proxy for in vivo SERT and DAT selectivity of ^{123}I-PE2I and ^{123}I-FP-CIT, individual specific-to-nonspecific ratio in thalamus to individual specific-to-nonspecific ratio in striatum is shown. Ratio for ^{123}I-FP-CIT is significantly higher than for ^{123}I-PE2I (*t* test, $P < 0.005$, $n = 16$).

^{123}I-FP-CIT binding ratio disappeared after citalopram infusion: ^{123}I-FP-CIT, 3.3 ± 0.4, and ^{123}I-PE2I, 3.3 ± 0.4 (Wilcoxon, $P > 0.2$).

There was no significant difference in BP_{ND} and simple binding ratio obtained from 180 to 240 min after ^{123}I-FP-CIT injection (Wilcoxon, $P > 0.5$). The individual terminal venous plasma clearance was stable; on average, it decreased 5.9% per hour in the fourth hour after bolus injection.

DISCUSSION

To our knowledge, this is the first study of a head-to-head design to compare DAT and SERT binding properties of the 2 SPECT DAT radioligands ^{123}I-PE2I and ^{123}I-FP-CIT and to assess the contribution of SERT to the total signal. In this study, we found 3-fold higher brain counting rates per injected megabecquerel for ^{123}I-FP-CIT than for ^{123}I-PE2I. The ratio of striatal specific to nondisplaceable binding for ^{123}I-FP-CIT was almost 20% higher than the BP_{ND} of ^{123}I-PE2I, but after acute blocking of SERT with citalo-

pram no significant difference in the specific-to-nondisplaceable striatal binding of ^{123}I-FP-CIT versus ^{123}I-PE2I was observed. Although ^{123}I-PE2I BP_{ND} was unaffected by citalopram infusion, ^{123}I-FP-CIT BP_{ND} declined significantly. Citalopram infusion increased the plasma concentration of ^{123}I-FP-CIT but not of ^{123}I-PE2I; this increase supported the finding that peripheral SERT binding sites, particularly in the lung tissue (*4*), were blocked, resulting in a higher availability of ^{123}I-FP-CIT but not of ^{123}I-PE2I.

Count statistics per injected megabecquerel for ^{123}I-FP-CIT are superior to those for ^{123}I-PE2I; these better count statistics are particularly beneficial in patients with low DAT binding. In addition, the higher brain uptake of ^{123}I-FP-CIT is beneficial and, compared with ^{123}I-PE2I, its higher uptake can be translated into a better determination of the target-to-background ratio or into a lower dose of radioactivity by shortening the scanning time.

We chose to compare the 2 radioligands using experimental setups most commonly used in the clinical setting—that is, bolus (^{123}I-FP-CIT) and bolus–infusion (^{123}I-PE2I) schedules. At the time of measurement, ^{123}I-FP-CIT was not in a steady-state condition in plasma or in tissue but was in a transient equilibrium. In theory, the ^{123}I-FP-CIT binding ratio overestimates the steady-state BP_{ND} because of the effect of the terminal plasma clearance rate—a problem originally addressed by Carson et al. in 1993 (*6*). We found, however, that the actual terminal plasma clearance rate was stable, with an average of an approximately 6% decline per hour; second, there was no difference between BP_{ND} calculated using SRTM and the binding ratio obtained as a mean from 180 to 240 min after ^{123}I-FP-CIT injection. Thus, transient equilibrium analysis of ^{123}I-FP-CIT does not explain the higher ratio for ^{123}I-FP-CIT than for ^{123}I-PE2I in healthy individuals. As a note of caution, however, altered plasma clearance may occur in patients with, for example, renal diseases or with altered metabolism of ^{123}I-FP-CIT.

We also evaluated the potential confounding effect of SERT on the total striatal signal in what is presumed to be cerebral DAT imaging. Because of the following reasons, our results confirmed in vitro data, suggesting that the higher in vivo binding ratio of nondisplaceable radioligand for ^{123}I-FP-CIT than for ^{123}I-PE2I was related to SERT binding. First, a significantly higher binding was seen in a SERT high-density region, the thalamus, for ^{123}I-FP-CIT than for ^{123}I-PE2I, both in absolute terms and when assessed as the thalamus-to-striatum ratio. Second, acute blockade of SERT before ^{123}I-FP-CIT administration was associated with significantly increased plasma ^{123}I-FP-CIT levels, because of the lower peripheral binding of ^{123}I-FP-CIT. This increased plasma was not seen with ^{123}I-PE2I. Finally, a significant decrease in BP_{ND} (average, 24%) of ^{123}I-FP-CIT was observed in the striatum after SERT blocking, whereas no significant change in BP_{ND} for ^{123}I-PE2I was observed.

We found a considerable interindividual variability in ^{123}I-FP-CIT binding, both in comparison to ^{123}I-PE2I binding and in response to SERT blockade, with striatal BP_{ND} decreases of between −8% and 43% for ^{123}I-FP-CIT. This variability could be because of the SERT density (density of transporters available to radioligand binding [B_{avail}]), or affinity (K_d) of the SERT for ^{123}I-FP-CIT, K_d of citalopram, or relative DAT versus SERT density ratio in that region. We considered the K_d of citalopram a less likely reason because we did not observe any correlation between the effect of citalopram on BP_{ND} for SERT low- and high-density regions.

In theory, if the observed higher striatal target-to-background ratio for ^{123}I-FP-CIT than for ^{123}I-PE2I should be explained by variations in the relative striatal densities of DAT and SERT, and assuming published in vitro K_i values for the radioligands, then the striatal $B_{avail,\ DAT}$–to–$B_{avail,\ SERT}$ ratio would need to be below 5:1 (Supplemental Appendix; supplemental materials are available online only at http://jnm.snmjournals.org). Human postmortem brain studies point toward a $B_{avail,\ DAT}$–to–$B_{avail,\ SERT}$ ratio of 20:1 in the putamen (~200:10 pmol/g) (*20,21*). This ratio could probably vary somewhat in healthy subjects, and a large variation in BP_{ND} has indeed been reported in in vivo studies (SD of BP_{ND} for SERT, 23% of mean (*22,23*), and for DAT, 13% of mean (*11,24*)). Hence, our large decrease in ^{123}I-FP-CIT signal after citalopram blocking suggests that the superiority of ^{123}I-PE2I over ^{123}I-FP-CIT is even more selective in vivo than in vitro.

Acute blocking of the SERT decreased striatal BP_{ND} as measured with ^{123}I-FP-CIT, to the same level as that for ^{123}I-PE2I. On the basis of the available in vitro data on ^{123}I-FP-CIT DAT versus SERT selectivity and affinity, the extent to which SERT blocking decreased striatal BP_{ND} was larger than expected (Supplemental Appendix). Three previous studies have investigated the striatal ^{123}I-FP-CIT binding in response to semichronic selective serotonin reuptake inhibitor treatment (*25–27*), and despite reporting significant binding to SERT sites in the lungs, increased—and not decreased—striatal binding ratios were reported. The main difference between these studies and our study is that selective serotonin reuptake inhibitor treatment was not administered acutely or intravenously, but over days and orally. It is possible that the more chronic administration induced alterations in both DAT and SERT, preventing a straightforward interpretation of the data.

Finally, we want to address the fact that BP_{ND} is proportional to the free fraction of the nondisplaceable radioligand in the brain (f_{ND}). It is hard to imagine that infusion of citalopram should occupy the total amount of protein binding sites in the brain affecting the f_{ND} and thereby the nondisplaceable binding of ^{123}I-FP-CIT. Further, if such an effect would occur, it would increase the f_{ND} and not decrease it, leading to an increase in ^{123}I-FP-CIT BP_{ND}.

CONCLUSION

In the clinic, ^{123}I-FP-CIT has the advantage of the experimental simplicity of a bolus-alone setup, and as we have shown here, this radioligand has a substantially higher brain

uptake than ^{123}I-PE2I. The interval between ^{123}I-FP-CIT injection and scanning is 3 h, compared with 2 h for ^{123}I-PE2I, but patients scanned with ^{123}I-PE2I are connected to an infusion pump and therefore restricted in their physical activities during these hours. The bolus–infusion setup is easily implemented for routine use. In our SPECT laboratory, we conduct more than 100 diagnostic ^{123}I-PE2I SPECT scans annually. The number of acquisitions is the same for both radiotracers.

Yet, the simplicity of ^{123}I-FP-CIT administration may compromise exact quantification of the binding. The mode of administration of ^{123}I-FP-CIT makes it susceptible to interindividual variation in the terminal plasma clearance rate of the tracer, which may be a particular problem in medicated patients or in patients with concomitant medical disorders. However, for the healthy unmedicated subjects studied here, the influence of the terminal plasma clearance rate on the outcome parameter is not quantitatively important. The variation in terminal plasma clearance rate is, in theory, eliminated using the bolus–infusion approach we used for ^{123}I-PE2I.

As we have shown in this study, the most important disadvantage of ^{123}I-FP-CIT, compared with ^{123}I-PE2I, is the lack of selectivity for DAT. This lack of selectivity is quantitatively important, as we demonstrated after citalopram blocking or displacement in healthy volunteers. The outcome parameter of a ^{123}I-FP-CIT SPECT experiment is clearly more susceptible to up- and downregulation of striatal SERT and to coadministration of SERT blocking or modulating pharmaceuticals. The inferior DAT selectivity of ^{123}I-FP-CIT, compared with ^{123}I-PE2I, is likely to be more pronounced in patients with low DAT density in the striatum, as demonstrated in the Supplemental Appendix. This inferior selectivity has to be examined in similar studies of patients with low DAT density.

ACKNOWLEDGMENTS

We thank Svitlana Olsen and Glenna Skouboe for expert technical assistance and Kirsten Møller, PhD, DMSc, Jesper Poulsen, and Ronni Plovsing for precautionary measures during citalopram infusion. This work was supported by Rigshospitalet, the Lundbeck Foundation, the EC-FP6-project DiMI LSHB-CT-2005-512146, the Toyota Foundation, the University of Copenhagen, and HR (the Capital Region of Denmark). Part of the data were acquired in conjunction with the establishment of a European database of ^{123}I-FP-CIT SPET scans of healthy controls (ENC-DAT) sponsored by the EANM/European Network of Excellence for Brain Imaging.

REFERENCES

1. Fowler JS, Volkow ND, Wolf AP, et al. Mapping cocaine binding sites in human and baboon brain in vivo. *Synapse.* 1989;4:371–377.
2. Neumeyer JL, Wang SY, Milius RA, et al. [^{123}I]-2 β-carbomethoxy-3 β-(4-iodophenyl)tropane: high-affinity SPECT radiotracer of monoamine reuptake sites in brain. *J Med Chem.* 1991;34:3144–3146.
3. Neumeyer JL, Wang S, Gao Y, et al. *N*-ω-fluoroalkyl analogs of (1R)-2 β-carbomethoxy-3 β-(4-iodophenyl)-tropane (β-CIT): radiotracers for positron emission tomography and single photon emission computed tomography imaging of dopamine transporters. *J Med Chem.* 1994;37:1558–1561.
4. Booij J, Busemann Sokole E, Stabin MG, Janssen AG, de Bruin K, van Royen EA. Human biodistribution and dosimetry of [^{123}I]FP-CIT: a potent radioligand for imaging of dopamine transporters. *Eur J Nucl Med.* 1998;25:24–30.
5. Abi-Dargham A, Gandelman MS, DeErausquin GA, et al. SPECT imaging of dopamine transporters in human brain with iodine-123-fluoroalkyl analogs of β-CIT. *J Nucl Med.* 1996;37:1129–1133.
6. Carson RE, Channing MA, Blasberg RG, et al. Comparison of bolus and infusion methods for receptor quantitation: application to [^{18}F]cyclofoxy and positron emission tomography. *J Cereb Blood Flow Metab.* 1993;13:24–42.
7. Booij J, Kemp P. Dopamine transporter imaging with [^{123}I]FP-CIT SPECT: potential effects of drugs. *Eur J Nucl Med Mol Imaging.* 2008;35:424–438.
8. Emond P, Garreau L, Chalon S, et al. Synthesis and ligand binding of nortropane derivatives: *N*-substituted 2β-carbomethoxy-3β-(4′-iodophenyl)nortropane and *N*-(3-iodoprop-(2E)-enyl)-2β-carbomethoxy-3β-(3′,4′-disubstituted phenyl)nortropane—new high-affinity and selective compounds for the dopamine transporter. *J Med Chem.* 1997;40:1366–1372.
9. Kuikka JT, Baulieu JL, Hiltunen J, et al. Pharmacokinetics and dosimetry of iodine-123 labelled PE2I in humans, a radioligand for dopamine transporter imaging. *Eur J Nucl Med.* 1998;25:531–534.
10. Pinborg LH, Ziebell M, Frokjaer VG, et al. Quantification of ^{123}I-PE2I binding to dopamine transporter with SPECT after bolus and bolus/infusion. *J Nucl Med.* 2005;46:1119–1127.
11. Ziebell M, Thomsen G, Knudsen GM, et al. Reproducibility of [^{123}I]PE2I binding to dopamine transporters with SPECT. *Eur J Nucl Med Mol Imaging.* 2007;34:101–109.
12. Delorenzo C, Kumar JD, Zanderigo F, Mann JJ, Parsey RV. Modeling considerations for in vivo quantification of the dopamine transporter using [^{11}C]PE2I and positron emission tomography. *J Cereb Blood Flow Metab.* 2009;29:1332–1345.
13. Seibyl JP, Marek K, Sheff K, et al. Iodine-123-β-CIT and iodine-123-FPCIT SPECT measurement of dopamine transporters in healthy subjects and Parkinson's patients. *J Nucl Med.* 1998;39:1500–1508.
14. Videbaek C. G.M. K, K. B. Octanol extraction yields similar results as HPLC for quantitation of [^{123}I]PE2I metabolism [abstract]. *Eur J Nucl Med.* 1999;26:1139.
15. Ziebell M, Pinborg LH, Thomsen G, et al. MRI-guided region-of-interest delineation is comparable to manual delineation in dopamine transporter SPECT quantification in patients: a reproducibility study. *J Nucl Med Technol.* 2010;38:61–68.
16. Kretschmann H-J, Weinrich W. *Neuroanatomy and Cranial Computed Tomography.* Stuttgart, Germany: Thieme; 1986.
17. Innis RB, Cunningham VJ, Delforge J, et al. Consensus nomenclature for in vivo imaging of reversibly binding radioligands. *J Cereb Blood Flow Metab.* 2007; 27:1533–1539.
18. Lammertsma AA, Hume SP. Simplified reference tissue model for PET receptor studies. *Neuroimage.* 1996;4:153–158.
19. Hall H, Halldin C, Guilloteau D, et al. Visualization of the dopamine transporter in the human brain postmortem with the new selective ligand [^{125}I]PE2I. *Neuroimage.* 1999;9:108–116.
20. Madras BK, Gracz LM, Fahey MA, et al. Altropane, a SPECT or PET imaging probe for dopamine neurons: III. Human dopamine transporter in postmortem normal and Parkinson's diseased brain. *Synapse.* 1998;29:116–127.
21. Varnas K, Halldin C, Hall H. Autoradiographic distribution of serotonin transporters and receptor subtypes in human brain. *Hum Brain Mapp.* 2004;22:246–260.
22. Matsumoto R, Ichise M, Ito H, et al. Reduced serotonin transporter binding in the insular cortex in patients with obsessive-compulsive disorder: a [^{11}C]DASB PET study. *Neuroimage.* 2009;49:121–126.
23. Frankle WG, Slifstein M, Gunn RN, et al. Estimation of serotonin transporter parameters with ^{11}C-DASB in healthy humans: reproducibility and comparison of methods. *J Nucl Med.* 2006;47:815–826.
24. Booij J, Habraken JB, Bergmans P, et al. Imaging of dopamine transporters with iodine-123-FP-CIT SPECT in healthy controls and patients with Parkinson's disease. *J Nucl Med.* 1998;39:1879–1884.
25. Booij J, de Jong J, de Bruin K, Knol R, de Win MM, van Eck-Smit BL. Quantification of striatal dopamine transporters with ^{123}I-FP-CIT SPECT is influenced by the selective serotonin reuptake inhibitor paroxetine: a double-blind, placebo-controlled, crossover study in healthy control subjects. *J Nucl Med.* 2007;48: 359–366.
26. de Win MM, Habraken JB, Reneman L, van den Brink W, den Heeten GJ, Booij J. Validation of [^{123}I]β-CIT SPECT to assess serotonin transporters in vivo in humans: a double-blind, placebo-controlled, crossover study with the selective serotonin reuptake inhibitor citalopram. *Neuropsychopharmacology.* 2005;30:996–1005.
27. Kugaya A, Seneca NM, Snyder PJ, et al. Changes in human in vivo serotonin and dopamine transporter availabilities during chronic antidepressant administration. *Neuropsychopharmacology.* 2003;28:413–420.

Appendix

It is possible to simulate the amount of total striatal signal that originates from the SERT binding as a function of DAT density. In the case of the current DAT radioligands, BP_{ND} is equal to the product of the free fraction of ligand in the non-displaceable tissue compartment (f_{ND}) and the sum of available monoamine transporters in tissue of interest (B_{avail}) divided with the affinities for the individual monoamine transporters (K_d) for each radioligand.

$$BP_{ND} = f_{ND}\left(\frac{B_{avail,SERT}}{K_{d,SERT}} + \frac{B_{avail,DAT}}{K_{d,DAT}} + \left(\frac{B_{avail,NET}}{K_{d,NET}}\right)\right)$$

As mentioned in the discussion, the *in vitro* $B_{avail, DAT}$: $B_{avail, SERT}$ ratio in putamen is 20:1, but highly variable within individuals so it may also be 10:1. The literature suggests that in contrast to DAT, SERT binding is less affected with age (Brust *et al* 2006; Buchert *et al* 2006; van Dyck *et al* 2002). If $B_{avail, SERT}$ remains unchanged in healthy volunteers we can estimate SERT signal as function of $B_{avail, DAT}$:

$$\frac{SERTsignal}{TOTALsignal}\left(B_{avail,DAT}\right) = \frac{B_{avail,SERT}}{B_{avail,SERT} + \frac{K_{d,SERT}}{K_{d,DAT}} * B_{avail,DAT}}$$

$SERTsignal = B_{avail,SERT}/K_{d,SERT}$, $TOTALsignal = B_{avail,SERT}/K_{d,SERT} + B_{avail,DAT}/K_{d,DAT.}$

The binding of the radioligand to NET is neglected. Since K_d values are not available K_i are used instead and the ratio of K_i values are comparable to that of the K_d ratio.

The equation is presented in Figure appendix 1a & b. As one can appreciate from the figures, in [^{123}I]FP-CIT SPECT imaging, SERT signal may contribute to 20% of total striatal signal when $B_{avail, DAT}$ is between 60-40 % of normal, opposite in [^{123}I]PE2I SPECT imaging where the SERT signal is below 5 %. (60-40 % of normal $B_{avail, DAT}$ is typical what is present of $B_{avail, DAT}$ when PD patients experience their first Parkinson symptoms and is referred to a DAT SPECT scanning).

Appendix 1a & b: The figures shows the theoretical proportion of SERT signal of total striatal signal in: a) [^{123}I]PE2I and b) [^{123}I]FP-CIT in a 20/1, 10/1 and 5/1 ratio of DAT/SERT distribution.

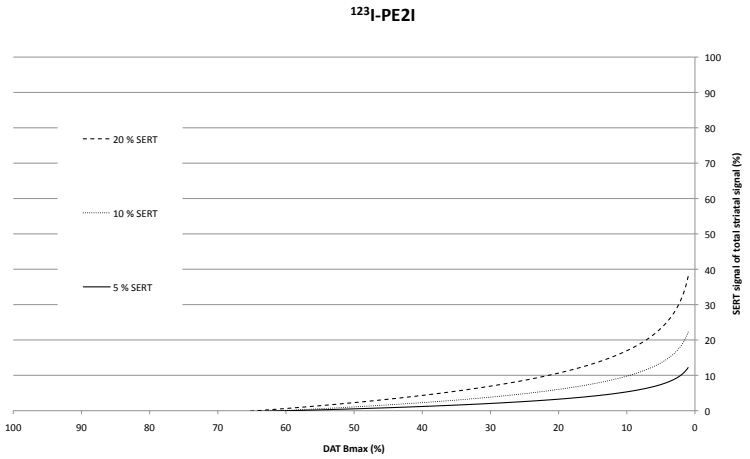

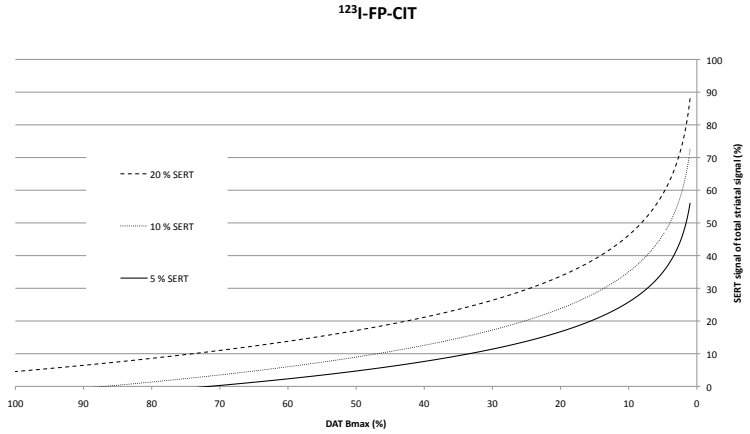

References

Abi-Dargham A, Gandelman MS, DeErausquin GA, Zea-Ponce Y, Zoghbi SS, Baldwin RM, Laruelle M, Charney DS, Hoffer PB, Neumeyer JL, Innis RB (1996) SPECT imaging of dopamine transporters in human brain with iodine-123-fluoroalkyl analogs of beta-CIT. *J Nucl Med* 37:1129-33.

Anden NE, Carlsson A, Dahlstroem A, Fuxe K, Hillarp NA, Larsson K (1964) Demonstration and Mapping out of Nigro-Neostriatal Dopamine Neurons. *Life Sci* 3:523-30.

Arthur Harris J (1913) On the Calculation of Intra-Class and Inter-Class Coefficients of Correlation from Class Moments when the Number of Possible Combinations is Large. *Biometrika* 9:446-72.

Barger G, Dale HH (1910) Chemical structure and sympathomimetic action of amines. *J Physiol* 41:19-59.

Booij J, Busemann Sokole E, Stabin MG, Janssen AG, de Bruin K, van Royen EA (1998a) Human biodistribution and dosimetry of [123I]FP-CIT: a potent radioligand for imaging of dopamine transporters. *Eur J Nucl Med* 25:24-30.

Booij J, Habraken JB, Bergmans P, Tissingh G, Winogrodzka A, Wolters EC, Janssen AG, Stoof JC, van Royen EA (1998b) Imaging of dopamine transporters with iodine-123-FP-CIT SPECT in healthy controls and patients with Parkinson's disease. *J Nucl Med* 39:1879-84.

Booij J, Kemp P (2008) Dopamine transporter imaging with [(123)I]FP-CIT SPECT: potential effects of drugs. *Eur J Nucl Med Mol Imaging* 35:424-38.

Brooks DJ, Frey KA, Marek KL, Oakes D, Paty D, Prentice R, Shults CW, Stoessl AJ (2003) Assessment of neuroimaging techniques as biomarkers of the progression of Parkinson's disease. *Exp Neurol* 184 Suppl 1:S68-79.

Brown WD, Taylor MD, Roberts AD, Oakes TR, Schueller MJ, Holden JE, Malischke LM, DeJesus OT, Nickles RJ (1999) FluoroDOPA PET shows the nondopaminergic as well as dopaminergic destinations of levodopa. *Neurology* 53:1212-8.

Brunoni AR, Lopes M, Fregni F (2008) A systematic review and meta-analysis of clinical studies on major depression and BDNF levels: implications for the role of neuroplasticity in depression. *Int J Neuropsychopharmacol* 11:1169-80.

Brust P, Hess S, Müller U, Szabo Z (2006) Neuroimaging of the Serotonin Transporter — Possibilities and Pitfalls. *Current Psychiatry Reviews* 2:111-49.

Buchert R, Schulze O, Wilke F, Berding G, Thomasius R, Petersen K, Brenner W, Clausen M (2006) Is correction for age necessary in SPECT or PET of the central serotonin transporter in young, healthy adults? *J Nucl Med* 47:38-42.

Carlsson A, Lindqvist M, Magnusson T (1957) 3,4-Dihydroxyphenylalanine and 5-hydroxytryptophan as reserpine antagonists. *Nature* 180:1200.

Carson RE, Channing MA, Blasberg RG, Dunn BB, Cohen RM, Rice KC, Herscovitch P (1993) Comparison of bolus and infusion methods for receptor quantitation: application to [18F]cyclofoxy and positron emission tomography. *J Cereb Blood Flow Metab* 13:24-42.

Catafau AM, Tolosa E (2004) Impact of dopamine transporter SPECT using 123I-Ioflupane on diagnosis and management of patients with clinically uncertain Parkinsonian syndromes. *Mov Disord* 19:1175-82.

Catafau AM, Corripio I, Perez V, Martin JC, Schotte A, Carrio I, Alvarez E (2006) Dopamine D2 receptor occupancy by risperidone: implications for the timing and magnitude of clinical response. *Psychiatry Res* 148:175-83.

Chen JJ (2010) Parkinson's disease: health-related quality of life, economic cost, and implications of early treatment. *Am J Manag Care* 16 Suppl Implications:S87-93.

Ciliax BJ, Heilman C, Demchyshyn LL, Pristupa ZB, Ince E, Hersch SM, Niznik HB, Levey AI (1995) The dopamine transporter: immunochemical characterization and localization in brain. *J Neurosci* 15:1714-23.

Corripio I, Catafau AM, Perez V, Puigdemont D, Mena E, Aguilar Y, Carrio I, Alvarez E (2005) Striatal dopaminergic D2 receptor occupancy and clinical efficacy in psychosis exacerbation: a 123I-IBZM study with ziprasidone and haloperidol. *Prog Neuropsychopharmacol Biol Psychiatry* 29:91-6.

Damier P, Hirsch EC, Agid Y, Graybiel AM (1999) The substantia nigra of the human brain. II. Patterns of loss of dopamine-containing neurons in Parkinson's disease. *Brain* 122 (Pt 8):1437-48.

Daws LC, Callaghan PD, Moron JA, Kahlig KM, Shippenberg TS, Javitch JA, Galli A (2002) Cocaine increases dopamine uptake and cell surface expression of dopamine transporters. *Biochem Biophys Res Commun* 290:1545-50.

de Lau LM, Breteler MM (2006) Epidemiology of Parkinson's disease. *Lancet Neurol* 5:525-35.

Delorenzo C, Kumar JD, Zanderigo F, Mann JJ, Parsey RV (2009) Modeling considerations for in vivo quantification of the dopamine transporter using [(11)C]PE2I and positron emission tomography. *J Cereb Blood Flow Metab* 29:1332-45.

Dick FD, De Palma G, Ahmadi A, Scott NW, Prescott GJ, Bennett J, Semple S, Dick S, Counsell C, Mozzoni P, Haites N, Wettinger SB, Mutti A, Otelea M, Seaton A, Soderkvist P, Felice A (2007) Environmental risk factors for Parkinson's disease and parkinsonism: the Geoparkinson study. *Occup Environ Med* 64:666-72.

Eller M, Williams DR (2009) Biological fluid biomarkers in neurodegenerative parkinsonism. *Nat Rev Neurol* 5:561-70.

Emond P, Garreau L, Chalon S, Boazi M, Caillet M, Bricard J, Frangin Y, Mauclaire L, Besnard JC, Guilloteau D (1997) Synthesis and ligand binding of nortropane derivatives: N-

substituted 2beta-carbomethoxy-3beta-(4'-iodophenyl)nortropane and N-(3-iodoprop-(2E)-enyl)-2beta-carbomethoxy-3beta-(3',4'-disubstituted phenyl)nortropane. New high-affinity and selective compounds for the dopamine transporter. *J Med Chem* 40:1366-72.

Eriksen J, Rasmussen SG, Rasmussen TN, Vaegter CB, Cha JH, Zou MF, Newman AH, Gether U (2009) Visualization of dopamine transporter trafficking in live neurons by use of fluorescent cocaine analogs. *J Neurosci* 29:6794-808.

Eriksen J, Jorgensen TN, Gether U (2010) Regulation of dopamine transporter function by protein-protein interactions: new discoveries and methodological challenges. *J Neurochem* 113:27-41.

Eskow KL, Dupre KB, Barnum CJ, Dickinson SO, Park JY, Bishop C (2009) The role of the dorsal raphe nucleus in the development, expression, and treatment of L-dopa-induced dyskinesia in hemiparkinsonian rats. *Synapse* 63:610-20.

Evans AH, Lawrence AD, Potts J, MacGregor L, Katzenschlager R, Shaw K, Zijlmans J, Lees AJ (2006) Relationship between impulsive sensation seeking traits, smoking, alcohol and caffeine intake, and Parkinson's disease. *J Neurol Neurosurg Psychiatry* 77:317-21.

Fahn S, Oakes D, Shoulson I, Kieburtz K, Rudolph A, Lang A, Olanow CW, Tanner C, Marek K (2004) Levodopa and the progression of Parkinson's disease. *N Engl J Med* 351:2498-508.

Falck B, Hillarp NA, Thieme G, Torp A (1982) Fluorescence of catechol amines and related compounds condensed with formaldehyde. *Brain Res Bull* 9:xi-xv.

Fearnley JM, Lees AJ (1991) Ageing and Parkinson's disease: substantia nigra regional selectivity. *Brain* 114 (Pt 5):2283-301.

Fernandez HH, Friedman JH, Fischman AJ, Noto RB, Lannon MC (2001) Is altropane SPECT more sensitive to fluoroDOPA PET for detecting early Parkinson's disease? *Med Sci Monit* 7:1339-43.

Ferri CP, Prince M, Brayne C, Brodaty H, Fratiglioni L, Ganguli M, Hall K, Hasegawa K, Hendrie H, Huang Y, Jorm A, Mathers C, Menezes PR, Rimmer E, Scazufca M (2005) Global prevalence of dementia: a Delphi consensus study. *Lancet* 366:2112-7.

Fowler JS, Volkow ND, Wolf AP, Dewey SL, Schlyer DJ, Macgregor RR, Hitzemann R, Logan J, Bendriem B, Gatley SJ, et al. (1989) Mapping cocaine binding sites in human and baboon brain in vivo. *Synapse* 4:371-7.

Frankle WG, Slifstein M, Gunn RN, Huang Y, Hwang DR, Darr EA, Narendran R, Abi-Dargham A, Laruelle M (2006) Estimation of serotonin transporter parameters with 11C-DASB in healthy humans: reproducibility and comparison of methods. *J Nucl Med* 47:815-26.

Frey KA, Koeppe RA, Kilbourn MR (2001) Imaging the vesicular monoamine transporter. *Adv Neurol* 86:237-47.

Garnett ES, Firnau G, Chan PK, Sood S, Belbeck LW (1978) [18F]fluoro-dopa, an analogue of dopa, and its use in direct external measurements of storage, degradation, and turnover of intracerebral dopamine. *Proc Natl Acad Sci U S A* 75:464-7.

Gasser T (2007) Update on the genetics of Parkinson's disease. *Mov Disord* 22 Suppl 17:S343-50.

Geng DY, Li YX, Zee CS (2006) Magnetic resonance imaging-based volumetric analysis of basal ganglia nuclei and substantia nigra in patients with Parkinson's disease. *Neurosurgery* 58:256-62; discussion -62.

Gether U, Andersen PH, Larsson OM, Schousboe A (2006) Neurotransmitter transporters: molecular function of important drug targets. *TRENDS in Pharmacological Sciences* 27:375-83.

Girault JA, Greengard P (2004) The neurobiology of dopamine signaling. *Arch Neurol* 61:641-4.

Group PS (2002) Dopamine transporter brain imaging to assess the effects of pramipexole vs levodopa on Parkinson disease progression. *JAMA* 287:1653-61.

Hall H, Halldin C, Guilloteau D, Chalon S, Emond P, Besnard J, Farde L, Sedvall G (1999) Visualization of the dopamine transporter in the human brain postmortem with the new selective ligand [125I]PE2I. *Neuroimage* 9:108-16.

Haugbol S, Pinborg LH, Arfan HM, Frokjaer VM, Madsen J, Dyrby TB, Svarer C, Knudsen GM (2007) Reproducibility of 5-HT2A receptor measurements and sample size estimations with [18F]altanserin PET using a bolus/infusion approach. *Eur J Nucl Med Mol Imaging* 34:910-5.

Hersch SM, Yi H, Heilman CJ, Edwards RH, Levey AI (1997) Subcellular localization and molecular topology of the dopamine transporter in the striatum and substantia nigra. *J Comp Neurol* 388:211-27.

Hesse S, Meyer PM, Strecker K, Barthel H, Wegner F, Oehlwein C, Isaias IU, Schwarz J, Sabri O (2009) Monoamine transporter availability in Parkinson's disease patients with or without depression. *Eur J Nucl Med Mol Imaging* 36:428-35.

Holtz P (1959) Role of L-DOPA decarboxylase in the biosynthesis of catecholamines in nervous tissue and the adrenal medulla. *Pharmacol Rev* 11:317-29.

Hughes AJ, Daniel SE, Kilford L, Lees AJ (1992) Accuracy of clinical diagnosis of idiopathic Parkinson's disease: a clinico-pathological study of 100 cases. *J Neurol Neurosurg Psychiatry* 55:181-4.

Hwang WJ, Yao WJ, Wey SP, Ting G (2004) Reproducibility of 99mTc-TRODAT-1 SPECT measurement of dopamine transporters in Parkinson's disease. *J Nucl Med* 45:207-13.

Innis RB, Cunningham VJ, Delforge J, Fujita M, Gjedde A, Gunn RN, Holden J, Houle S, Huang SC, Ichise M, Iida H, Ito H, Kimura Y, Koeppe RA, Knudsen GM, Knuuti J, Lammertsma AA, Laruelle M, Logan J, Maguire RP, Mintun MA, Morris ED, Parsey R, Price JC, Slifstein M, Sossi V, Suhara T, Votaw JR, Wong DF, Carson RE (2007) Consensus nomenclature for in vivo imaging of reversibly binding radioligands. *J Cereb Blood Flow Metab* 27:1533-9.

Katzenschlager R, Head J, Schrag A, Ben-Shlomo Y, Evans A, Lees AJ (2008) Fourteen-year final report of the randomized PDRG-UK trial comparing three initial treatments in PD. *Neurology* 71:474-80.

Kilbourn MR, Kuszpit K, Sherman P (2000) Rapid and differential losses of in vivo dopamine transporter (DAT) and vesicular monoamine transporter (VMAT2) radioligand binding in MPTP-treated mice. *Synapse* 35:250-5.

Kimmel HL, Carroll FI, Kuhar MJ (2000) Dopamine transporter synthesis and degradation rate in rat striatum and nucleus accumbens using RTI-76. *Neuropharmacology* 39:578-85.

Kirk R. (1982). *Experimental design: procedures for the behavioral sciences*. Pacific Grove, CA: Brooks/Cole.

Kish SJ, Tong J, Hornykiewicz O, Rajput A, Chang LJ, Guttman M, Furukawa Y (2008) Preferential loss of serotonin markers in caudate versus putamen in Parkinson's disease. *Brain* 131:120-31.

Koch W, Radau PE, Hamann C, Tatsch K (2005) Clinical testing of an optimized software solution for an automated, observer-independent evaluation of dopamine transporter SPECT studies. *J Nucl Med* 46:1109-18.

Kuhl D, Edwards R (1963) Image separation radioisotope scanning. *Radiology* 80:653-61.

Kuikka JT, Baulieu JL, Hiltunen J, Halldin C, Bergstrom KA, Farde L, Emond P, Chalon S, Yu M, Nikula T, Laitinen T, Karhu J, Tupala E, Hallikainen T, Kolehmainen V, Mauclaire L, Maziere B, Tiihonen J, Guilloteau D (1998) Pharmacokinetics and dosimetry of iodine-123 labelled PE2I in humans, a radioligand for dopamine transporter imaging. *Eur J Nucl Med* 25:531-4.

Kung MP, Stevenson DA, Plossl K, Meegalla SK, Beckwith A, Essman WD, Mu M, Lucki I, Kung HF (1997) [99mTc]TRODAT-1: a novel technetium-99m complex as a dopamine transporter imaging agent. *Eur J Nucl Med* 24:372-80.

Lammertsma AA, Hume SP (1996) Simplified reference tissue model for PET receptor studies. *Neuroimage* 4:153-8.

Laruelle M, Baldwin RM, Malison RT, Zea-Ponce Y, Zoghbi SS, al-Tikriti MS, Sybirska EH, Zimmermann RC, Wisniewski G, Neumeyer JL, et al. (1993) SPECT imaging of dopamine and serotonin transporters with [123I]beta-CIT: pharmacological characterization of brain uptake in nonhuman primates. *Synapse* 13:295-309.

Laruelle M, Abi-Dargham A, van Dyck CH, Gil R, D'Souza CD, Erdos J, McCance E, Rosenblatt W, Fingado C, Zoghbi SS, Baldwin RM, Seibyl JP, Krystal JH, Charney DS, Innis RB (1996) Single photon emission computerized tomography imaging of amphetamine-induced dopamine release in drug-free schizophrenic subjects. *Proc Natl Acad Sci U S A* 93:9235-40.

Lassen NA, Henriksen L, Paulson OB (1981) Regional cerebral blood flow by radioxenon-113 inhalation and dynamic emission tomography. *Prog Nucl Med* 7:110-7.

Lee CS, Samii A, Sossi V, Ruth TJ, Schulzer M, Holden JE, Wudel J, Pal PK, de la Fuente-Fernandez R, Calne DB, Stoessl AJ (2000) In vivo positron emission tomographic evidence for compensatory changes in presynaptic dopaminergic nerve terminals in Parkinson's disease. *Ann Neurol* 47:493-503.

Letchworth SR, Nader MA, Smith HR, Friedman DP, Porrino LJ (2001) Progression of changes in dopamine transporter binding site density as a result of cocaine self-administration in rhesus monkeys. *J Neurosci* 21:2799-807.

Lichtensteiger W, Hefti F, Felix D, Huwyler T, Melamed E, Schlumpf M (1982) Stimulation of nigrostriatal dopamine neurones by nicotine. *Neuropharmacology* 21:963-8.

Litvan I, MacIntyre A, Goetz CG, Wenning GK, Jellinger K, Verny M, Bartko JJ, Jankovic J, McKee A, Brandel JP, Chaudhuri KR, Lai EC, D'Olhaberriague L, Pearce RK, Agid Y (1998) Accuracy of the clinical diagnoses of Lewy body disease, Parkinson disease, and dementia with Lewy bodies: a clinicopathologic study. *Arch Neurol* 55:969-78.

Logan J, Fowler JS, Volkow ND, Wolf AP, Dewey SL, Schlyer DJ, MacGregor RR, Hitzemann R, Bendriem B, Gatley SJ, et al. (1990) Graphical analysis of reversible radioligand binding from time-activity measurements applied to [N-11C-methyl]-(-)-cocaine PET studies in human subjects. *J Cereb Blood Flow Metab* 10:740-7.

Luxen A, Guillaume M, Melega WP, Pike VW, Solin O, Wagner R (1992) Production of 6-[18F]fluoro-L-dopa and its metabolism in vivo--a critical review. *Int J Rad Appl Instrum B* 19:149-58.

Madras BK, Gracz LM, Fahey MA, Elmaleh D, Meltzer PC, Liang AY, Stopa EG, Babich J, Fischman AJ (1998) Altropane, a SPECT or PET imaging probe for dopamine neurons: III. Human dopamine transporter in postmortem normal and Parkinson's diseased brain. *Synapse* 29:116-27.

Maeda T, Kannari K, Shen H, Arai A, Tomiyama M, Matsunaga M, Suda T (2003) Rapid induction of serotonergic hyperinnervation in the adult rat striatum with extensive dopaminergic denervation. *Neurosci Lett* 343:17-20.

Marshall VL, Reininger CB, Marquardt M, Patterson J, Hadley DM, Oertel WH, Benamer HT, Kemp P, Burn D, Tolosa E, Kulisevsky J, Cunha L, Costa D, Booij J, Tatsch K, Chaudhuri KR, Ulm G, Pogarell O, Hoffken H, Gerstner A, Grosset DG (2009) Parkinson's disease is overdiagnosed clinically at baseline in diagnostically uncertain cases: a 3-year European multicenter study with repeat [123I]FP-CIT SPECT. *Mov Disord* 24:500-8.

Matsumoto R, Ichise M, Ito H, Ando T, Takahashi H, Ikoma Y, Kosaka J, Arakawa R, Fujimura Y, Ota M, Takano A, Fukui K, Nakayama K, Suhara T (2009) Reduced serotonin transporter binding in the insular cortex in patients with obsessive-compulsive disorder: A [(11)C]DASB PET study. *Neuroimage* 49:121-6.

McKeith I, O'Brien J, Walker Z, Tatsch K, Booij J, Darcourt J, Padovani A, Giubbini R, Bonuccelli U, Volterrani D, Holmes C, Kemp P, Tabet N, Meyer I, Reininger C (2007) Sensitivity and specificity of dopamine transporter imaging with 123I-FP-CIT SPECT in dementia with Lewy bodies: a phase III, multicentre study. *Lancet Neurol* 6:305-13.

Michaeli S, Oz G, Sorce DJ, Garwood M, Ugurbil K, Majestic S, Tuite P (2007) Assessment of brain iron and neuronal integrity in patients with Parkinson's disease using novel MRI contrasts. *Mov Disord* 22:334-40.

Minati L, Grisoli M, Carella F, De Simone T, Bruzzone MG, Savoiardo M (2007) Imaging degeneration of the substantia nigra in Parkinson disease with inversion-recovery MR imaging. *AJNR Am J Neuroradiol* 28:309-13.

Mintun MA, Raichle ME, Kilbourn MR, Wooten GF, Welch MJ (1984) A quantitative model for the in vivo assessment of drug binding sites with positron emission tomography. *Ann Neurol* 15:217-27.

Missale C, Nash SR, Robinson SW, Jaber M, Caron MG (1998) Dopamine receptors: from structure to function. *Physiol Rev* 78:189-225.

Mortensen OV, Amara SG (2003) Dynamic regulation of the dopamine transporter. *Eur J Pharmacol* 479:159-70.

Neumeyer JL, Wang SY, Milius RA, Baldwin RM, Zea-Ponce Y, Hoffer PB, Sybirska E, al-Tikriti M, Charney DS, Malison RT, et al. (1991) [123I]-2 beta-carbomethoxy-3 beta-(4-iodophenyl)tropane: high-affinity SPECT radiotracer of monoamine reuptake sites in brain. *J Med Chem* 34:3144-6.

Neumeyer JL, Wang S, Gao Y, Milius RA, Kula NS, Campbell A, Baldessarini RJ, Zea-Ponce Y, Baldwin RM, Innis RB (1994) N-omega-fluoroalkyl analogs of (1R)-2 beta-carbomethoxy-3 beta-(4-iodophenyl)-tropane (beta-CIT): radiotracers for positron emission tomography and single photon emission computed tomography imaging of dopamine transporters. *J Med Chem* 37:1558-61.

Olanow CW, Rascol O, Hauser R, Feigin PD, Jankovic J, Lang A, Langston W, Melamed E, Poewe W, Stocchi F, Tolosa E (2009) A double-blind, delayed-start trial of rasagiline in Parkinson's disease. *N Engl J Med* 361:1268-78.

Parkinson J. (1817). *An essay on the shaking palsy*. London: Sherwood, Neely, and Jones.

Paulsen JS (2009) Functional imaging in Huntington's disease. *Exp Neurol* 216:272-7.

Piccini PP (2003) Dopamine transporter: basic aspects and neuroimaging. *Mov Disord* 18 Suppl 7:S3-8.

Pinborg LH, Videbaek C, Knudsen GM, Swahn CG, Halldin C, Friberg L, Paulson OB, Lassen NA (2000) Dopamine D(2) receptor quantification in extrastriatal brain regions using [(123)I]epidepride with bolus/infusion. *Synapse* 36:322-9.

Pinborg LH, Videbaek C, Hasselbalch SG, Sorensen SA, Wagner A, Paulson OB, Knudsen GM (2001) Benzodiazepine receptor quantification in Huntington's disease with [(123)I]omazenil and SPECT. *J Neurol Neurosurg Psychiatry* 70:657-61.

Pinborg LH, Videbaek C, Svarer C, Yndgaard S, Paulson OB, Knudsen GM (2002) Quantification of [(123)I]PE2I binding to dopamine transporters with SPET. *Eur J Nucl Med Mol Imaging* 29:623-31.

Pinborg LH, Adams KH, Svarer C, Holm S, Hasselbalch SG, Haugbol S, Madsen J, Knudsen GM (2003) Quantification of 5-HT2A receptors in the human brain using [18F]altanserin-PET and the bolus/infusion approach. *J Cereb Blood Flow Metab* 23:985-96.

Pinborg LH, Ziebell M, Frokjaer VG, de Nijs R, Svarer C, Haugbol S, Yndgaard S, Knudsen GM (2005) Quantification of 123I-PE2I binding to dopamine transporter with SPECT after bolus and bolus/infusion. *J Nucl Med* 46:1119-27.

Pirker W, Djamshidian S, Asenbaum S, Gerschlager W, Tribl G, Hoffmann M, Brucke T (2002) Progression of dopaminergic degeneration in Parkinson's disease and atypical parkinsonism: a longitudinal beta-CIT SPECT study. *Mov Disord* 17:45-53.

Rice ME, Cragg SJ (2008) Dopamine spillover after quantal release: rethinking dopamine transmission in the nigrostriatal pathway. *Brain Res Rev* 58:303-13.

Schou M, Steiger C, Varrone A, Guilloteau D, Halldin C (2009) Synthesis, radiolabeling and preliminary in vivo evaluation of [18F]FE-PE2I, a new probe for the dopamine transporter. *Bioorg Med Chem Lett* 19:4843-5.

Seibyl JP, Laruelle M, van Dyck CH, Wallace E, Baldwin RM, Zoghbi S, Zea-Ponce Y, Neumeyer JL, Charney DS, Hoffer PB, Innis RB (1996) Reproducibility of iodine-123-beta-CIT SPECT brain measurement of dopamine transporters. *J Nucl Med* 37:222-8.

Seibyl JP, Marek K, Sheff K, Baldwin RM, Zoghbi S, Zea-Ponce Y, Charney DS, van Dyck CH, Hoffer PB, Innis RB (1997) Test/retest reproducibility of iodine-123-betaCIT SPECT brain measurement of dopamine transporters in Parkinson's patients. *J Nucl Med* 38:1453-9.

Seibyl JP, Marek K, Sheff K, Zoghbi S, Baldwin RM, Charney DS, van Dyck CH, Innis RB (1998) Iodine-123-beta-CIT and iodine-123-FPCIT SPECT measurement of dopamine transporters in healthy subjects and Parkinson's patients. *J Nucl Med* 39:1500-8.

Solinas M, Ferre S, You ZB, Karcz-Kubicha M, Popoli P, Goldberg SR (2002) Caffeine induces dopamine and glutamate release in the shell of the nucleus accumbens. *J Neurosci* 22:6321-4.

Stern MB, Braffman BH, Skolnick BE, Hurtig HI, Grossman RI (1989) Magnetic resonance imaging in Parkinson's disease and parkinsonian syndromes. *Neurology* 39:1524-6.

Strecker K, Wegner F, Hesse S, Becker GA, Patt M, Meyer PM, Lobsien D, Schwarz J, Sabri O (2010) Preserved serotonin transporter binding in de novo Parkinson's disease: negative correlation with the dopamine transporter. *J Neurol* [Epub ahead of print].

Tedroff J, Ekesbo A, Rydin E, Langstrom B, Hagberg G (1999) Regulation of dopaminergic activity in early Parkinson's disease. *Ann Neurol* 46:359-65.

Tossici-Bolt L, Hoffmann SM, Kemp PM, Mehta RL, Fleming JS (2006) Quantification of [(123)I]FP-CIT SPECT brain images: an accurate technique for measurement of the specific binding ratio. *Eur J Nucl Med Mol Imaging* 33:1491-9.

Tsuchida T, Ballinger JR, Vines D, Kim YJ, Utsunomiya K, Lang AE, Ichise M (2004) Reproducibility of dopamine transporter density measured with 123I-FPCIT SPECT in normal control and Parkinson's disease patients. *Ann Nucl Med* 18:609-16.

Uhl GR (2003) Dopamine transporter: basic science and human variation of a key molecule for dopaminergic function, locomotion, and parkinsonism. *Mov Disord* 18 Suppl 7:S71-80.

Vaillancourt DE, Spraker MB, Prodoehl J, Abraham I, Corcos DM, Zhou XJ, Comella CL, Little DM (2009) High-resolution diffusion tensor imaging in the substantia nigra of de novo Parkinson disease. *Neurology* 72:1378-84.

van Dyck CH, Seibyl JP, Malison RT, Laruelle M, Zoghbi SS, Baldwin RM, Innis RB (2002) Age-related decline in dopamine transporters: analysis of striatal subregions, nonlinear effects, and hemispheric asymmetries. *Am J Geriatr Psychiatry* 10:36-43.

Varnas K, Halldin C, Hall H (2004) Autoradiographic distribution of serotonin transporters and receptor subtypes in human brain. *Hum Brain Mapp* 22:246-60.

Videbaek C, G.M. K, K. B (1999) Octanol extraction yields similar results as HPLC for quantitation of [123I]PE2I metabolism. *Eur J Nucl Med* 26:1139.

Vingerhoets FJ, Schulzer M, Ruth TJ, Holden JE, Snow BJ (1996) Reproducibility and discriminating ability of fluorine-18-6-fluoro-L-Dopa PET in Parkinson's disease. *J Nucl Med* 37:421-6.

Vlaar AM, van Kroonenburgh MJ, Kessels AG, Weber WE (2007) Meta-analysis of the literature on diagnostic accuracy of SPECT in parkinsonian syndromes. *BMC Neurol* 7:27.

Vlaar AM, de Nijs T, Kessels AG, Vreeling FW, Winogrodzka A, Mess WH, Tromp SC, van Kroonenburgh MJ, Weber WE (2008) Diagnostic value of 123I-ioflupane and 123I-iodobenzamide SPECT scans in 248 patients with parkinsonian syndromes. *Eur Neurol* 59:258-66.

Wagner HN, Jr., Burns HD, Dannals RF, Wong DF, Langstrom B, Duelfer T, Frost JJ, Ravert HT, Links JM, Rosenbloom SB, Lukas SE, Kramer AV, Kuhar MJ (1983) Imaging dopamine receptors in the human brain by positron tomography. *Science* 221:1264-6.

Walker Z, Jaros E, Walker RW, Lee L, Costa DC, Livingston G, Ince PG, Perry R, McKeith I, Katona CL (2007) Dementia with Lewy bodies: a comparison of clinical diagnosis, FP-CIT single photon emission computed tomography imaging and autopsy. *J Neurol Neurosurg Psychiatry* 78:1176-81.

WHO. (2010) Neurological disorders: public health challenges. http://www.who.int/mental_health/neurology/neurodiso/en/index.html

Wilson JM, Kish SJ (1996) The vesicular monoamine transporter, in contrast to the dopamine transporter, is not altered by chronic cocaine self-administration in the rat. *J Neurosci* 16:3507-10.

Wise RA (2004) Dopamine, learning and motivation. *Nat Rev Neurosci* 5:483-94.

Ziebell M, Thomsen G, Knudsen GM, de Nijs R, Svarer C, Wagner A, Pinborg LH (2007) Reproducibility of [123I]PE2I binding to dopamine transporters with SPECT. *Eur J Nucl Med Mol Imaging* 34:101-9.

Ziebell M, Holm-Hansen S, Thomsen G, Wagner A, Jensen P, Pinborg LH, Knudsen GM (2010a) Serotonin transporters in dopamine transporter imaging: A head-to-head comparison of dopamine transporter SPECT radioligands [123I]FP-CIT and [123I]PE2I. *J Nucl Med* 51: 1885-91.

Ziebell M, Pinborg LH, Thomsen G, de Nijs R, Svarer C, Wagner A, Knudsen GM (2010b) MRI-guided region-of-interest delineation is comparable to manual delineation in dopamine transporter SPECT quantification in patients: a reproducibility study. *J Nucl Med Technol* 38:61-8.

Zigmond MJ, Abercrombie ED, Berger TW, Grace AA, Stricker EM (1990) Compensations after lesions of central dopaminergic neurons: some clinical and basic implications. *Trends Neurosci* 13:290-6.

Zuccato C, Cattaneo E (2009) Brain-derived neurotrophic factor in neurodegenerative diseases. *Nat Rev Neurol* 5:311-22.